Synthesis and Reactivity Studies of Square Pyramidal Complexes on Group 5 and 6 Metals for Nitrogen and Small Molecule Fixation

Richard Morris

A THESIS SUBMITTED TO
THE FACULTY OF GRADUATE STUDIES
IN PARTIAL FULFILLMENT OF THE REQUIREMENTS
FOR THE DEGREE OF
MASTERS OF SCIENCE

Graduate Program in
Chemistry
York University
Toronto, Ontario
August 2015

Abstract

I have completed work in the Lavoie Group which has resulted in the synthesis of new square pyramidal complexes supported by the *tert*-butyl-substituted (ethenediylidene)tetraphenoxide spectator ligand "TPO" ligand system. 2,2',2",2"'-(1,2-Ethenediylidene)tetrakis[4-*tert*-butylphenol], $(TPO)H_4$, was synthesized in four steps by literature procedures. The TPO ligand system was used to coordinate to tantalum. Complexes **6**, 2,2',2",2"'-(1,2-ethenediylidene)tetrakis[4-*tert*-butylphenoxo] tantalum(V) ethoxide and **7**, 2,2',2",2"'-(1,2-ethenediylidene)tetrakis[4-*tert*-butylphenoxo] tantalum(V) dimethylamide were synthesized and structurally characterized. Crystal structures of complexes **6** and **7** were also elucidated. The crystal structures confirmed that the geometry of complexes **6** and **7** is square pyramidal with the TPO ligand coordinating to tantalum slightly below the xy plane on which the metal resides. In addition, the ethoxo and dimethylamido ligands coordinate to tantalum on the z axis. Analyzing the X-ray structures gives valuable insight into π-interactions between the metal center and the apical ligands. Bond lengths and angles from the structures indicate significant double bond character between the metal and the apical ligand. Very short metal–oxygen and metal–nitrogen bonds in **6** and **7**, respectively, that results from donation of π-electron density from the heteroatom into empty metal dπ-orbitals. Reaction of (TPO)Ta(OEt) (**6**) and $(TPO)Ta(NMe_2)$ (**7**) with trimethylaluminum gave the methyl complex $(TPO)Ta(CH_3)$ (**8**). Complexes **6** and **7** were cleanly regenerated by addition of ethanol and dimethylamine to complex **8**. Reactivity studies with complexes **6**, **7**, and **8** are also reported. Reactions are reported with weak and strong acids, hydrides, amines, acid chlorides, isocyanides, and anhydrides. Reactivity studies with complex **6** and chlorotrimethylsilane also shows potential of forming a tantalum chloride species. Bonding in the tantalum complexes, specifically the

interactions between tantalum and the dimethylamido ligand on complex **7** were further explored using density functional theory calculations. Work on group 6 tungsten(VI) and molybdenum(VI) oxychloride precursors has also been completed with the synthesis of square pyramidal (TPO)tungsten(VI) oxide and (TPO)molybdenum(VI) oxide species being promising.

Table of Contents

List of Figures

List of Schemes

List of Tables

List of Abbreviations

Å	angstrom
acacH	acetylacetone
atm	atmosphere
Ar	aryl
^{13}C	carbon-13
calc	calculated
Cp	cyclopentadiene
Cp^*	pentamethylcyclopentadiene
d	doublet
DFT	density functional theory
DME	dimethoxyethane
Et	ethyl
^{1}H	proton
$\{^{1}H\}$	proton decoupled
hfacacH	hexafluoroacetylacetone
HIPT	hexaisopropylterphenyl
HOMO	highest occupied molecular orbital
LUMO	lowest unoccupied molecular orbital
MacacH	hexamethylacetylacetone
MAO	methylaluminoxane
Me	methyl group
MO	molecular orbital

NMR	nuclear magnetic resonance
O/N	overnight
ORTEP	Oak Ridge Thermal Ellipsoid Plot
Ph	phenyl group
PNP	2,6-bis(dialkylphosphinomethyl)pyridine
ppm	parts per million
q	quartet
rt	room temperature
s	singlet
salen	N,N'-bis(salicylaldehydo)ethylenediamine
t	triplet
*t*Bu	*tert*-butyl group
THF	tetrahydrofuran
TIBA	triisobutylaluminum
TPO	2,2',2",2"'-(1,2-ethenediylidene)tetrakis[4-*tert*-butylphenoxide]
$(TPO)H_4$	2,2',2",2"'-(1,2-ethenediylidene)tetrakis[4-*tert*-butylphenol]

Acknowledgements

Firstly, I would like to thank Prof. Gino G. Lavoie for accepting me as an MSc degree candidate as well as for his supervision throughout my project to date. Also, I would like to thank Profs. Sylvie Morin and Pierre G. Potvin for being part of my supervisory committee. In addition, I would like to thank Dr. Alan Lough from the University of Toronto for his help with X-ray analysis and Dr. Howard Hunter for his help with many NMR experiments. I would also like to thank the members of the Lavoie Group, past Michael Harkness, Jameel Al-Thagfi, Anna Badaj, Tim Larocque, Naseeb Fahahrim and present Lauren Keyes, and Faidh Hana for their help and support throughout my time at York University.

Last, but definitely not least important, I would like to thank my family for their love and support throughout my degree, especially my parents Eva and Stephen.

Some of the work herein reported has been accepted for publication. Received 13 May 2015, Revised 3 June 2015, Accepted 4 June 2015, Available online 16 June 2015.

Morris, R. S.; Lavoie, G. G. *Inorganica Chim. Acta* **2015**, *435*, 1–6.

1.0 Introduction

1.1 General Introduction

The developments of inorganic catalysts have played a valuable role in the advancement of synthetic chemistry over many decades. Many research groups around the world have been developing catalysts and the field has become an ever increasing area of research. The effectiveness of catalysts depends on the metal–ligand combination, namely, the types of ligands employed and the transition metals used. Catalysts that are comprised of *d*-block metals are of great importance to the chemical industry for two reasons: they provide cost-effective syntheses and they have excellent selectivity over the products formed. Transition metal inorganic complexes are used frequently in catalysis; allowing for the enhancement of activity as well as the exploration of new synthetic pathways. The chemical industry is worth billions of dollars per year and the search for new catalysts is a major driving force behind inorganic chemistry research. One of the most challenging tasks facing inorganic chemists to date is the conversion of N_2 to NH_3 using a homogenous catalyst under ambient conditions.[1-5]

One of the biggest warnings about nitrogen depletion in the soil was first given by William Crookes in 1898; he stated that this was an immense threat to the growing human population.[6] At the time, it was known that bacteria could use molecular nitrogen to help plants grow; additionally farming practices needed nitrogen supplements to increase crop production.[7] Unfortunately sources of cheap nitrogen, such as guano, were in short supply. The timely invention by Haber in the early 20th century for the synthetic process of ammonia formation was a monumental discovery; a Nobel Prize in Chemistry was awarded for the work in 1918.[8] Applying the discovery to the practical industrial process in 1913 by Bosch was also an

extraordinary accomplishment, also deserving a share in the Nobel Prize for Chemistry in 1931. The Haber-Bosch process did in fact significantly help the agricultural industry by making ammonia readily available as fertilizer, but there is still the need to understand the mechanism of this process.[7]

1.2 The Nitrogen Molecule

Unlike CO, NO or H_2, which are highly reactive species, the N_2 molecule is inert not only at ambient conditions (20 °C, 1 bar), but also at elevated temperatures and pressures.[9] The N_2 molecule is nonpolar, with tightly bound σ and π orbitals, and has a negative electron affinity. It also has very high ionization energy (15.58 eV) similar to that of argon (15.75 eV). Furthermore, the N_2 molecule has a triple bond that is particularly stable (944 kJ/mol); therefore making N–N bond cleavage very difficult.[9-11] Lastly, the N_2 molecule has a large HOMO-LUMO gap meaning it is reluctant to accept or lose electrons. This makes redox reactions with dinitrogen difficult despite the fact that dinitrogen has a range of oxidation states when incorporated in organic molecules.[11] All of these properties of dinitrogen explain why the Haber-Bosch process requires extreme temperatures and pressures to convert N_2 and H_2 to NH_3. This process is quite different to that which is found in nature; nature can convert thousands of tons of molecular nitrogen into ammonia every day at 20°C and 1 atm of pressure.[9]

1.3 Nitrogen Fixation Overview – Heterogeneous Catalysis

Ammonia (NH_3) has been produced for more than 100 years by reacting dinitrogen (N_2) and dihydrogen (H_2) over a Fe-based heterogeneous catalyst under forcing conditions, 150–250 bar and 300–550 °C.[12] Ammonia synthesis is one of the most important processes in the chemical industry, which was developed at BASF over 100 years ago by Fritz Haber and Carl

Bosch. Gas feed recycling in combination with high pressure and a catalyst such as osmium was used to attain large conversions of nitrogen.[13] Because of their successes, there is now a large-scale production of artificial fertilizers. Since 2011, approximately 80% of the world's production of ammonia (136 megatons per year) is used for that purpose.[13,14] This process is still significantly inefficient with little that has changed since its discovery 100 years ago. Even at such high temperatures and pressures, the ammonia concentration in the exhaust gas is still only 18 vol%. [13] An important step in the modern Haber-Bosch process was the development of the unique catalyst in the early 20th century by Alwin Mittasch at BASF.[13,15] To obtain this very active iron catalyst, magnetite (Fe_3O_4) is fused with oxides (K_2O, Al_2O_3, later also CaO) in an oxide melt. The magnetite is then mechanically granulated and reduced in the syngas feed to give the α-Fe catalyst. This synthesis imparts essential properties to the α-Fe catalyst and this same catalyst is still employed in the industry to date.[13,16]

1.4 Nitrogen Fixation Overview – Biological Catalysis

Reducing dinitrogen is an important reaction in nature. Dinitrogen is an essential molecule but in its diatomic form unusable to many living organisms.[17] Ever since scientists have discovered nitrogen fixing bacteria and plants, there has been a push to find chemical systems capable of fixing dinitrogen catalytically under mild conditions.[9,18] Firstly, there were attempts to isolate the enzymes and observe the reaction of N_2 in vitro of destroyed cells, but these attempts failed, which in turn slowed down the investigation of the reduction of N_2 chemistry.[18] In 1960 though, the first dinitrogen reduction was observed in supernatant solution from cells, which stimulated the biochemical investigation of nitrogenase chemistry.[18] Nitrogen fixation is mediated by singular enzymes, nitrogenase, that catalyze the conversion of N_2 to ammonia with the following stoichiometry:[17,19]

$N_2 + 8\,H^+ + 8e^- + 16\,MgATP \rightarrow 2\,NH_3 + H_2 + 16\,(MgADP + P_i)$

In this reaction there are eight protons and eight electrons involved that generate not only two molecules of ammonia but a molecule of hydrogen.[19] Additionally, there is the hydrolysis of 16 magnesium adenosine triphosphate (MgATP) molecules for every dinitrogen reduction cycle.[17,20] Physiological nitrogen fixation therefore consumes a lot of energy to produce ammonia.[17] To date, there are three types of nitrogenase enzymes known: Mo/Fe, V/Fe, and the Fe only centers.[9,21] Additionally, a single Fe_4S_4 cubane cluster is present in each nitrogenase enzyme. This allows for the reduction process since the cluster is responsible for electron transport.[22] Trapping intermediates, as well as spectroscopic characterization of different dinitrogen reduction intermediates have provided insight into the reduction to ammonia by nitrogenase.[23] Though the structures of many of these nitrogenase enzymes are known in great detail, the full mechanisms by which dinitrogen is reduced is far from being fully understood.[9,24]

It is apparent that the enzymatic system is one of the systems reducing dinitrogen in protic media.[18] Mo-Fe cofactors were also isolated from one of the proteins involved in the nitrogen fixing process playing a vital role in the activation and reduction of dinitrogen.[18] Though the exact mechanistic route for dinitrogen fixation is not fully understood, there is now insight into the process and there is less freedom of choice between possible schemes.[18]

Research on biological nitrogen fixation has yielded remarkable progress. The detailed make-up of the Fe-Mo cofactor of nitogenase is further understood, such as the characterization of the central atom in the Fe-Mo-co cluster (a carbide moiety).[25] Unfortunately, the mechanism of N_2 binding or reduction of N_2 in the nitrogenase is relatively unknown. Interestingly, it was thought that once the active site of nitrogenase was elucidated then it would provide valuable

information for development of synthetic systems; systems that would catalytically synthesize ammonia or other nitrogen compounds from dinitrogen.[7] It is important to note that nitrogenase is very complex. Additionally, the framework and all the parts that make up the enzyme are required for reactivity.[25] Research groups have attempted to make models of the system. Tremendous effort has been put in to construct Fe-Mo sulfidoclusters, but all the systems have failed to show any tendency to react with dinitrogen to form ammonia.[7]

1.5 Nitrogen Fixation Overview – Transition Metal Complexes

Since the discovery of cell-free nitrogenase over 40 years ago, the catalytic reduction of dinitrogen to ammonia at room temperature and pressure has gained much interest.[9,26] Obtaining a source of cheap fertilizer has seemingly been almost within reach with so much early progress in this field.[9]

During the same time period that biological N_2 fixation was being invested, the first reactions of dinitrogen where observed in the presence of transition metals. Dinitrogen transition complexes were discovered and surprisingly found to be very stable.[18] At the beginning, these complexes showed no chemical reactivity besides liberating N_2 from the metal.[18] Shortly thereafter, dinitrogen complexes were reacted to produce reduced products such as hydrazine as well as ammonia.[18]

The main principle that coordination chemists look for when dealing with small molecules is activation; primarily how they bind, to one or more metal centers and thus possibly become transformed. The fact that there is a lack of reactivity of the free N_2 molecule makes it challenging to reduce, the promise of N_2 coordination is a way of dealing with this inertness. Therefore, after a few years of the first discovery of dinitrogen complexes, by Allen and Senoff,

more complexes were discovered and this was an intense period of research in the field of molecular dinitrogen coordination chemistry.[27,28] Though Allen and Senoff did discover the $[Ru(NH_3)_5N_2]^{2+}$ species serendipitously, the complex shows little to no reactivity towards the transformation of dinitrogen.[7] Complexes with end-on binding modes were first targeted, many findings were published and reactivity studies were conducted such as protonation studies.[25] It was clear that most of the complexes showed little activity; simply releasing the coordinated dinitrogen ligand after an acid was introduced to the complex.

Dinitrogen is coordinated to the transition metal center by the Dewar–Chatt–Duncanson σ-donor/π-acceptor model of ligand bonding.[29,30] This is despite the fact that the dinitrogen ligand is a poor σ donor and a poor π acceptor (a very poor coordinating ligand). For example, if the dinitrogen molecule is bound end-on to a single metal center, the filled N_2 non-bonding orbitals will form a dative bond with the empty metal orbitals (d_z^2 and $d_{x^2-y^2}$). Filled orbitals of d_{xz}, d_{yz}, and d_{xy} of the metal will then back-donate to the vacant π^* of N_2 stabilizing the metal-N_2 complex further and weakening the N≡N bond.[29] This is the first step in effectively activating dinitrogen towards reduction. Unfortunately, the large HOMO-LUMO gap diminishes the overlap between the metal center and dinitrogen orbital making it a weak Lewis base (e.g. comparison to CO).[29]

Strongly reducing early metals have the ability to activate coordinated dinitrogen more than by simply bonding. Schrock has demonstrated that Ta(III) and W(IV) species have been prepared and reacted with dinitrogen to form imido-like ligands bridging two metal centers.[29,31,32] The donation of electrons in to the N_2 ligand reduces the bonding order; because of this the N–N bond length can correlate to the bond order. The longer the bond length from that of free N_2 (1.0975 Å) the more the molecule has been activated.[29] There are different binding

modes for the dinitrogen ligand; firstly there is the terminal end-on binding mode which is most common also it is the most prevalent especially in late transition metal chemistry (examples shown in Figure 1)[33,34].[29] Additionally greater activation can be achieved when the metal center is bridging the dinitrogen ligand, increasing the basicity of the N–N bond because of back-donation. This binding mode is more common for early transition metal dinitrogen complexes as the formation of strong multiple bonds to nitrogen ligands is made possible by additional reduction from the second metal-nitrogen bond. This can be shown in the case for Ta(V) and W(IV) species, which are known to have dinuclear end-on dinitrogen coordination.[32,35] For example, Schrock has shown that early transition metals, such as tantalum, can be reduced by sodium amalgam under argon gas in the presence of PMe_3, to give $TaCl_3(PMe_3)_3$.[31] Furthermore, $Ta(CHCMe_3)(PMe_3)_4Cl$ can be made by the reduction of $Ta(CHCMe_3)(PMe_3)_2C1_3$ under the same conditions. $[Ta(CHCMe_3)(PMe_3)_2Cl]_2(\mu\text{-}N_2)$ is therefore made by reacting a mixture of $Ta(CHCMe_3)(PMe_3)_2C1_3$ in ether with dinitrogen gas (1 atm).[29,31,36] In those complexes the N–N bond lengths are similar to a N=N double bond. However, since the formal oxidation states are Ta(V) and W(VI) indicating $(N_2)^{-4}$ therefore N–N is best represented as a single bond. The last most common binding mode is side-on bound dinitrogen ligand.[29] The binding mode is commonly observed in dinuclear complexes of early transition metals, possibly due to the fact that there is a lack of a second available d orbital for back-donation into the nitrogen (Figure 2).[29]

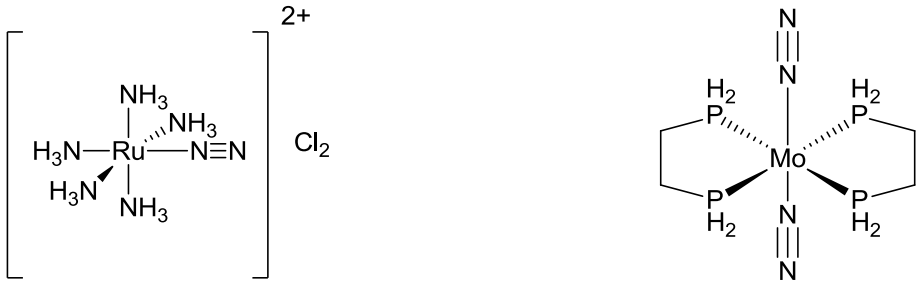

Figure 1. Example of Terminal Binding Mode Complexes.[33,34]

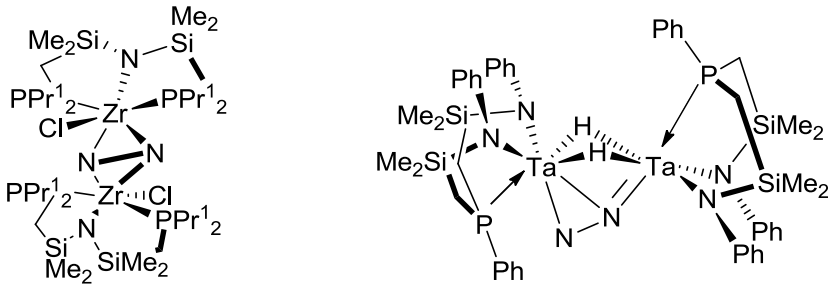

Figure 2. Dinuclear Side-on Bound Dinitrogen Complexes.[37,38]

More recently, molybdenum complexes coordinated by bulky aryl-substituted triamidoamine tripodal ligands $[N(CH_2CH_2NR)_3]^{3-}$, Schrock has created another 'high oxidation' system where N_2 is activated by electrophiles.[39-41] Schrock first reported the catalytic reduction of dinitrogen to ammonia at a monomeric molybdenum site.[40] In order to prevent formation of the relatively stable and unreactive bimetallic $[N(CH_2CH_2NAr)_3]$Mo-N=N-Mo$[N(CH_2CH_2NAr)_3]$ complexes, Schrock synthesized a complex containing the triamidoamine ligand ($[(RNCH_2CH_2)_3N]^{3-}$) in which the R group is 3,5-(2,4,6-*i*-$Pr_3C_6H_2)_2C_6H_3$ (HexaIsoPropylTerphenyl or HIPT), not only an extremely sterically shielding substituent but one that would provide increased solubility of the complex.[40,42] Coordination of N_2 to the [Mo(HIPTN_3N)] created a dinitrogen complex where the N_2 ligand coordinates in the trigonal binding pocket of the Mo(III) metal (Figure 3).[43]

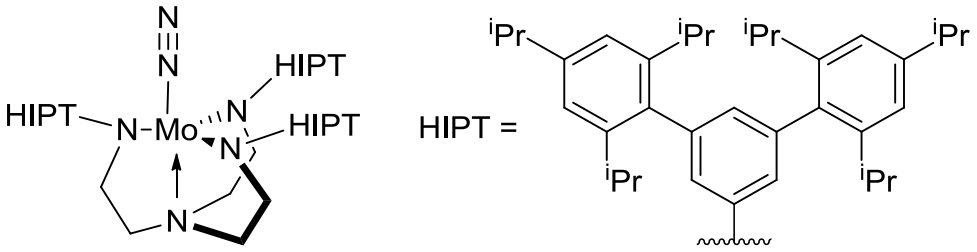

Figure 3. The Schrock [HIPTN$_3$N]Mo(N$_2$) Complex.[40]

Reducing the [HIPTN$_3$N]Mo(N$_2$) with either cobaltocene or decamethylchromocene, as an electron source, in the presence of {2,6-lutidinium}BAr‘$_4$, a proton source, in benzene leads to the catalytic formation of ammonia (7-8 equivalents). DFT calculations and isolation of key intermediates led to the proposed "Schrock cycle" (Scheme 1), which involves sequential one-electron reduction and protonation steps. This catalytic system has been studied extensively over the last decade and is still studied to date at length.[44-47] X-ray diffraction studies show that the HIPT backbone creates a symmetric pocket that protects a variety of dinitrogen reduction products against bimolecular decomposition reactions.[40] Although the three-fold symmetric cavity is protected, the metal is still available for reactions near the equatorial amido ligands.[40]

To acquire more knowledge on the catalytic properties of the Mo-triamidoamine systems different “hybrid” triamidoamine ligands have also been synthesized and investigated. Unfortunately, none were as successful at reducing dinitrogen as the [HIPTN$_3$N]Mo system.[48-51] Quite surprisingly many of these “hybrid” complexes (Figure 4) failed completely at catalyzing dinitrogen to ammonia. This demonstrates how sensitive the system is to changes in electronic structure and steric shielding at the metal center. Importantly, steric shielding is a decisive factor

when preventing the formation of binuclear complexes and the decomposition of unstable intermediates in the catalytic cycle in particular the diazenido complex.[17] One other feature that was noted was that electron donating-ligands might increase the rate of ammonia to dinitrogen exchange, a key step in the Schrock cycle. Schrock and co-workers developed complexes by tuning one of the arms of the of [HIPTN$_3$N]Mo(N$_2$) complex, running catalytic trials showed that most of the complexes were either ineffective at reducing dinitrogen or only catalytic to a slight degree (2 equiv).[48]

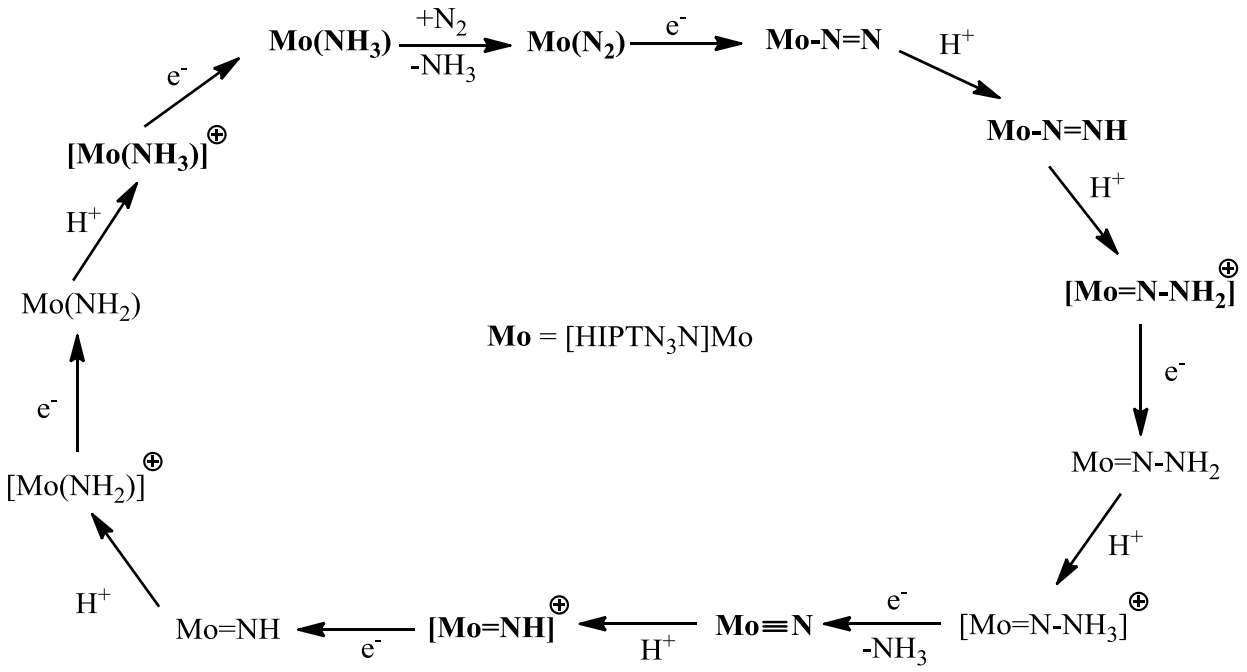

Scheme 1. The Schrock Cycle, a Model Synthetic Nitrogen Fixation Pathway. **Bolded** Intermediates Have Been Synthesized and Characterized.[42]

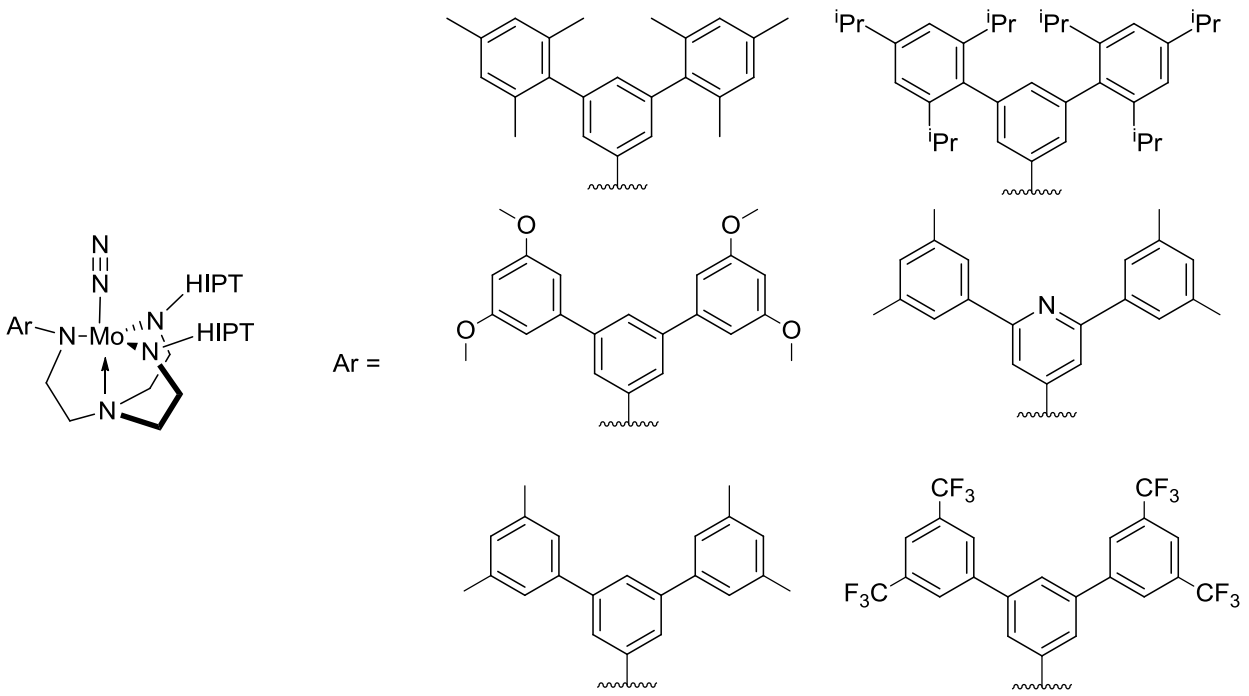

Figure 4. Examples of "Hybrid" Triamidoamine Ligands.[48]

In addition to Schrock's catalytic system for nitrogen fixation, many other researchers have tried to achieve catalytic transformation of dinitrogen to ammonia using very different transition metal complexes. Peters and co-workers have recently reported the coordination of neutral tetradentate tris(phosphino)borane ligands to iron (Figure 5). The resulting complexes also adopt trigonal bipyramidal geometries with dπ metal frontier orbitals similar to those of Schrock's complexes, approximately d_{xz} and d_{yz}.[52] Peters' complex mediated the reduction of dinitrogen to ammonia with comparable productivities to that of Schrock. The iron complex containing the anionic tris(phosphino)methyl ligand was found to be active. However, it was not thermally stable at standard temperatures, 20°C and 1 atm. The complex required lower temperatures to perform catalytic transformations, −78°C under 1 atm of N_2, yielding worse catalytic productivity.[53]

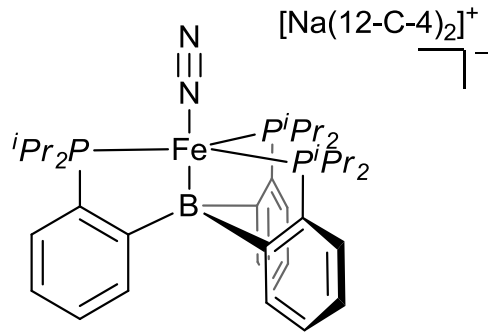

Figure 5. The Peters [(TPB)Fe(N_2)][Na(12-crown-4)$_2$] Complex.[52]

More recently, Nishibayashi and co-workers have reported activities exceeding 25 equivalents of ammonia per metal center using bimetallic molybdenum complexes based on neutral 2,6-bis(dialkylphosphinomethyl)pyridine, PNP pincer, ligands.[54] In their system, the strategy was to use mixed P/N ligands in synthetic nitrogen fixation. This would combine the π-accepting capabilities of the phosphine moieties with the high σ-donor ability of the amine. Nishibayashi's system showed that dinitrogen can be converted to ammonia catalytically, under atmospheric pressure, in the presence of proton and electron sources.[55] Treating Nishibayashi's complex (Figure 7) with 2,6-lutidinium triflate and cobaltocene in high excess under an atmosphere of N_2 catalytically produced ammonia. This further demonstrates the successful catalytic conversion of dinitrogen to ammonia under ambient conditions.[56] Interestingly, modifying the proton and/or the electron source had dramatic effects on ammonia yields. For example, using chromocene did not work at all as a reducing agent. Additionally, when [LutH]BAr'_4 (Ar' = 3,5-$(CF_3)_2C_6H_3$) or [LutH]Cl were used as acids, the yield of ammonia

decreased dramatically.[56] This is yet again another example of how extremely sensitive the nitrogen fixation catalytic cycle is with regards to the use of different reagents; simply changing the proton source slightly can decrease or stop the activity of a catalyst.

Nishibayashi and co-workers have also shown that slight modifications of bis(dialkylphosphinomethyl)pyridine pincer ligand drastically changes the catalytic efficiency of the complex (Figure 6).[57] The backbone can be modified by replacing the methyl group for a methoxy group; this was shown to dramatically change the catalytic behavior. The methyl complex shows catalytic activity for 2 h with a turnover rate of 44 equiv. of NH_3 (22 equiv. per metal center) then abruptly halts. On the contrary, catalysis of the methoxy complex occurred at a slower rate, over 10 h, with a turnover rate of 52 equiv. of NH_3 (26 equiv. per metal center).[57] The mechanism for this system is still unknown. Moreover, once the catalytic cycle has ended, it has been determined that only the free PNP ligands remain, indicating catalyst decomposition over time.

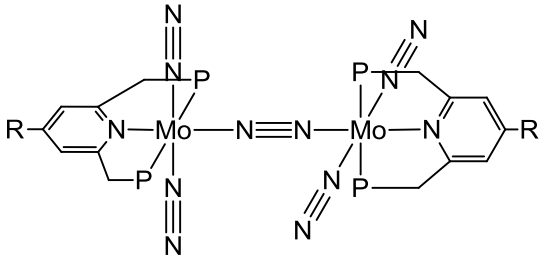

P = P^tBu_2 R = H, Me vs R= MeO

Figure 6. The Nishibayashi Molybdenum Complex Featuring the PNP-Pincer Ligand.[54,55,57]

1.6 Metal Ligand Multiple Bonds & Square Pyramidal Transition Metal Complexes

Multiple bonds between metals and main group elements such as oxygen, nitrogen and carbon are a common component of transition metal complexes. Double and triple bond reactivities in inorganic complexes have greatly expanded the chemical field and introduced a wealth of knowledge.[58] Complexes containing metal oxo groups have shown to be quite reactive for the epoxidation of alkenes,[59,60] atom-transfer reactions to compounds containing C=O, C=N, C=C and C≡C bonds,[61] C–H bond activation/cleavage,[62-64] as well as several other important small molecule transformations.[65] Similarly, the analogous metal imido complexes have been used in several associated reactions. Reactions include the formation of imines from ketones and aldehydes,[66] the aziridination of alkenes,[67,68] catalytic reduction of organic compounds containing C=X functional groups (X = O, N, or C),[61] and H_2 activation and hydrogenation.[69] Moreover, transition metal complexes that contain nitrido moieties have been used in numerous stoichiometric and catalytic reactions.[65,70,71] Complexes containing these metal imido and nitrido moieties are essential intermediates in the reduction of dinitrogen. Metal imido and nitrido complexes are vital to the nitrogen fixation pathway. The e^-/H^+ transfer process leads to the formation of ammonia.[65,71,72] For example, Schrock and co-workers have shown that both metal imido and nitrido complexes are key reactive intermediates in the nitrogen fixation pathway.[73,74]

Metal–atom multiple bonds occur from interactions between dπ orbitals on the metal and p-orbitals on the main group atom. An M–N σ-bond is formed by the interaction between an orbital of σ-symmetry on the metal (a d_z^2 orbital, assuming the M–N axis is also the z axis) and an nitrogen p_z orbital; π bonds are then formed by the overlap of the nitrogen p_x and p_y orbitals with suitable orbitals of π-symmetry on the metal, d_{xy}, d_{xz}, and d_{yz}.[70] Several factors impact the ability of the metal to participate in these π-interactions, including the energy of the dπ orbitals,

the identity of the spectator ligands and the geometry of the complex.[75] The ability of five-coordinate complexes with a three-fold geometry to participate in π-interactions with the apical ligand has been well demonstrated in the literature. Recently, trigonal bipyramidal and trigonal planar complexes have shown great promise in the field of nitrogen fixation, due to π-interactions between the metal center and the apical nitrogen atom.[73,74,76-81]

Laplaza and Cummins have reported the synthesis of a three coordinate molybdenum(III) system, [Mo{N(R)Ar}$_3$] (R = *t*Bu, Ar = 3,5-$C_6H_3Me_2$), that has trigonal planar geometry around the molybdenum metal center.[82] The molybdenum(III) complex reacts readily with dinitrogen to provide a terminal nitrido complex NMo[N(R)Ar]$_3$ through a μ-N_2 intermediate.[78,83] Additionally, Fryzuk has reported the synthesis of a four-coordinate trigonal-bipyramidal chloride complex, [P_2N_2]NbCl (where [P_2N_2] = PhP($CH_2SiMe_2NSiMe_2CH_2$)$_2$PPh).[84] Fryzuk was able to demonstrate that the reduction of [P_2N_2]NbCl with potassium graphene compound, KC_8, under dinitrogen leads to the formation of the dinuclear dinitrogen complex, ([P_2N_2]Nb)$_2$(μ-N_2).[84,85] Schrock's molybdenum complex contains three HexaIsoPropylTerphenyl (HIPT) substituents attached at each equatorial amide nitrogen around the complex creating a well protective pocket.[40] The amide groups on the triamidoamine ligand have a strong π-donor ability, this leads to a considerable activation of the N_2 ligand for reduction. The electron density of the Lewis base, N_2, into the empty orbital on the molybdenum center (d_z^2) creates an σ bond. Furthermore, when the dinitrogen binds to molybdenum, the filled metal orbital (approximately d_{xy} and d_{xz}) back-donates electron density to the anti-bonding LUMO of N_2, resulting in the formation of a M–N π bond and a decrease in the N≡N bond order. The activation of the N≡N bond is dependent upon the degree of back-donation from the metal center since electron density from the filled metal orbital enters the antibonding orbital of N_2. In Schrock's [HIPT]Mo(N_2)

complex, the backdonation from the metal center to the π* orbital of N_2 is quite substantial. Therefore [HIPT]Mo(N_2) is efficient in activating the dinitrogen triple bond.[86] Surprisingly, these π-interactions in square pyramidal complexes have been studied much less despite the known impact of angles between ligands in five-coordinate complexes on spin state and thereby on reactivity.[87,88]

1.7 2,2',2",2"'-(1,2-Ethenediylidene)tetraphenoxide (TPO) Ligand vs. Calixarene

For our work, we became interested in studying square pyramidal transition metal complexes since they offer unique opportunities for the activation of molecular nitrogen. Square pyramidal complexes have dπ-orbitals (approximately d_{xz} and d_{yz} in character, assuming the z-axis as the principal axis of rotation) available for interactions with the substrate at the apical position. The metal center could transfer electron density to the empty π*-orbitals of dinitrogen. This would then reduce the N≡N bond order, polarizing it, effectively activating the molecule for subsequent reactions. There are very few square pyramidal dinitrogen complexes which contain a tetradentate ligand coordinated to the metal center that have been structurally characterized; additionally many are dimeric.[89,90] Few ligands exist that when coordinated to metals conform to square pyramidal geometries with no isomerization to the trigonal bipyramidal isomer, while being able to easily change their steric and electronic parameters; examples include calixerenes or salen ligands.[91-94] The small energy difference between the trigonal bipyramidal and the targeted square pyramidal geometries is evidenced through fluxional behavior observed both in solution and in the solid state.[95-99]

Stryker has recently reported the synthesis of substituted 2,2',2",2"'-(1,2-ethenediylidene) tetraphenols (herein referred to as $(TPO)H_4$; Figure 7) and derivatives thereof in good to

excellent yields.[100-103] He was interested in designing a preorganized polydentate ligand system similar to calix[4]arenes but with more conformational rigidity.[103] Calix[4]arenes have been used as a polyaryloxide structural motif for coordination complex and modeling oxide supports.[104,105] Calix[4]arenes promote chelating over bridging coordination modes since they lack the conformational rigidity at the binding sites.[11] Furthermore, calix[4]arenes renders metal complexes prone to uncontrolled intermolecular aggregation because they lack sterically isolating substituents adjacent to the binding sites.[103] Substituted calix[4]arenes have been reported, on the methylene bridges, but the substituents do not sufficiently isolate the phenol oxygens.[106] The TPO ligand exploits the relative planarity of the ethylene core but still exhibits conformational freedom associated with free rotation of the aryl groups.[103]

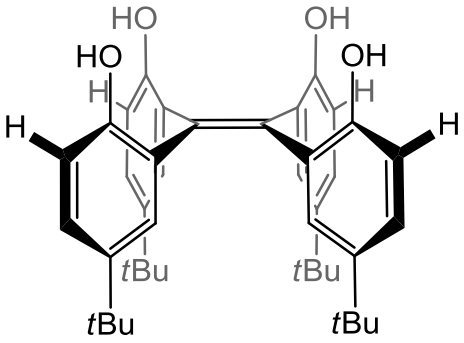

(TPO)H$_4$

Figure 7. Structure of 2,2',2",2"'-(1,2-Ethenediylidene)tetrakis(4-*tert*-butylphenol), (TPO)H$_4$.[100,103]

The (ethenediylidene)tetrakis[phenoxide] ligand system, herein referred to as "TPO", has aryl groups oriented approximately perpendicular to the ethylene plane with the hydroxyl groups in an all-*syn* conformation.[103] This creates a square planar alignment of oxygen atoms for metal binding.[103] The ligand design also accommodates the addition of substituents *ortho* to the hydroxyl groups to protect the metal center from Lewis bases and to inhibit intermolecular

aggregation.[101,103] Calix[4]arene ligands, on the contrary, would not accommodate any substituents *ortho* to the hydroxyl groups. This is because calix[4]arene systems have CH_2 bridges in those *ortho* positions connecting each aryl group, thus substituents can only be added onto the methylene carbon. Moreover, calix[4]arene do not have backside protection and have an open cavity where molecules can enter or bind. Examples include the complexation of benzene, toluene, water or other neutral molecules in the calixarene cavity, or the ability of calixarenes to form bimetallic inclusion complexes.[106-109] This creates pseudo-octahedral complexes, not the desired square pyramidal geometry. The TPO structure has excellent backside protection against the coordination of Lewis bases; the ethene group serves perfectly as it hinders the formation of hexacoordinate complexes. Ethenediylidenetetrakis[phenol] and derivatives are thus topologically unique, versatile and conformationally constrained precursors to tetradentate aryloxy ligands.[103]

Additionally, when comparing TPO to the salen ligand system many of the same disadvantages can be established for the salen ligand. Salen, (N,N'-bis(salicylaldehydo)ethylenediamine), has four coordinating sites and binds in a tetradentate mode to metal centers when deprotonated. Therefore salen forms a square planar arrangement of atoms [O, N, O, N] around the metal with most salen complexes showing a bowl conformation.[110,111] Unlike TPO, salen, has two axial sites open to the chelation of ancillaryligands.[110] For example many early transition metal salen complexes (M = Ti, Zr) are prepared by reacting the metal amide with the salen. This reaction occurs by the elimination of phenolic proton on the salen with the formation of the volatile $NHMe_2$ at the same time. The product is a bis-amido Salen complex that has two amido groups situated in both axial positions therefore making it hexacoordinate. An analogues reaction can be completed with metal alkoxide

precursors but the formation of a single species is more difficult. Oligomeric complexes are formed because of the equilibrium of the reaction; different complexes can be present in different concentrations.[110,112,113] Bulky substituents can be added to the salen framework, on the phenolic arene rings, but cannot fully protect the metal complex from nucleophiles at the axial site when chelated to transition metals.[111,114,115] For example, oxovanadium (IV) salen complexes have been prepared with the solid state structures showing a polynuclear linear chain structure. Each vanadium metal center is bridged by an oxo group in the axial positions forming a polymeric complex.[116,117] Moreover, exceptionally bulky salen complexes with mesityl groups in the 3, 5 positions of the arene rings have been prepared. Solid state structures show that the complexes do not conform to a square pyramidal geometry but rather are trigonal bipyramidal.[118]

1.8 Square-Based Pyramidal and Trigonal Bipyramidal Crystal Field Splittings

Square pyramidal systems can be analyzed by using crystal field therory. An octahedral ML_6 fragment can be the starting point and one or more ligands can be removed creating different metal ligand fragments (ML_{6-n}).[119] For instance, by removing one axial ligand on an octahedral complex a five-coordinate, C_{4v}, species is formed; a square pyramidal system.[119] From the formation of a square pyramidal system one can now further distort the C_{4v} system into a D_{3h} system creating a trigonal bipyramidal system. Firstly, starting with the ML_6 *d* block of orbitals from the octahedron, the energy levels are established using crystal field theory. The lower set of orbitals consists of, d_{xz}, d_{yz}, and d_{xy}, all having t_{2g} symmetry. The much higher energy set e_g consists of $d_{x^2-y^2}$ and d_{z^2} orbitals and is antibonding.[119,120] When one ligand is removed from the octahedron by a first approximation the t_{2g} set is slightly altered; the levels are labeled $e + b_2$ in the C_{4v} point group fragment.[119,120] There may be a relatively small energy gap

between *e* (d_{xz} and d_{yz}) and b_2 (d_{xy}), depending on the ligand. Usually the d_{xz} and d_{yz} metal orbitals are slightly lower in energy compared to the d_{xy} orbital of a C_{4v} square pyramidal complex.[88,121] In addition, the $d_{x^2-y^2}$ component would remain unchanged, remaining strongly antibonding. The main difference will be in the d_{z^2} orbitals, now labeled a_1, which will be greatly stabilized. Removing one ligand in the apical position loses a strong antibonding interaction between the metal center and surrounding ligands. Therefore the orbital moves to lower energy since part of its antibonding interaction is lost (Figure 9).[119,120]

If the C_{4v} fragment, (as in Figure 8. (b)) is distorted, allowing the L_{apical}-M-L_{basal} angle θ to become greater than 90°, a variation of the square pyramid geometry is established. The $d_{x^2-y^2}$ orbital becomes significantly increased in energy. There is significant metal-ligand antibonding in complexes with C_{4v} geometries. When the ligands are situated exactly on the xy plane the *e* (d_{xz}, d_{yz}) and b_2 (d_{xy}) orbitals are almost degenerate. Complexes with π-acceptor ligands have d_{xz} and d_{yz} orbitals in the lowest energy positions and have the d_{xy} slightly greater in energy.[122-124] Furthermore, when complexes have π back-donating ligands the b_2 set is lower in energy than the *e* set. The crystal-field model predicts the d_{xy} orbital as being destabilized; however the d_{xy} orbital becomes more stable than d_{xz}, d_{yz} because it overlaps orbitals of π symmetry on all four equatorial π back-donating ligands.[123] Pushing the equatorial ligands below the xy plane will cause the *e* set to rise in energy. The b_2 set will only rise slightly in energy as the L_{apical}-M-L_{basal} angle θ becomes larger.[119,120]

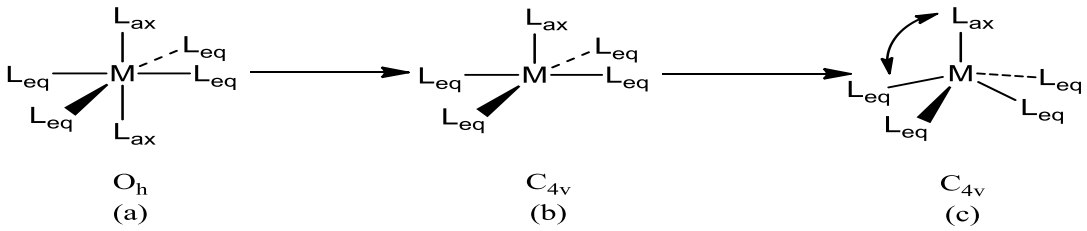

Figure 8. Converting from Octahedral to Square Pyramidal Geometries.

When comparing the square pyramidal geometry with trigonal bipyramidal, similarities and differences in the orbital arrangements can be established. The d_z^2 and $d_{x^2-y^2}$ orbitals switch in energy. The d_z^2 orbital points directly at the 2 axial ligands thus is destabilized the most, this now has a_1' symmetry. Two of the ligands on the yz plane move to the nodal plane of this $d_{x^2-y^2}$ orbital. This level becomes stabilized and is part of the e' symmetry set of the trigonal pyramidal geometry, $d_{x^2-y^2}$ and d_{xy}. When going from square pyramidal geometry to trigonal bipyramidal geometry one L_{eq}–M–L_{eq} ligand is decreased 90° below the xy plane and while the remaining 3 ligands are equally distanced on the xy plane. The d_{xy} orbital therefore becomes slightly higher in energy when converting to a trigonal bipyramidal geometry, but d_{yz} orbital is now lower in energy. Lastly, the two orbitals, d_{xz} and d_{yz}, are lowest in energy and are members of e'' symmetry set in trigonal bipyramidal geometries (Figure 9).[119,125]

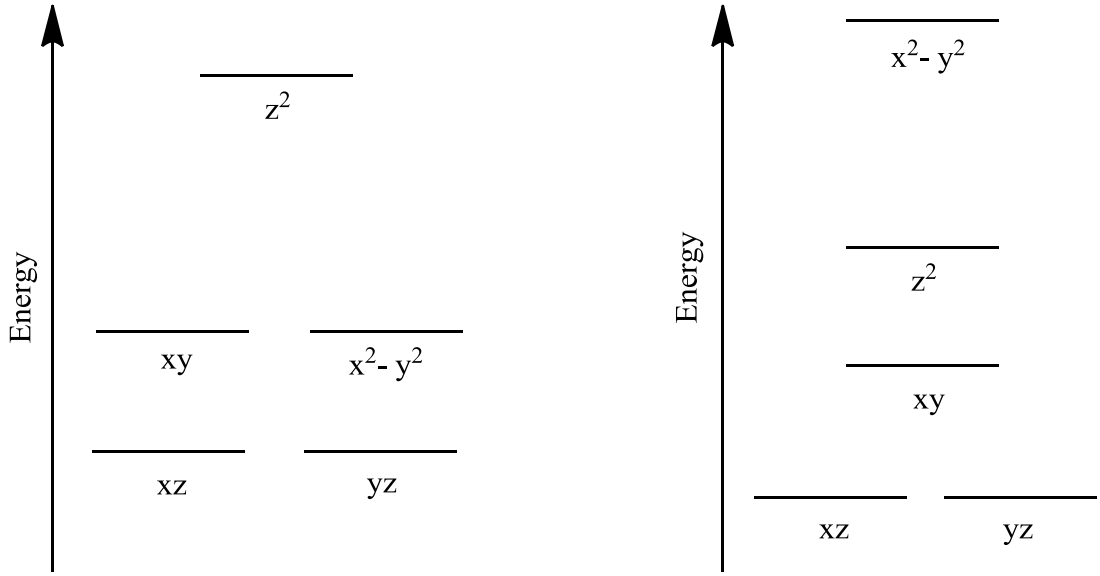

Figure 9. Crystal Field Splitting Diagrams for Trigonal Bipyramidal, (Left) and Square-Based Pyramidal, (Right) Fields.[119,125,126]

1.9 Comparing Schrock's [$HIPTN_3N$] Ligand System with the TPO Ligand System

Schrock's [$HIPTN_3N$] ligand enforces a trigonal bipyramidal geometry on the [$HIPTN_3N$]Mo(N_2) complex.[127] The [$HIPTN_3N$]Mo(N_2) complex is a low-spin d^3 species (S = $^1/_2$); in inorganic chemistry it is one of the rarest configurations.[127] A low-spin d^3 ion in the trigonal-bipyramidal coordination environment of [$HIPTN_3N$]Mo(N_2) exhibits a doubly degenerate ^2E ground state that is subject to a Jahn-Teller (JT) distortion as a consequence of vibronic coupling to doubly degenerate *e* vibrations.[127] Electron paramagnetic resonance (EPR) studies of the [$HIPTN_3N$]Mo(N_2) complex establishes that the complex exhibits the ls [e^3] electronic configuration.[128] Additionally in the e^3 configuration, the antibonding a_1 (d_{z2}) orbital has considerably higher energy than e'' (d_{xz}, d_{yz}), probably due to interactions with the axial nitrogen atoms.[128]

When looking at the TPO ligand system and its coordination mode to *d*-block metals, comparisons can be made to Schrock's [$HIPTN_3N$] ligand and [$HIPTN_3N$]Mo(N_2) complex. Schrock's complex is a four-coordinate trigonal-bipyramidal complex [Mo(N_3N)] (N_3N=[$(RNCH_2CH_2)_3N$]$^{3-}$ where R is a bulky substituent).[129,130] It was shown to bind to a variety of transition metals of oxidation states of +3 or higher.[131] The triamidoamine ligand binds to transition metals in a tetradentate manner, therefore creating a sterically protected symmetric pocket in which small molecules can bind.[129] Most importantly, this complex system can only accommodate ligands that bind in the apical position; along top of the z axis. This leaves only 3 orbitals available to bind to a ligand in the apical position, an σ orbital (approximately d_z^2) as well as two degenerate π orbitals (approximately d_{xz} and d_{yz}).[129,131] The two frontier π orbitals are both degenerate in the C_3 symmetric triamidoamine complexes; creating a well-suited environment for forming a metal–ligand triple bond.[131] In contrast to Schrock's [$HIPTN_3N$]

ligand and its trigonal planar binding mode, the TPO ligand system creates a square planar alignment of oxygen atoms for metal binding.[103] The TPO system, when coordinated to transition metals, has rigidity constraints therefore creating square pyramidal geometries (Figure 10). Backside hindrance can be observed in Schrock's $[HIPTN_3N]Mo(N_2)$ complex where an amine nitrogen (Figure 4) serves as backside protection. Similarities can be drawn from both systems, with the frontier molecular orbitals of both the $[HIPTN_3N]Mo(N_2)$ and TPO complexes having their d_{xz} and d_{yz} orbitals in the lowest energy (Figure 10).

In square pyramidal complexes reactivity with small molecules can take place at the apical position. When a small molecule such as dinitrogen where to bind end-on at that position, it would donate 2-electrons forming a σ-bond. Furthermore, if the square pyramidal complex has its lowest lying orbitals, d_{xz} and d_{yz}, populated with electrons the metal would donate electrons into the π^*-MO of dinitrogen. This would reduce the N≡N bond order and therefore activate the molecule.

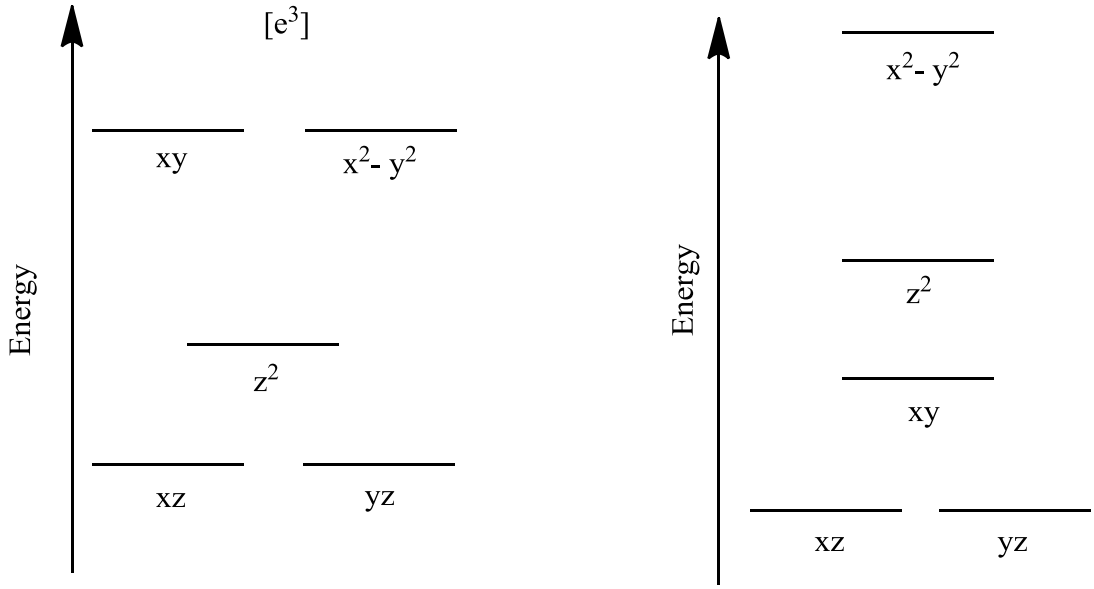

Figure 10. Electronic Configuration of the $[HIPTN_3N]Mo(N_2)$ Complex, Left, Compared to the Crystal Field Structure of Square Pyramidal Geometries, Right.[128]

2.0 Results and Discussion

2.1 Project Goals and Plan of Study

In the last few decades, much effort has been made to synthesize novel monometallic complexes for the reduction of dinitrogen. Until recently, only a few examples of complexes have been shown to homogeneously catalyze dinitrogen into some higher-value nitrogen species, such as ammonia, amines or other related nitrogen-containing compounds.[132] The catalytic transformation of molecular dinitrogen using complexes as catalysts under mild reaction conditions is really only limited to few examples.[17,18,133]

For this project, two major steps must be achieved: ligand synthesis and the study of its coordination chemistry. In our research, synthesizing (TPO)H_4 compounds, both *tert*-butyl substituted and unsubstituted, will be achieved using literature procedures. The coordination chemistry of the ligands will be first assessed on group 5 transition metals such as tantalum before looking into group 6 and 7 metals. The TPO system will be coordinated to tantalum primarily to gain insight into the chemistry of the complex and to assess the geometry that is enforced. Group 5 metals are easier to study since the corresponding complexes are diamagnetic, thus much easier to characterize by NMR spectroscopy than paramagnetic species. Halide (Cl or Br) complexes are targeted since they can be reduced under atmospheres of N_2 and CO. Reduction under those atmospheres could lead to the formation of complexes with bound N_2 or CO which is the first step in the functionalization those molecules. Another important aspect of halides is that they are common precursors to amides and alkoxides. A range of complexes can be more easily prepared when starting with a metal halide. This will be important when completing reactivity studies. Additionally, investigating complexes containing metal-nitrogen bonds such as M–NR_2, M–NHR, M–N_2H_3 will be of great interest. The metal nitrogen bond is of

great importance in homogenous nitrogen fixation as reduction occurs on the metal center. Dinitrogen is reduced on the metal center. Therefore, studying complexes with such a bond will be targeted. For example, complexes containing a hydrazido ligand could lead into the nitrogen reduction cycle; bound hydrazido is a key intermediate in the cycle.[134]

Upon the coordination of TPO to group 5 metals, the resulting complexes will be studied to gain knowledge on the bonding interactions. π-Interactions between the TPO ligand and apical ligands on the metal center will be investigated. Solid state structures will be analyzed for bond lengths and angles that the TPO ligand and the apical ligands enforce on the metal center. Analysis of the complexes, bond lengths and angles will provide evidence of π-bonding between the ligands and the metal. In addition, DFT calculations of the solid state structures will be performed to further provide validation of any π-interactions between the apical ligands and the TPO ligand on the metal center.

2.2 Synthesis of 2,2',2",2"'-(1,2-Ethenediylidene)tetrakis[4-*tert*-butylphenol]

An efficient four-step synthesis (Schemes 2 and 3), which has been developed by Stryker,[103] of 2,2',2",2"'-(1,2-ethenediylidene)tetrakis[4-*tert*-butylphenol] from 4-(*tert*-butyl)phenol. Additionally, a three-step pathway (Scheme 2) to 2,2',2",2"'-(ethenediylidene)tetrakis[phenol] was developed from anisole. In our research, two ligands were synthesized: the unsubstituted 2,2',2",2"'-(ethenediylidene)tetrakis[phenol] as well as the substituted 2,2',2",2"'-(1,2-ethenediylidene)tetrakis[4-*tert*-butylphenol]. A *tert*-butyl substituent was employed in the *para* position of each arene ring, for the synthesis of 2,2',2",2"'-(1,2-ethenediylidene)tetrakis[4-*tert*-butylphenol]. This was made so that later in subsequent research, *ortho* substituents, such as bromide and silyl groups,[101] could be added to the ligand framework.

Having a *tert*-butyl group *para* to the hydroxyl group eliminates bromination in that position and only leads to bromides in the *ortho* position. The synthesis of $(TPO)H_4$ starts with 4-(*tert*-butyl)phenol, **1**, which is methylated to form 4-(*tert*-butyl)anisole, **2b**. Compound **2b** is commercially available but due to its high cost and the fact that it can easily be prepared, the synthetic route was favoured. Subsequently, preparing the 2,2'-(dimethoxybenzo)phenone (**3a/b**) was completed by ortho-metalation of the anisole.[103] Afterwards, reductive coupling of the substituted benzophenone was accomplished by the McMurry olefination reaction.[100] The final step in the synthesis was the deprotection of the methoxy groups, using BBr_3 to obtain either the substituted or unsubstituted protonated $(TPO)H_4$ (**5a/b**).[103]

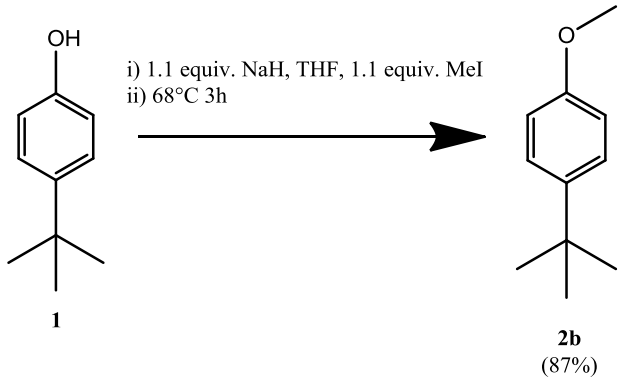

Scheme 2. Synthesis of 4-(*Tert*-butyl)anisole (**2b**)

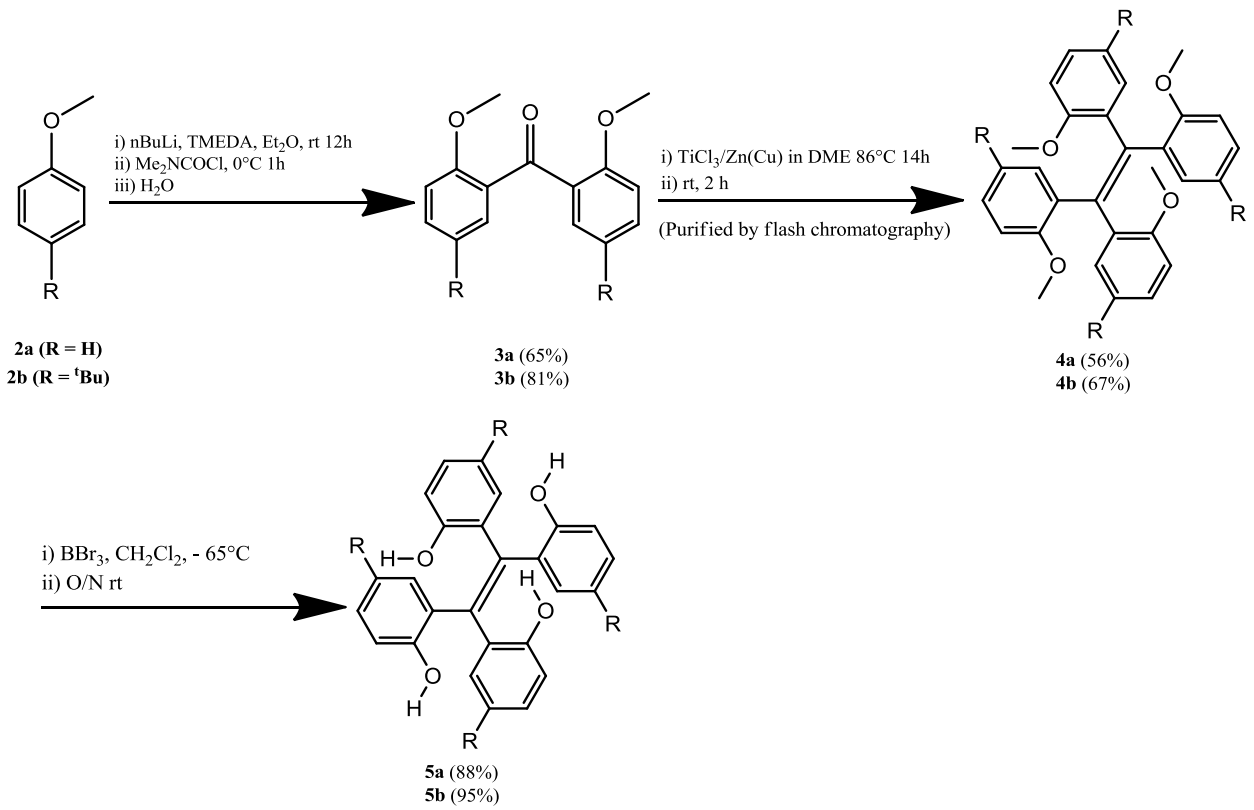

Scheme 3. Synthesis of 2,2',2",2"'-(1,2-Ethenediylidene)tetrakis[phenol] (**5a**) and 2,2',2",2"'-(1,2-Ethenediylidene)tetrakis[4-*tert*-butylphenol] (**5b**).

2.3 Coordination of 2,2',2",2"'-(1,2-Ethenediylidene)tetrakis[4-*tert*-butylphenol] **5b** to Group 5 Metals

Styker has shown that the TPO ligand system has potential in coordination chemistry by investigating the coordination of TPO to both main group and transition metals.[103] The main goal of his work was to form quasi-planar, raft-like, polymetallic coordination complexes.[102] The ligand would provide topologically consistent structural models for metal coordination to "oxo-surfaces" such as silica- and alumina.[102] Styker focused his attention on the coordination to magnesium, aluminum and titanium and the corresponding complexes were prepared.[101,102,135] These metal complexes were all either dimeric or oligomeric, with each molecule containing more than one metal center.

Stryker has reported only one example of the ligand chelating to a single polyvalent metal ion in a tetradente fashion.[103] A dark blue monomeric half-piano stool molybdenum(V) complex was isolated in good yield by reacting Cp^*MoCl_4 with the tetranionic ligand, prepared in situ by addition of NaH to $(TPO)H_4$.[103] X-ray analysis showed that all the Mo–O bonds were nearly equidistant with the ligand conforming to a distorted propeller formation. Each aryl ring was titled off by 76-86° from the ethene plane.[103]

In our work, early attempts to coordinate either the *tert*-butyl TPO (5b) or unsubstituted TPO (5a) were made with $TaCl_5$ and Cp^*TaCl_4 in aprotic polar solvents such as THF, MeCN or diethyl ether. The procedure reported by Styker for the preparation of CpMoTPO was used. $(TPO)H_4$ was deprotonated in situ by the addition of NaH followed by treatment of the tetranionic salt, $Na_4(TPO)$, with the metal precursor. Several attempts have been conducted using various ratios of base to ligand (4 to 8 equiv), employing different solvents (THF, MeCN, diethyl ether or toluene) or changing the base used (e.g. NaH, $NaN(SiMe_3)_2$, MeLi or Et_3N). None of

these methods produced a pure characterizable complex. When utilizing $TaCl_5$ as a metal precursor in the early reactions, THF or MeCN were used as solvents. The solvents would coordinate to the metal center as well since THF and MeCN both are coordinating solvents. This was a common occurrence, with coordinated THF observed in crude ^1H NMR spectra. Additionally, when $TaCl_5$ or Cp^*TaCl_4 was used as a metal precursor, the reactions did not produce the desired products: the majority of the resonances in the aromatic region of the ^1H NMR spectra was not as predicted nor could any single product be isolated or purified. Washing with different solvents, in attempts to purify any products formed, or crystallization techniques did not result in an isolated product. The ^1H NMR spectrum showed many more resonances than expected, which may indicate that one or more hydroxyl groups may be binding to other Ta metal centers, creating aggregations or oligomeric species, as reported by Stryker for Mg and Al.[102] Scheme 4 shows an example of the unsubstituted TPO ligand coordinating to 2.5 metal centers. This could be an example of an aggregation which might have occurred.

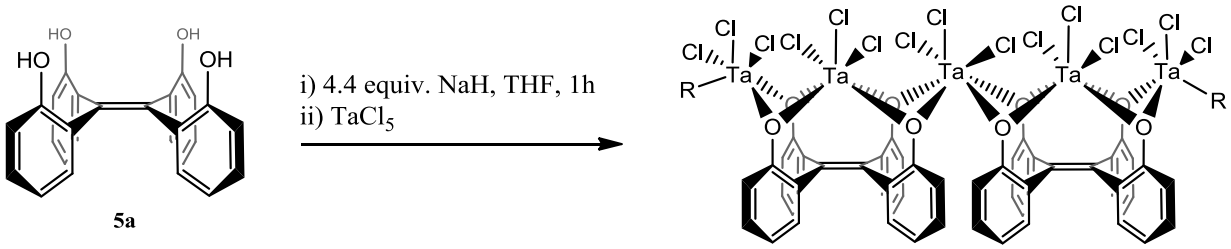

Scheme 4. Example of Aggregation when Reacting a $TaCl_5$ Precursor with $(TPO)H_4$.

Since attempts to synthesize tantalum complexes bearing a chloride or Cp^* in the apical position did not produce any complexes that were hoped for, a different synthetic approach was developed. Upon completing some research, Verkade et al. used $Ta(OC_2H_5)_5$ as a metal precursor in a reaction using a tridentate hydroxyl ligand, tris(2-hydroxy-3,5-dimethylbenzyl)amine.[136] In their research, they synthesized a 6-coordinate complex bearing

their tridentate ligand and 3 ethoxide ligands. The reaction was accomplished by the addition of $Ta(OC_2H_5)_5$ in toluene to a solution of their tris(hydroxyl) ligand in toluene. The reaction mixture was set to heat to reflux for 14 h.[136]

This synthetic approach was employed using the *tert*-butyl substituted $(TPO)H_4$, **5b**. The reaction mixture was not set to heat on reflux. The preparation of $(TPO)Ta(OCH_2CH_3)$ was accomplished by protonolysis from the corresponding homoleptic tantalum(V) ethoxide complex with **5b** $(TPO)H_4$. Addition of one equivalent of $Ta(OCH_2CH_3)_5$ to $(TPO)H_4$ in toluene cleanly gave $(TPO)Ta(OCH_2CH_3)$ (**6**) as a pale yellow solid in excellent yield (97%), with the generation of ethanol as by-product (Scheme 5). The ^1H and ^{13}C NMR spectra, in benzene-d_6, showed only one set of resonances for the TPO scaffold, indicating a highly symmetrical structure (refer to section **6.0** NMR spectra). The TPO resonances in the ^1H NMR spectrum show 3 resonances in the aromatic region with a ratio of 1:1:1 and one in the aliphatic region with a ratio of 9:1 to that of one aromatic peak. Integrating each aromatic resonance as 4 leads to an integral of 36 on the aliphatic resonance that totals 48 for the TPO ligand. Most importantly, the characteristic proton resonances from the ethoxide moiety could be identified, a quartet at 4.27 ppm for the methylene and a triplet at 1.08 ppm for the methyl, integrating to 5 and with a ^3J coupling of 7.00 Hz. In the $^{13}C\{^1H\}$ NMR spectrum, 11 resonances were observed, which correspond to the 11 different carbons present in the complex. The characteristic resonances in the $^{13}C\{^1H\}$ NMR spectrum are recognized as the methylene, 74.8 ppm, and methyl, 17.7 ppm, from the ethoxide moiety. Results from microcombustion analysis are consistent with what was calculated for complex **6**, which further support the structure and its purity. The complex is thermally stable. No decomposition of complex **6** was observed upon prolonged heating at 70 °C.

The same reaction was attempted but with the unsubstituted $(TPO)H_4$ ligand, **5a**. Unlike the previous reaction, the results were not as predicted. The crude ^1H NMR spectrum showed multiple peaks in the aromatic and aliphatic region and the spectrum was uninterpretable. The multiple peaks may have been due to one hydroxyl group binding to a Ta center while another binds to a separate Ta center causing aggregation of ligands and metal centers. It seems as though the *tert*-butyl groups on **5b** forced complex **6** into the square pyramidal conformation, having a more sterically favourable orientation. The *tert*-butyl groups are in a conformation that maximizes the distance away from each other. Conversely, ligand **5a** does not have any bulky groups that would help stabilize the complex; therefore there is greater opportunity for uncontrolled reactions.

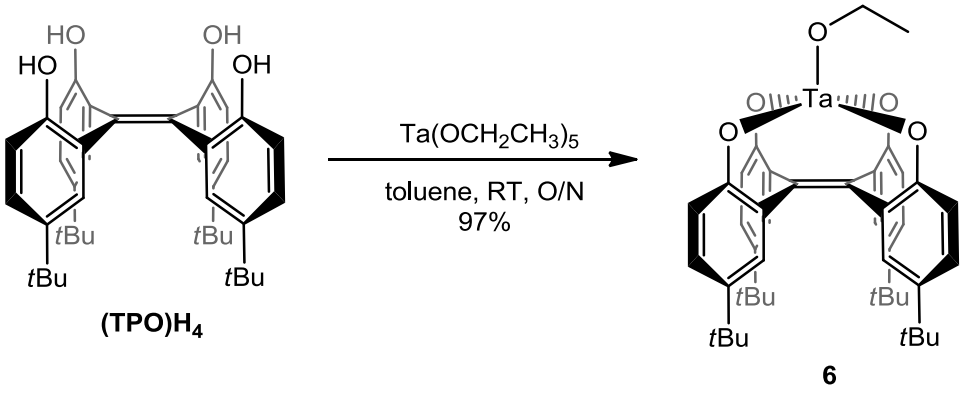

Scheme 5. Coordination of *tert*-butyl TPO to $Ta(OEt)_5$

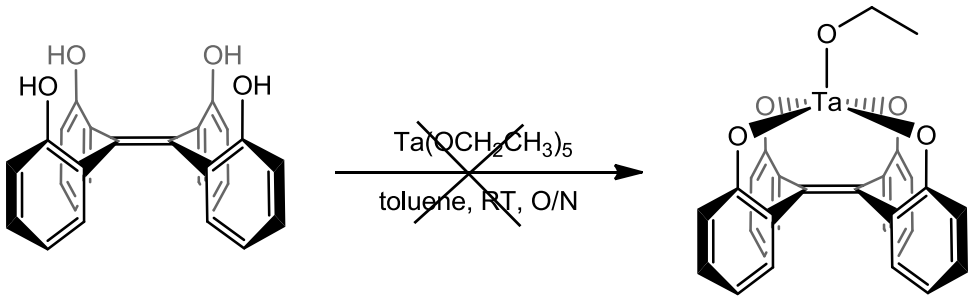

Scheme 6. Failed Coordination of Unsubstituted TPO to $Ta(OEt)_5$

Since the synthesis of complex **6** worked so effectively, a similar synthetic approach was adopted for the preparation of a tantalum dimethylamide complex (Scheme 7). $Ta(N(CH_3)_2)_5$ was dissolved in toluene, also a separately prepared suspension was made by the addition of **5b** to toluene. The suspension containing **5b** was next carefully added to the solution containing $Ta(N(CH_3)_2)_5$ and the resulting mixture was stirred overnight. This synthesis led to the desired complex **7** in a 52% yield, as a light yellow solid. The ^{1}H NMR spectrum showed very similar peaks to that of complex **6**: 3 peaks in the aromatic region in a ratio of 1:1:1 (a doublet at 7.44 ppm, a doublet of doublets at 6.86 ppm and a doublet at 6.69 ppm), as well as a large singlet in the aliphatic region, in a ratio of 9:1 relative to one of the aromatic resonances. The main characteristic peak in the ^{1}H NMR is the singlet at 3.40 ppm corresponding to the methyl protons on the dimethylamido substituent. In the $^{13}C\{^1H\}$ NMR spectrum, 10 peaks could be seen in the spectrum which correspond to 10 different carbons present in the complex (refer to section **6.0** NMR spectra). Results from microcombustion analysis are consistent with the calculated value of complex **7**; this further supports the structure and its purity.

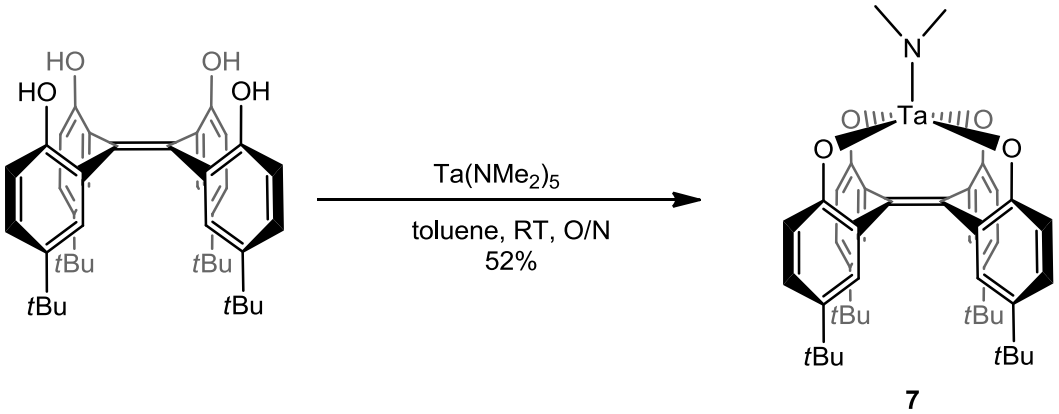

7

Scheme 7. Coordination of *Tert*-butyl $(TPO)H_4$ to $Ta(N(CH_3)_2)_5$, Complex **7**

In addition to working with 2,2',2",2"'-(1,2-ethenediylidene)tetrakis[4-*tert*-butylphenol], 2,2',2",2"'-(1,2-ethanediylidene)tetrakis[4-*tert*-butylphenol], a saturated version of $(TPO)H_4$, was also employed in the reactions with $Ta(N(CH_3)_2)_5$ and $Ta(OCH_2CH_3)_5$. 2,2',2",2"'-(1,2-Ethanediylidene)tetrakis[4-*tert*-butylphenol] was synthesized from 2,2'-dimethoxybenzo(*tert*-butylphenone) reductively coupling by the McMurry reaction.[100] This reaction leads to primarily 2,2',2",2"'-(1,2-ethenediylidene)tetrakis[4-*tert*-butylanisole] but over-reduction can also lead to the 1,1,2,2,-tetrasubstituted ethane. Purification by column chromatography on silica gel using a gradient solvent system of CH_2Cl_2/hexanes yields mostly 2,2',2",2"'-(1,2-ethenediylidene)tetrakis[4-*tert*-butylanisole] but the over-reduced product can be isolated in upwards of 20% yield. 2,2',2",2"'-(1,2-Ethanediylidene)tetrakis[4-*tert*-butylanisole] was then deprotected with BBr_3 to obtain 2,2',2",2"'-(1,2-ethanediylidene)tetrakis[4-*tert*-butylphenol], the saturated variant.

Next, the saturated $(TPO)H_4$ ligand was treated with both $Ta(OCH_2CH_3)$ and $Ta(N(CH_3)_2)_5$ in a 1:1 ratio in toluene, in an analogous reaction to that of $(TPO)H_4$. Interestingly, no reaction occurred between the ligand and either precursor, as the saturated version of $(TPO)H_4$ was not soluble in toluene and did not react. Different solvents were used diethyl ether

and THF. The ligand was not fully soluble in the solvents and formed a suspension. No reaction between the ligand and the metal precursor occurred and no product was isolated.

2.4 Crystal Structures of Complexes **6** and **7**

To further prove the synthesis and binding mode of complexes **6** and **7,** X-ray quality crystals were grown. Crystals were both achieved by slow liquid diffusion at room temperature under an inert atmosphere (N_2). Complexes were dissolved in a minimal amount of toluene and layered with *n*-pentane. The vial was loosely capped to allow solvents to evaporate.

Both complexes crystallized with P-1 symmetry with the crystals being triclinic. When analyzing the structure of complex **6**, it is consistent with what was predicted: the complex adopts the targeted square pyramidal geometry (Figure 11). The TPO ligand is bound to the tantalum center forming the base of the square pyramid while the ethoxide is directly on the z axis. The tantalum is positioned 0.451 Å above the basal plane formed by the TPO oxygen atoms (O1–O4), with O5–Ta1–O_{basal} bond angles ranging from 102.72(5) to 104.22(5)°. The Ta1–O5 vector is almost perfectly aligned with the pseudo-principal axis of rotation (formally the z-axis), with a bond angle between O5, Ta1 and the centroid formed by O1–O4 of 179.18°. When comparing complex **6** to Stryker's molybdenum (V) complex, Cp^*Mo(TPO) (containing the unsubstitued TPO ligand) similarities can be drawn. Both complexes are square pyramidal but in Stryker's case the metal center is slightly more above the xy plane, measuring from the centroid on the Cp^* moiety to Mo to oxygen the angle ranges from 103.98° – 108.03°.[103] The molybdenum on Stryker's complex is further above the xy plane, 0.563 Å in respect to the four oxygens from TPO.[103] Additionally, the four oxygens are in a more unsymmetrical orientation than compared to complex **6**. This may be due to the fact that in complex **6**, the *tert*-butyl groups

force the ligand into a more rigid conformation. When measuring the angle of Ta1 to the centroid, established by O1–O4, to O2 it is 13.6°. When comparing bond lengths on complex **6** to Stryker's Mo(V) complex, subtle differences can also be seen by looking at the oxygens bound to the metal center. The tantalum–oxygen bonds, on complex **6**, formed between the metal and the spectator ligand measure from 1.9211(12) to 1.9522(11) Å, and are shorter than that expected for a Ta–O single bond (2.09 Å).[137,138] The Ta–O bond lengths between TPO and Ta are shorter than an average Ta–O single bond possibly due to electron donation from the lone pairs on the oxygens to the tantalum metal center. This is evidence of π-interaction between the TPO ligand and tantalum. When analyzing Stryker's complex, the $Mo–O_{(1-4)}$ bond lengths range from 1.992(3) – 2.004(3) Å.[103] The bond lengths are slightly shorter than the expected Mo–O single bond length of 2.01 Å, but still significantly longer than a Mo=O double bond (1.78 Å).[137,138] This is evidence that π-interactions between TPO and molybdenum on Stryker's complex is not as significant as in complex **6**.

The bond between the metal and the apical ethoxide ligand is markedly shorter (1.8370(12) Å) than the Ta–O bonds with the spectator ligand, with only one monometallic tantalum ethoxide complex reported in the literature with a shorter Ta–O bond (1.802(14) Å).[139] Another example showed by Hayatifar et al reported a complex with ethoxide groups attached to a tantalum metal center where the bond lengths were (1.8814(18)–1.922(5)Å); significantly longer than the Ta–O bond length of the apical ethoxide moiety.[140] Most interestingly, the Ta1–O5 bond in **6** is only slightly longer than expected for a Ta=O double bond (1.83 Å).[137,138] This is evidence of double bond character, the electrons from O5 being donated into the empty dπ-orbitals on the metal. This double bond character is further supported by the Ta1–O5–C43 bond

angle of 146.29(13)°, which is particularly larger than that expected for an sp^3-hybridized oxygen. This angle indicates that the hybridization on O5 is neither pure sp^3 nor pure sp^2.

The C1–C2 bond length of 1.352(2) Å is comparable to those reported for the protonated ligands (1.328(9)–1.347(9) Å), ruling out any significant interaction between the alkene and the metal center.[101,103] This is further supported by the planarity of the alkene, with angles around C1 and C2 adding up to 359.9° and 360.0°, respectively. Complex **6** also has a C1–C2 bond length which is in agreement with what is reported for Al(III), Mg(II) and Mo(V) complexes (1.295(8)–1.347(8) Å).[102,103]

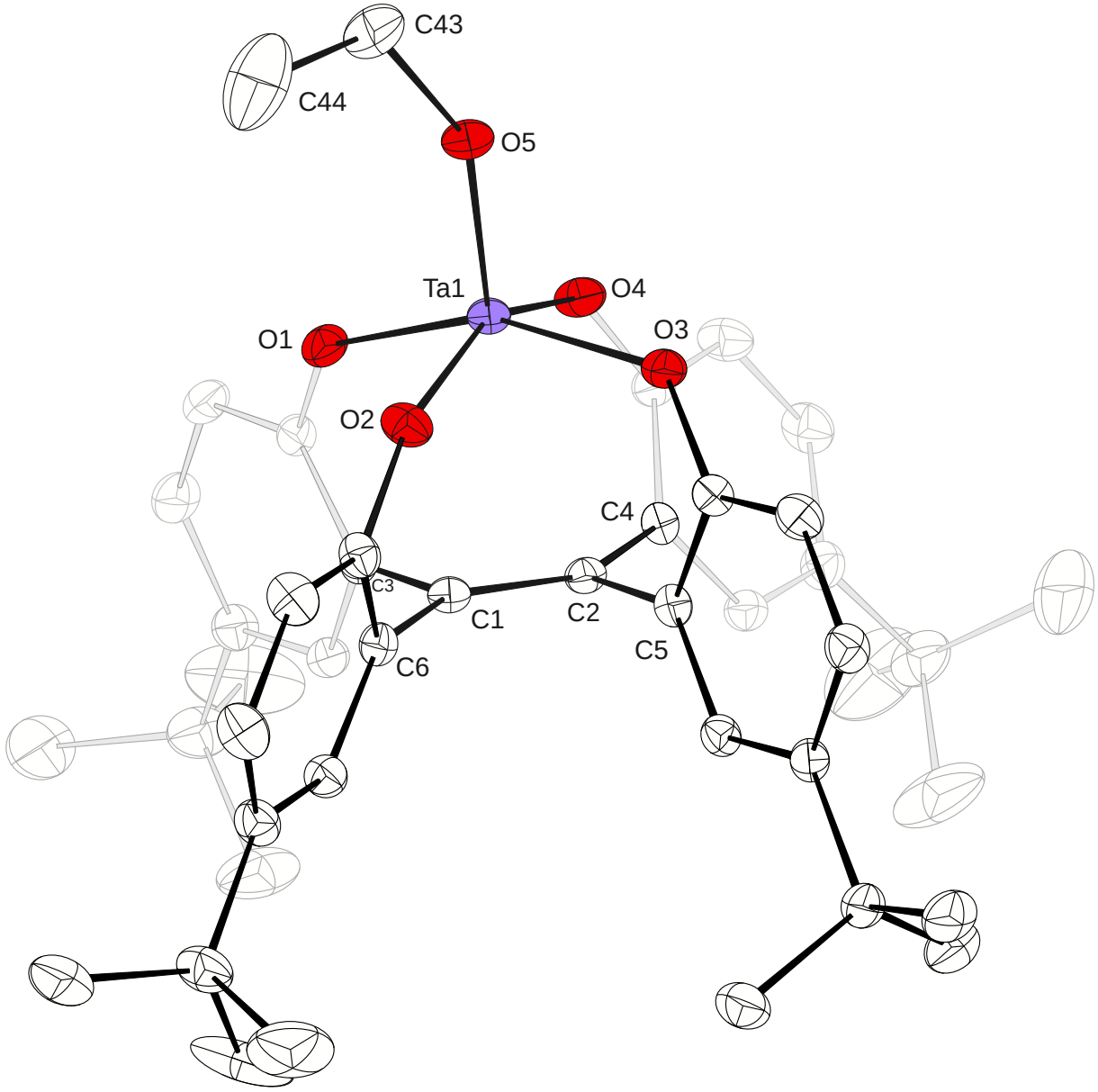

Figure 11. ORTEP diagram of complex **6** (50% probability level). Hydrogen atoms are omitted for clarity, and only major components of the disordered *tert*-butyl groups are shown.

Table 1. Selected Bond Lengths and Angles for Complexes **6** and **7**.

Selected Bond Lengths (Å)			
Complex **6**		Complex **7**	
Ta1–O1	1.9392(11)	Ta1–O1	1.964(3)
Ta1–O2	1.9211(12)	Ta1–O2	1.923(3)
Ta1–O3	1.9522(11)	Ta1–O3	1.979(3)
Ta1–O4	1.9396(12)	Ta1–O4	1.918(3)
Ta1–O5	1.8370(12)	Ta1–N1	1.922(3)
C1–C2	1.352(2)	C1–C2	1.332(6)
O5–C43	1.431(2)	N1–C43	1.454(6)
		N1–C44	1.464(6)
Selected Bond Angles (deg)			
Complex **6**		Complex **7**	
O5–Ta1–O1	102.74(5)	N1–Ta1–O1	102.22(14)
O5–Ta1–O2	104.22(5)	N1–Ta1–O2	106.18(14)
O5–Ta1–O3	102.72(5)	N1–Ta1–O3	103.96(14)
O5–Ta1–O4	104.19(5)	N1–Ta1–O4	103.06(15)
Ta1–O5–C43	146.29(13)	Ta1–N1–C43	122.8(3)
		Ta1–N1–C44	124.5(3)
		C43–N1–C44	112.7(4)
Selected Atom Distances (Å)			
Complex **6**		Complex **7**	
Ta1–C1	2.891	Ta1–C1	2.893
Ta1–C2	2.857	Ta1–C2	2.859

The structure of complex **7** is very similar to that of **6**. Complex **7** also adopts a square pyramidal geometry (Figure 12). The tantalum is 0.466 Å away from the basal plane established by the TPO oxygen atoms (O1–O4), with N1–Ta1–O_{basal} bond angles ranging from 102.2(1) to 106.2(1)°. The angle between N2, Ta1 and the centroid formed by O1–O4 measures 178.46°, only slightly off from 180°. This data is also consistent with what can be found in the literature of alkoxotantalum chemistry containing calixarenes, where the oxygens are bound to the tantalum metal center that is above the xy plane.[141] As previously observed in complex **6**, significant double bond character between the metal and the apical ligand is also demonstrated in the amido complex **7**. Firstly, the Ta1–N1 bond measures 1.922(3) Å. This is only slightly longer than the average Ta=N double bond (1.86 Å) but significantly shorter than the average Ta–N single bond (2.17 Å).[137,138] Further proof that there is double bond character between the metal and apical amido ligand is shown by the geometry around N1. The geometry around N1 is trigonal planar, with C44, C43, N1, Ta1 all in the same plane, as oppose to the expected tetrahedral orientation. There are three bonds to N1 as well as a lone pair of electrons which should correspond to a tetrahedral geometry, T_d, around N1. All three angles around the central atom add up to exactly 360.0°, with the C43–N1–C44 angle significantly smaller than the Ta1–N1–C43 and Ta1–N1–C44 angles. This means that the lone pair on the nitrogen is being donated to the tantalum metal center creating a π-bond, as anticipated. Interestingly, when looking into the literature of dimethylamido groups bound to tantalum, some complexes exhibit a similar trigonal planar orientation.[142,143] Bercaw made similar observations while studying π-interactions in tantalum amido complexes supported by a pyridine-linked bis(phenolate) pincer ligand. Their study showed that the tantalum–amide π-bond (as short as 1.9708(22) Å) is much stronger than the tantalum–phenoxide π-bond.[142] Only one tantalum dimethylamide complex has been reported

in the literature with a shorter Ta–N bond, further illustrating the excellent π-interaction between the metal and the apical ligand.[144]

The angle between the best planes formed by Ta1, N1, C43 and C44, and by Ta1, N1, O2 and O4 is 23.55°. The orientation of the NMe_2 group in the solid state leads to the two distinct sets of tantalum–oxygen bonds, with Ta1–O1 and Ta1–O3 markedly longer than Ta1–O2 and Ta1–O4 (Table 1). VT NMR spectroscopy was performed on complex **7** to determine if the energy barrier of rotation around the Ta1–N1 bond is large enough to be observed in the ^1H NMR spectrum. The experiment was conducted by dissolving complex **7** in anhydrous CD_2Cl_2, which was then added to an NMR tube and sealed. ^1H NMR spectra were obtained, first at room temperature (20°C), then by lowering 10°C intervals at a time until -80°C was attained. A total of 10 ^1H NMR spectra were acquired. If the energy of rotation was large enough, then rotation around Ta1–N1 bond would stop and two sets of proton resonances for the phenoxide rings would be observed. This was not the case for the Ta1–N1 bond on complex **7**. All the ^1H NMR spectra collected were nearly identical, with minor resonance broadening at low temperatures, indicating the energy barrier of rotation about the Ta1–N1 bond must be too small.

The C1–C2 bond length (1.332(6) Å) in complex **7** is slightly shorter than that observed in **6**, but in line with those reported in the literature.[101-103] Similar to that observed in complex **6**, the angles around C1 and C2 add up to 360.0° in both cases, indicative of no significant interactions of the alkene group with tantalum. This is further supported by the fact that the Ta1–C1 and Ta1–C2 atom distances are quite substantial, being 2.893 and 2.859 Å. Complexes found in the CSD database list tantalum–carbon distances all are significantly shorter than the distances in either complex **6** or **7**. The carbons on aliphatic alkenes to tantalum metal centers range from 2.3 Å to 2.5 Å. For example A.Nakamura et al. reported the synthesis of mononuclear tantalum

diene complexes, where the tantalum-carbon atom distances ranged from 2.398 to 2.324 Å.[145] The Ta1–C1/C2 distances are additionally much longer than any Ta–C bond. An average Ta–C single bond is 2.21 Å.[146] Selected bond lengths, angles and atom distances are listed in Table 1.

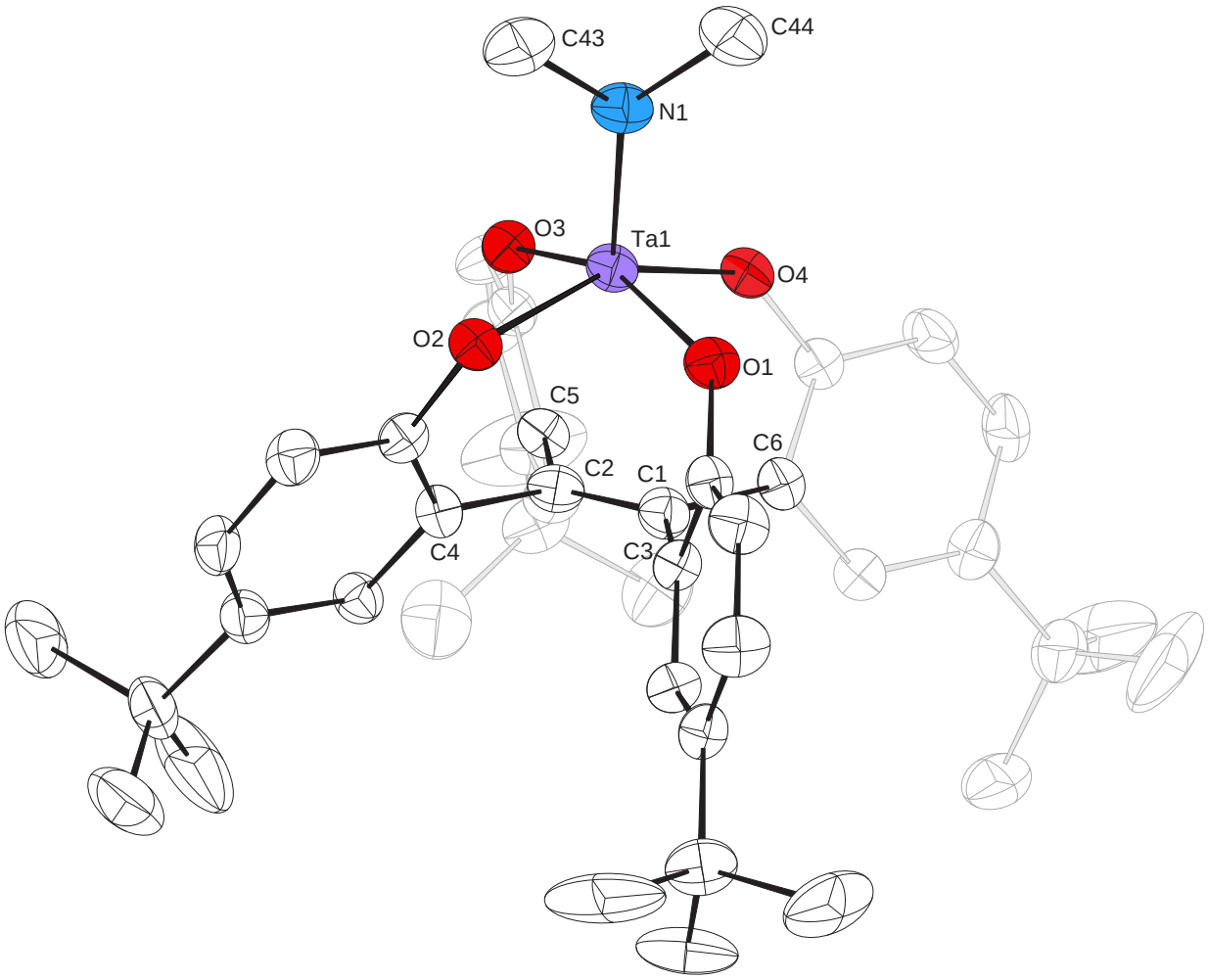

Figure 12. ORTEP diagram of complex **7** (50% probability level). Hydrogen atoms omitted for clarity, and only major components of the disordered *tert*-butyl groups are shown.

2.5 Activity Studies of Complexes **6** and **7**

Upon coordination of compound **5b** to tantalum, many reactivity studies were completed to see if the complexes had any activities with small molecules. Alkylation studies were completed mainly on complex **6.** Several alkylating agents were used such as diethylzinc, diethylaluminum chloride, triethylaluminum, triisobutylaluminum and trimethylaluminum. Preliminary experiments with triisobutylaluminum and trimethylaluminum showed encouraging results. In treating complex **6** with 2 equivalents of trimethylaluminum or triisobutylaluminum in C_6D_6, the corresponding alkyl complexes could be identified from the ^{1}H NMR spectra. Reactions were performed on small scales first, 10 to 15 mg, before scaling them up to 100 mg. The ^{1}H NMR spectrum of the $AlMe_3$ shows, over time, the disappearance of the ethoxide resonances and the appearance of a resonance at 1.63 ppm, assigned to the protons on the methyl group in complex **8** (refer to section **6.0** NMR spectra). All three resonances in the aromatic region were also slightly shifted from that of complex **6**. Treating complex **6** with 2 equivalents of trimethylaluminum in toluene followed by washing with cold *n*-pentane, to purify, afforded complex **8** (Scheme 8)**.** In the $^{13}C\{^1H\}$ NMR spectrum, 10 peaks could be seen in the spectrum, which correspond to 10 different carbons present in the complex. Results from microcombustion analysis are consistent with the calculated value of complex **8**; this further supports the structure and its purity. Efforts were taken to obtain crystals of X-ray quality but these attempts have not yet been successful.

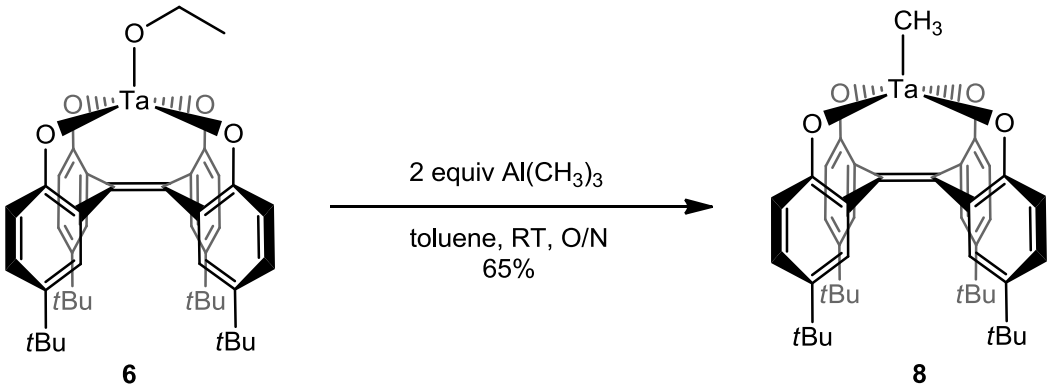

Scheme 8. Alkylation of Complex **6** to Form Complex **8**

The catalytic activity of complex **6** for ethylene polymerization was tested (1 atm of C_2H_4, room temperature). The first study was completed using 500 equivalents of triisobutylaluminum as the cocatalyst and a second study was performed using 1000 equivalents of methylaluminoxane (MAO) as the cocatalyst. The cocatalyst for the experiments is essential, since its role is to alkylate (Scheme 9) and to react with trace amounts of water which may be present in the solvent.[1] In the system, there must also be a vacant coordination site to facilitate alkyl migration.[1] The trials were run for 24 h and neither experiment produced any polyethylene nor was there any uptake of ethylene. The solution remained homogenous after both trials; there was no observation of anything solid within the solution. Additionally, there was no reduced pressure in either flask after the 24 h time period, indicting no uptake of ethylene gas. The cocatalyst may not have removed the ethoxide group, replacing it with an alkyl group. The Ta–O bond did not facilitate polymerization. One hypothesis would be that the bond was too strong to be broken. Also there is no coordinatively unsaturated, cationic metal center for the olefin to coordinate.[1] In the second step of the polymerization cycle, there must be a vacant site so that the double bond of the olefin can coordinate to the metal. The coordination of an ethylene molecule

by approaching from the xy plane would be very difficult. There are 4 oxygens that surround tantalum on the xy plane.

Additionally, the catalytic activity of complex **8** for ethylene polymerization was tested (1 atm of C_2H_4, room temperature). Polymerization trials were completed by exposing complex **8** to ethylene gas for 10 min as well as 24h. No cocatalyst was used in either case since complex **8** was already alkylated with a methyl group. Upon completing these experiments, no polymer was produced and no ethylene uptake was observed; therefore there must not have been any formation of oligomers either.

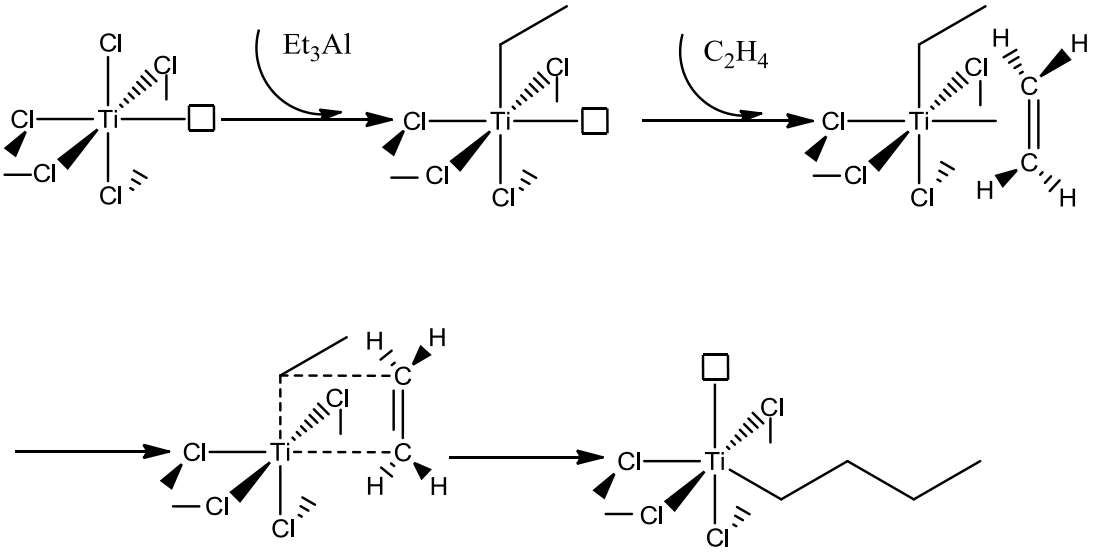

Scheme 9. Alkene Polymerization Employing Triethylaluminum.[1]

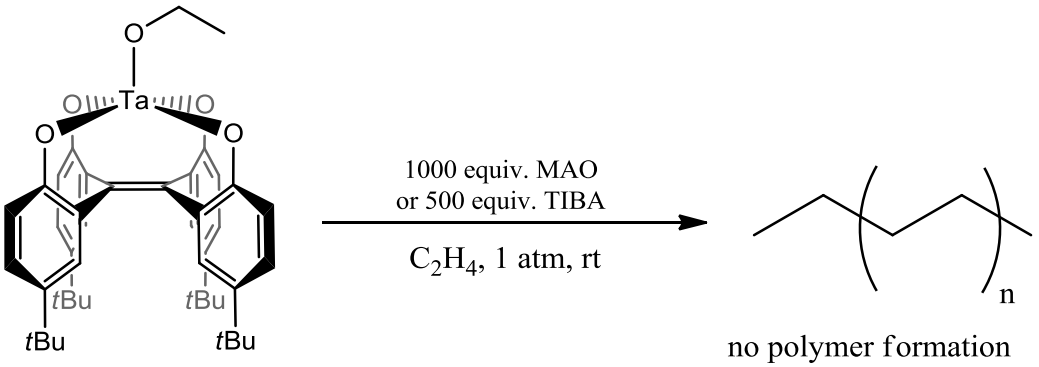

Scheme 10. Polymerization Study with Complex **6**.

Several other activity studies were performed on the tantalum complexes (Scheme 11). Exposing complex **8** to 1 equivalent of ethanol gave complex **6**. In addition, complex **7** can be synthesized by the reaction of complex **8** with 1 equivalent of dimethylamine in THF with heating to 60°C. Adding 2 equivalents of $AlMe_3$ to a solution of **8** and leaving to react overnight afforded a 50/50 mixture of complex **7** and **8**; no additional equivalents of $AlMe_3$ were added to complex **8**. Interestingly, treating complex **7** with 1 equivalent of ethanol leads directly back to complex **6**. Addition of dimethylamine to complex **6,** to obtain complex **7**, led to no reaction, even after heating at 70°C.

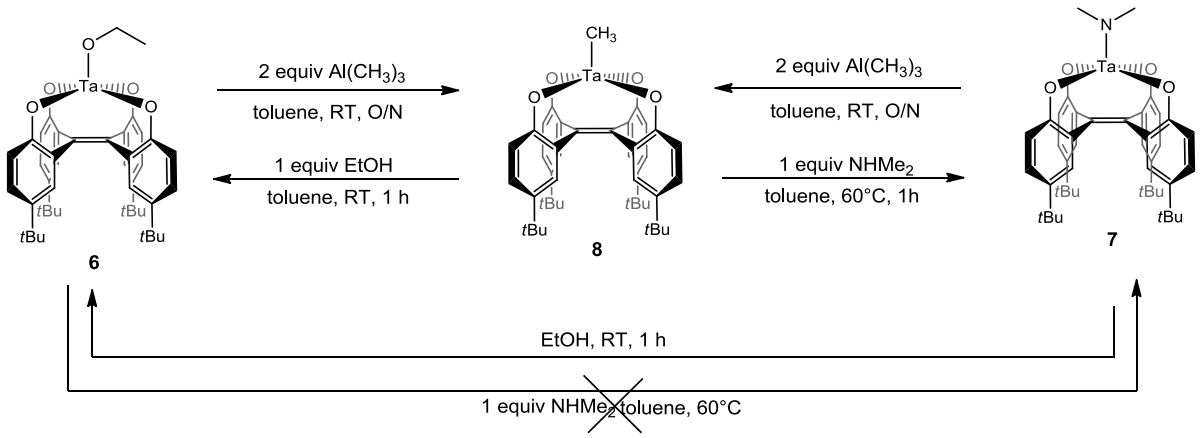

Scheme 11. Reactivity Studies of Complexes **6**, **7**, and **8**.

Several other activity studies were performed on complexes **6**, **7**, and **8** to gain more insight into the reactivity of the apical ligand. Treating complex **6** with excess methanol leads to what seemed to be the formation of a complex with a methoxide in the axial coordination site, complex **9** (Scheme 12). In the ^{1}H NMR spectrum, the ethoxide resonances from complex **6** were replaced by a new singlet. Additionally, ethanol resonances were observed, indicating the release of ethanol from the complex. Working-up the reaction by drying the solution in vacuo and washing the solids with pentane did not give a pure complex. Isolation of the product was not possible. With the knowledge of methanol being able to react with complex **6,** attempting synthesis of (TPO)TaX (X = $^{-}$OR) derivatives with stronger acids were conducted (Scheme 12). Adding phenol and benzoic acid to complex **6** was done in hopes that conversion would occur to the desired (TPO)TaX product. Unfortunately, both reactions did not proceed. Reactions were also attempted by adding excess benzoic acid or phenol (2 to 4 equiv.) or by heating to 70°C. No conversion was seen in either case, this could be because methanol is a much smaller molecule than either benzoic acid or phenol. It was thought that employing a reagent with a lower pK_a would be more desirable, but this was not the case. It seems as though sterics are favoured in the reactivity of complex **6**, not the pK_a of the substrate as previously hypothesized.

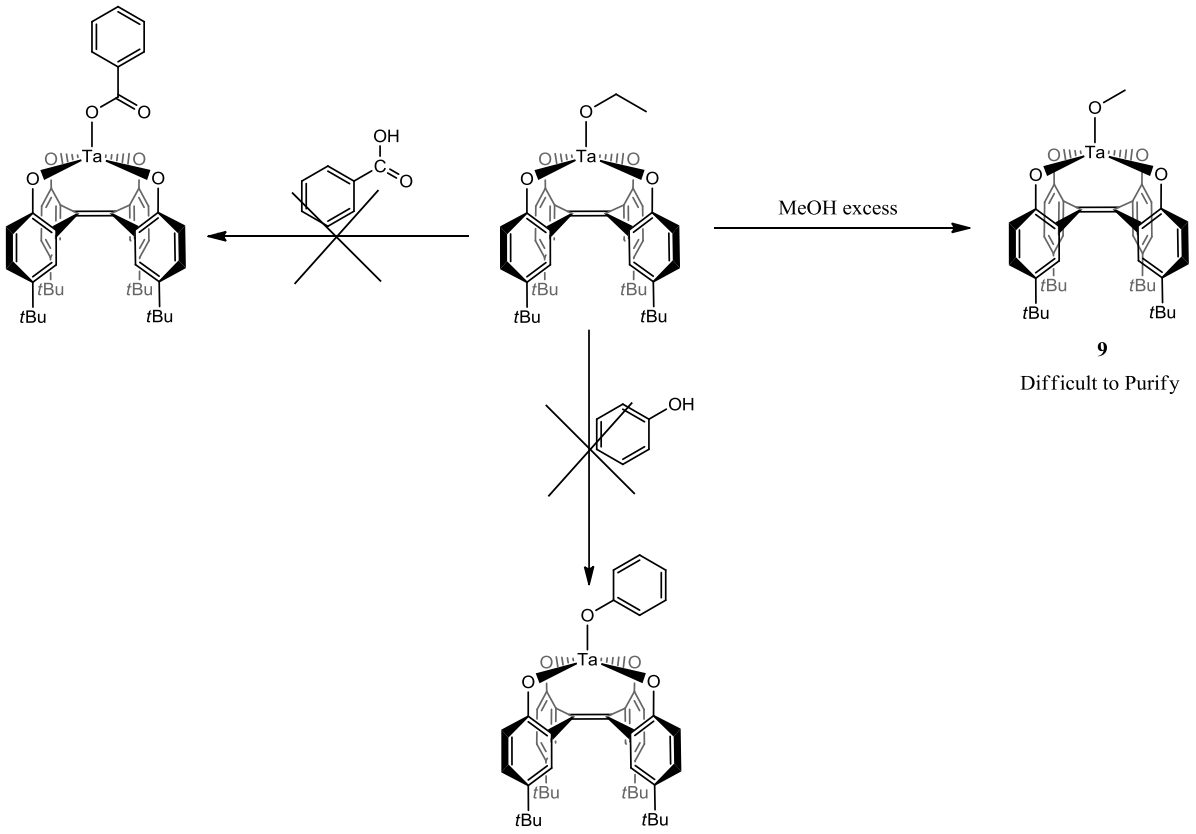

Scheme 12. Reactivity Studies of Complexes **6**, with Methanol, Phenol and Benzoic Acid

Reactions with weak acids mentioned above seemed quite challenging to accomplish. Other weak acids were also evaluated to gain insight into the reactivity of the apical ligand of complex **6**, **7**, or **8**. One such reaction was the reaction of cyclopentadiene, a weak acid with a pK_a of 16, with both complex **6** and **8**. Upon addition of cyclopentadiene to either complex **6** or **8** in benzene-d_6 no reaction occurred, as monitored by ^{1}H NMR spectroscopy. The solutions were left to react for 24 h, after which they were heated for several hours at 70°C. Even after heating for several hours the reaction did not proceed to completion. Both complexes seemed inert to cyclopentadiene even at elevated temperatures. ^{1}H NMR spectroscopy revealed no reactivity, and cyclopentadiene did not dimerize to dicyclopentadiene.

Additional reactivity studies with complexes **6**, **7**, and **8** were completed, one of which was to determine if the complexes would accommodate coordination from sigma donors. All three complexes were mixed with up to 4 equivalents of THF and left to react for several hours. Monitoring the reaction by using ^{1}H NMR spectroscopy showed no change in either the complex resonances nor the THF resonances, indicating no binding of THF had taken place.

One of the most challenging tasks in this research project was to replace the ethoxide, dimethylamido or methyl group on either complex with a halide (chloride or bromide) or triflate. (Scheme 13). This was attempted for two reasons: (1) a halide or pseudohalide complex would be a good precursor to other reactions, (2) implementing the chloride or bromide ligands may render the complex more crystalline. Using HCl in dioxane and HCl in ether were attempted to install a chloride group, but the experiments failed to produce the desired results. The reactions were completed on a small scale (10 to 15 mg of complex) by the addition of one equivalent of HCl (in dioxane or ether) to either **6**, **7**, or **8** in benzene-d_6. The complexes did not react as desired and the target complexes did not form under such conditions but led to mixtures of uncharacterized compounds. Competing protonation of the TPO ligand by these strong acids possibly explains the inability to cleanly prepare the tantalum chloride complex using this approach making the ^{1}H NMR difficult to analyze because of the mixtures of products. In attempts to circumvent this decomposition, the same reactions were performed at low temperatures (-42°C). These reactions were more controlled but still led to decomposition upon work-up, drying in vacuo and washing the solids with *n*-pentane.

Additionally, acetyl chloride, acetyl bromide, and benzoyl chloride were used as halide sources. It was hoped that the reactant, either acetyl chloride, acetyl bromide, or benzoyl chloride, would react with the ligand on apical position. The reagent would exchange the

ethoxide, dimethylamido or methyl ligand for a halide forming a tantalum chloride species as the product. The results were also not as anticipated and a pure complex could not be isolated. Reactions were completed using complexes **6**, **7**, and **8** on NMR tube scales, 10 to 15 mg of complex with the addition of the halide source. The reactions were then monitored over a period of several hours. The ^{1}H NMR spectra were unchanged showing the resonances from the complex and the reactant without any signs of reaction. Even at 70°C, for a period of several hours did not lead to any reactions.

In addition to the chloride sources mentioned, the weak acid triethylammonium chloride was employed as a chloride source. Addition of triethylammonium chloride to complex **6**, **7**, or **8** did not give clean conversion to the corresponding tantalum chloride complex, when monitored over a period of several hours, leading to uncharacterizable species.

Similarly, using triflic acid to install a triflate group did not lead to any isolatable products as the reactions were uncontrolled, at room temperature or when cooled to -42°C. The ^{1}H NMR spectra showed many resonances in the aromatic and aliphatic regions of the spectrum. Finally, after attempting different reagents without success, using chlorotrimethylsilane as a chloride source was used (Scheme 14). When treating complex **6** with chlorotrimethylsilane in a 5 to 10-fold excess, the resonances in the ^{1}H NMR spectrum corresponding to complex **6** were shown to be diminishing while new resonances could be seen with appropriate integrations. The ethoxide moiety would be attached to the silane, forming ethoxysilane. If the chloride moiety were to replace the ethoxide in the apical position then the resonances in the ^{1}H NMR spectrum would change. After reacting for more than 24 h, the reaction did not proceed any further, as seen in the ^{1}H NMR spectrum. For this reason, more chlorotrimethylsilane was added to shift the equilibrium of the reaction to the products. Performing the reaction using a 25-fold excess of

chlolotrimethylsilane to complex **6** did not afford total conversion. In further attempts to force the reaction to completion, chlolotrimethylsilane was used as the solvent and the reagent. This procedure did not produce the product: the ^{1}H NMR showed an uncontrolled reaction, and attempting to isolate a pure product was unsuccessful.

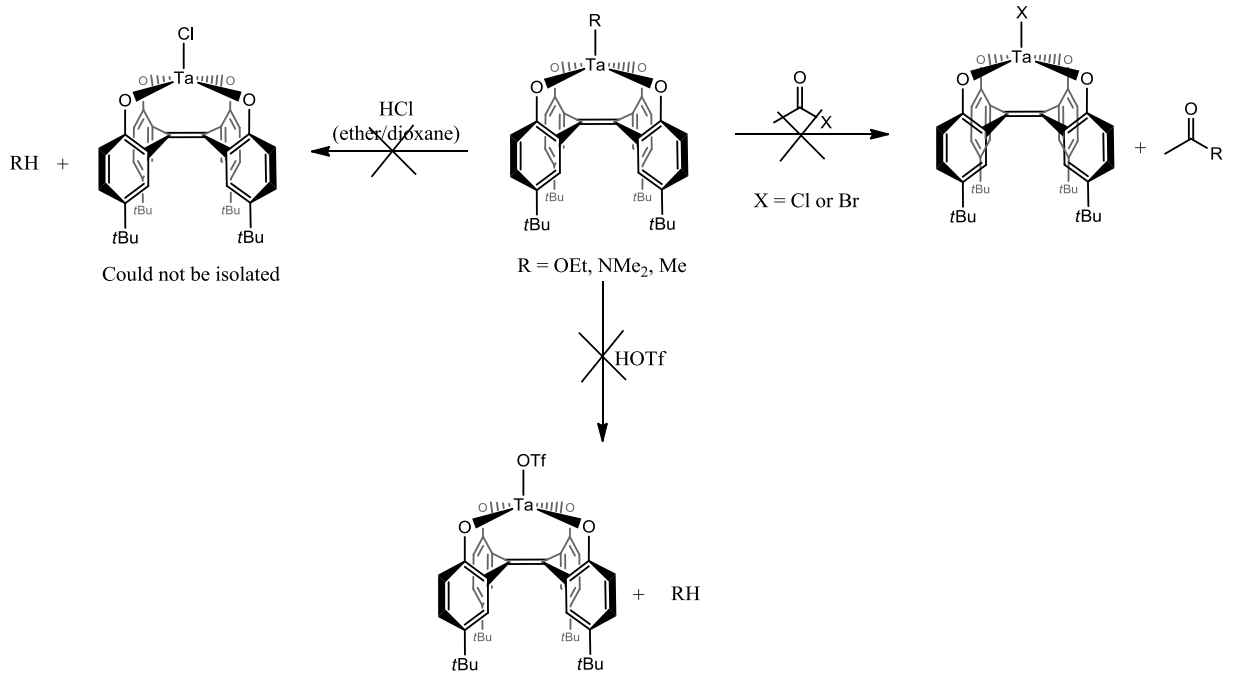

Scheme 13. Reactivity Studies of **6**, **7**, and **8** with HCl, Acetyl Chloride/Bromide and Triflic Acid.

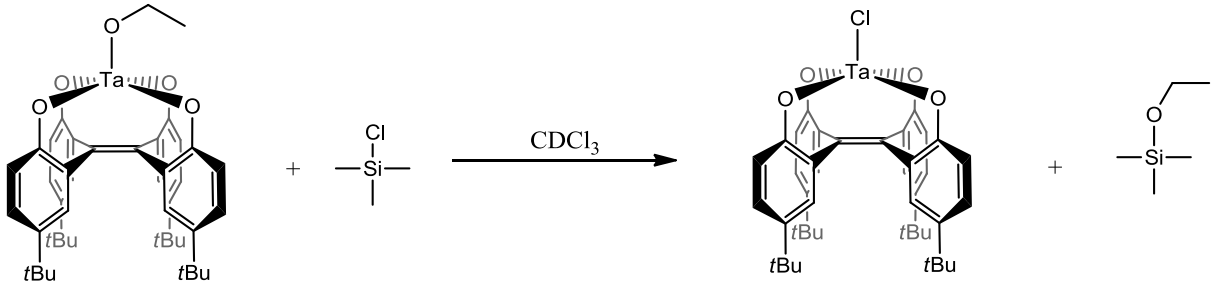

Scheme 14. Reaction of Complex **6** with Chlorotrimethylsilane.

In addition to using chlorotrimethylsilane, trimethylsilyl trifluoromethanesulfonate was used to install a triflate group in the apical position of the (TPO)TaX complex. NMR-scale reactions were completed with complex **6**, 10 to 15 mg, in benzene-d_6, with a 2-fold excess of silyltriflate. The solutions were monitored over time by ^{1}H NMR. The reaction proceeded slowly over time, but then became uncontrolled as the reaction progressed. When a ten-fold excess of silyltriflate was added, the reaction became uncontrolled quite rapidly. When analyzing the ^{1}H NMR spectrum, the complex decomposed, because of the many resonances in the aromatic and aliphatic regions of the ^{1}H NMR spectrum.

Continuing with reactivity studies, on the TPO complexes, reactions with a hydride source was also attempted. Unfortunately, the reactivity toward triethylsilane and diphenylsilane were nonexistent, showing no reaction even after heating at 70°C in benzene-d_6 (Scheme 15). Using H_2 as a hydride source was also attempted. Reactions were carried out in J. Young NMR tubes by dissolving the complex in a deuterated solvent (benzene-d_6 or $CDCl_3$) and exposing it to one atmosphere of H_2. No reactivity was observed by ^{1}H NMR spectroscopy. These results were quite surprising since one would expect hydrogen to react at the axial coordination site, removing the ligand and replacing with a hydride. Fryzuk et al. have shown that the $[(PhP(CH_2SiMe_2NPh)_2)TaMe_3]$ species undergoes hydrogenolysis upon exposure to 1-4 atm of dihydrogen to produce the purple, dinuclear, diamagnetic Ta(IV) hydride $[(PhP(CH_2SiMe_2NPh)_2)Ta(\mu\text{-}H)_2]_2$ along with the elimination of methane gas.[147] Whereby the methyl groups can easy be replaced with hydride ligands, forming a bridging species. Furthermore, exposing the bridging species to N_2 gas resulted in the loss of H_2 to form a dinitrogen complex $[(PhP(CH_2SiMe_2NPh)_2))TaH]_2((\mu\text{-}\eta^1\text{-}\eta^2\text{-}N_2)$.

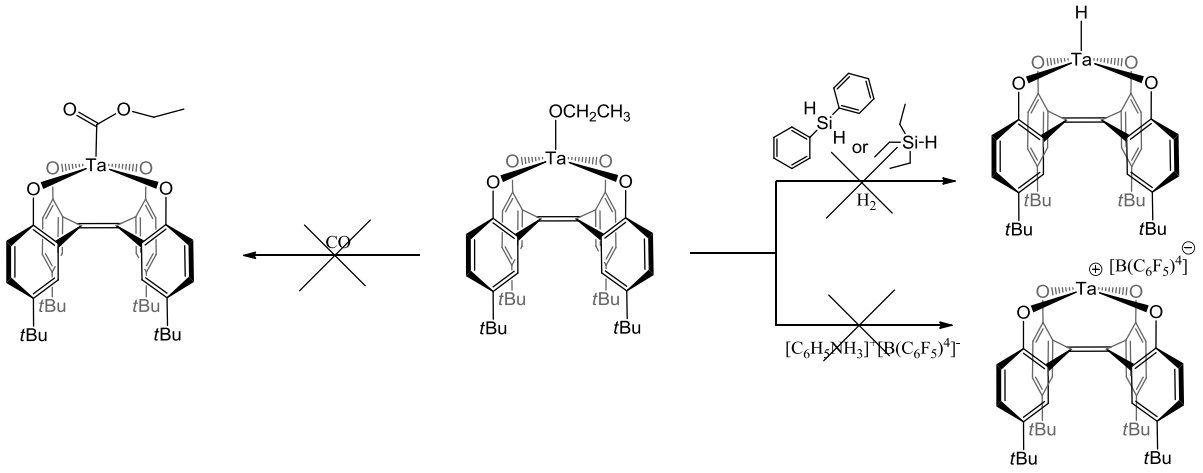

Scheme 15. Hydride, CO and $[C_6H_5NH_3]$ $[B(C_6F_5)_4]$ Reactivity Studies with Complex **6**.

Another important reactivity study was conducted with anilinium tetrakis(pentafluorophenyl)borate ($C_6H_5NH_3^+$ $[B(C_6F_5)_4]^-$) on complex **6**. The $[B(C_6F_5)_4]^-$ anion is a non-coordinating and non-nucleophile anion, and would serve as a counterion to the tantalum complex.[148] Therefore tantalum would have a coordination sphere that is unsaturated. The goal was to treat $[C_6H_5NH_3][B(C_6F_5)_4]$ with complex **6** to remove the ethoxide and have a free coordination site, [(TPO)Ta][$B(C_6F_5)_4$] (Scheme 15). Unfortunately, this reaction failed despite several attempts. Further attempts to create a cationic species by displacing apical ligands in **6**, **7**, and **8** with weakly coordinating donors were undertaken. Ammonium hexafluorophosphate was used in hopes that the proton from ammonium would react with the ethoxide in **6** or methyl in **8** liberating ethanol or methane. This would then create a cationic tantalum(V) species with hexafluorophosphate as the counterion. Attempting the reactions in deutrated NMR solvents did not succeed as ammonium hexafluorophosphate was neither soluble in benzene-d_6 nor $CDCl_3$. Therefore, the complexes were dissolved in THF along with ammonium hexafluorophosphate and stirred for 2 hours. Upon work-up, removing the volatiles in vacuo, ^{1}H NMR spectra were recorded. The reaction performed with complex **6** was

uncontrolled as the spectra were extremely disordered. The related reaction with complex **7** showed no reactivity towards ammonium hexafluorophosphate and complex **7** was recovered.

Furthermore, reactivity studies were completed by attempting to synthesize complexes containing tantalum-nitrogen bonds, in addition to complex **7**. Complexes **6** and **8** were reacted with different types of amines, including *tert*-butylamine, *n*-butylamine and hydrazine (Scheme 16). Complex **6** did not react with hydrazine at all but, when exposed to *n*-butylamine, reacted uncontrollably. In contrast, while complex **8** reacted uncontrollably with hydrazine, it did not react at all with either *tert*-butylamine or *n*-butylamine. The uncontrolled reaction of hydrazine with complex **8** may be due to the fact that hydrazine has two reactive ends, leading to bridging to two tantalum metal centers. Additionally, when comparing complex **6** to complex **8,** the ethoxide is relatively bulkier, possibly explaining why hydrazine showed no reaction in the presence of complex **6**.

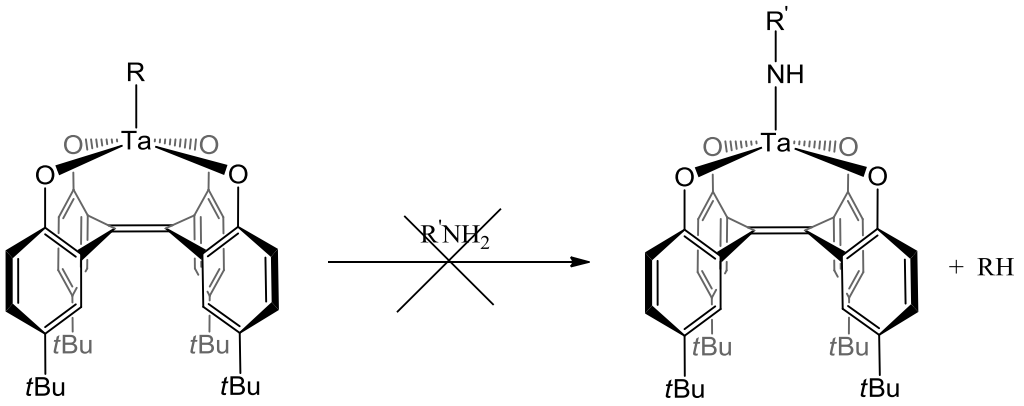

R = OEt or Me.
R'NH_2 = *tert*-butylamine, *n*-butylamine, hydrazine.

Scheme 16. Reactions of Amines with Complexes **6** and **8**.

Reactions were attempted to see if the complexes could react with the σ-donor/π-accepter isocyanide. Addition of *tert*-butyl- and 2,6-xylylisocyanide to complexes **6** and **8** in benzene-d_6 led to no reaction and there was no spectroscopic evidence for coordination of the isocyanide, even after several days (Scheme 17). These results further imply that there must be coordination of the substrate to the metal for any reaction with the apical ligand to take place. The results also suggest a relatively electron-rich metal center, a result of donation of π-electron density, both from the TPO ligand and from the apical ligand. CO studies on **6** were completed but also showed unfavourable results with the crude ^{1}H NMR spectra being uninterpretable (Scheme 16).

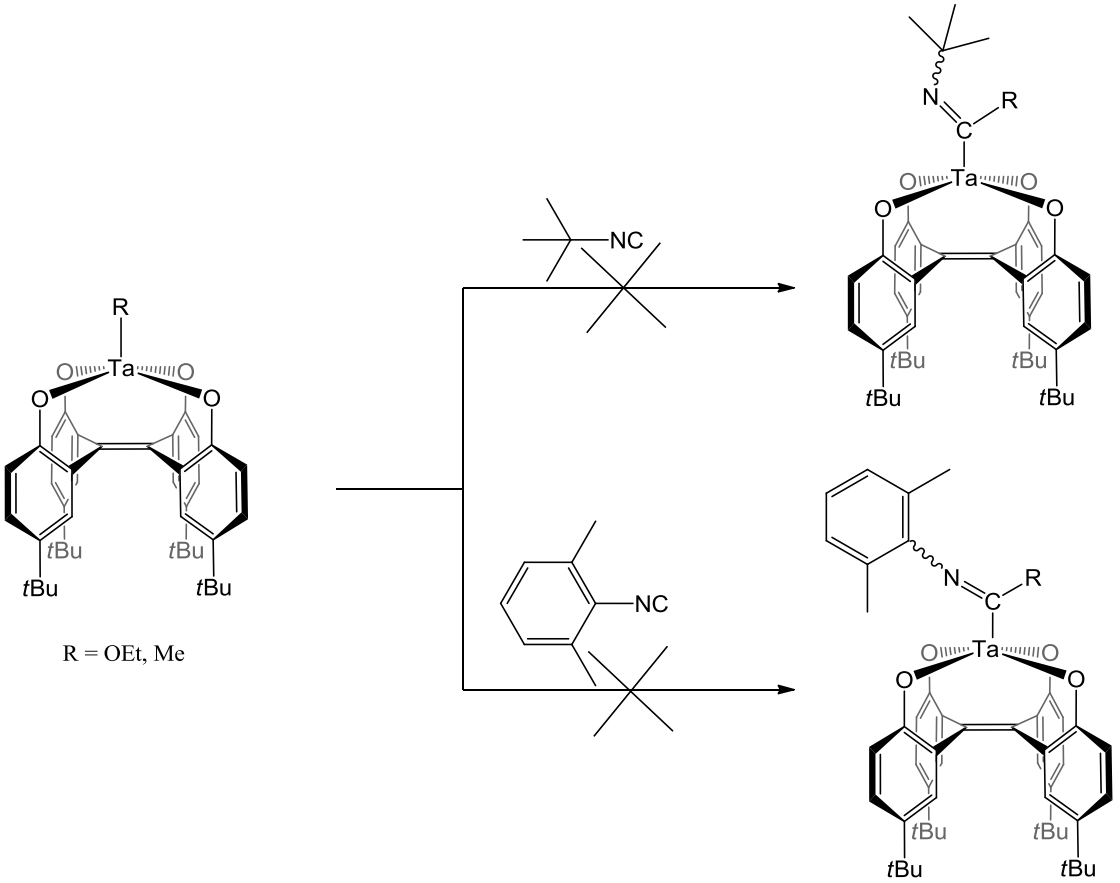

Scheme 17. Reactions of Isocyanides with TPO Complexes **6** and **8**.

To further explore and gain insight into the reactivity of the apical ligand in our TPO complexes, reactivity studies were completed using chelating weak acids. The reactants employed were acetylacetone (acacH), hexafluoroacetylacetone (hfacH), and hexamethylacetylacetone (MacacH). The acetylacetones are weak acids with pK_a values of 13.3 (in DMSO) for acetylacetone and a pK_a of 4.6 for hexafluoroacetylacetone.[149,150] Hexamethylacetylacetone is also a weak acid, similar acidic strength to acacH, but has significantly more steric bulk. Complexes **6**, **7**, and **8** were reacted with three different acetylacetones to assess the difference of reactivity of each..

Prior to reacting complex **6** with acacH, ^{1}H NMR spectra of the two were acquired separately in benzene-d_6, this was to understand the relative resonances of each reactant. All the experiments were conducted on small scales, dissolving 10-15 mg of complex in benzene-d_6 then adding 1 equivalent of the reactant and monitoring by ^{1}H NMR spectroscopy over time. When the reagents were added to one another it was noted that a reaction was progressing. Interestingly, there were no resonances corresponding to ethanol, it was predicted that acacH would protonate the ethoxide moiety liberating ethanol and bind the acac ligand. Instead it seemed as though the acac ligand bound to the metal center without releasing ethanol (Scheme 18). The resonances corresponding to acac had now been shifted, relative to free acacH. Additionally, there were now several more resonances in the aromatic ^{1}H NMR spectrum, protonation of an oxygen on the TPO ligand would render it unsymmetrical thus accounting for the many resonances in that region. It was hypothesized that the acac ligand was bound onto the tantalum metal center uncoordinating a phenoxide rather than the ethoxide moiety. Attempts to isolate a complex were unsuccessful. Heating the solution to 70°C to force the reaction to completion by attempting to bind the acac in a bidentate fashion and liberate ethanol led to an

uncontrolled reaction. The same reaction procedure was employed for both hfacH and MacacH with complex **6**, as with acacH. Unfortunately, the reactions did not yield an isolated complex as they were also uncontrolled.

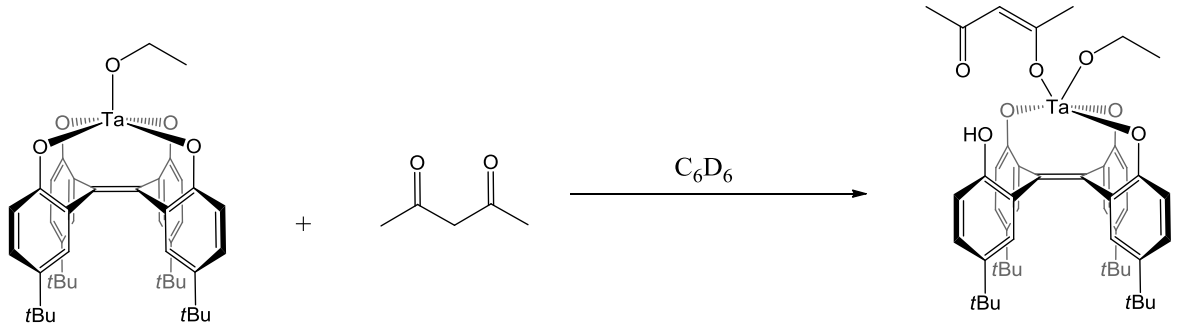

Scheme 18. Predicted Coordination of acacH to Complex **6**.

Complex **7** was also reacted with acacH in a 1:1 ratio but reacted more uncontrollably than complex **6**, and no species could be isolated (Scheme 19). The addition of one equivalent of acacH to complex **7** led to an uncontrolled reaction almost immediately. The ^{1}H NMR spectrum was very cluttered, with many resonances in the aromatic and aliphatic regions making it very difficult to interpret. Since neither complex **6** nor **7** reacted cleanly with acacH, the methyl complex **8** was also employed in the attempt to synthesize a new complex. Treating complex **8** with 1 equivalent of acacH showed slow reactivity. The reaction seemed to be progressing towards the desired product since there was formation of methane gas as well as the slow disappearance of the methyl resonance in **8**. The reaction was left to proceed over several hours though this did not yield the desired product and no product could be isolated. Initially, it seemed as though the reaction was proceeding favourably, as seen by ^{1}H NMR spectroscopy. Regrettably, after several hours the reaction became uncontrolled and no species could be characterized.

In an attempt to circumvent the problem of the complex decomposing over several hours, 5 equivalents of acacH were used. This was an attempt to force the reaction to completion, by adding excess acacH to drive the reaction to the products. The target complex could then be worked up quickly by simply drying in vacuo. The reaction did not proceed as predicted. Analysis with ^{1}H NMR spectroscopy after 30 min showed complete decomposition of the complex. The excess acacH possibly reacted with the phenoxide groups as well as the methyl moiety, completely destroying the species. When using hfacH as a stronger acid, it was hoped that it would react more cleanly with complex **8.** Regrettably, as with complex **6,** the reaction was just as uncontrolled. Additionally, MacacH was used as a reactant with complex **8**, but did not lead to a species being formed; no reaction occurred.

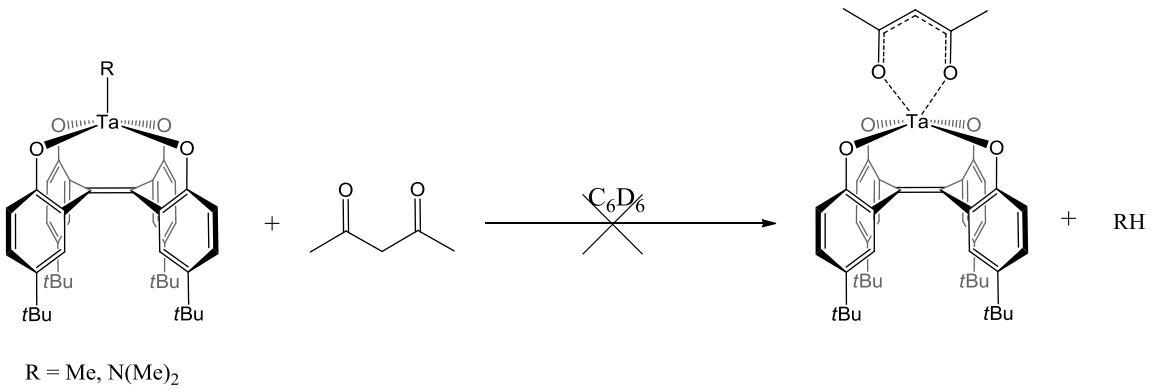

R = Me, $N(Me)_2$

Scheme 19. Attempted Synthesis of Acetylacetonate TPO Complex.

Lastly, complex **6** and **7** were reacted with 1 equivalent of acetic anhydride in benzene-d_6. Complex **6** showed no reactivity towards acetic anhydride, over several hours at 70°C, as was seen in the ^{1}H NMR spectra. In contrast, complex **7** reacted slowly to what seemed to be the predicted product (Scheme 20). The original protons from the phenoxide ring on complex **7** diminished and new resonances appeared in the aromatic region. Moreover, the resonance corresponding to the *tert*-butyl group diminished and new resonance slowly began to appear in

the aliphatic region of the spectrum. However, over time the reaction became uncontrolled, as observed by ^{1}H NMR spectroscopy. As the reaction further progressed the spectra became very difficult to analyze as there were far more peaks than predicted both in the aliphatic and aromatic regions. No product could therefore be isolated from the reaction.

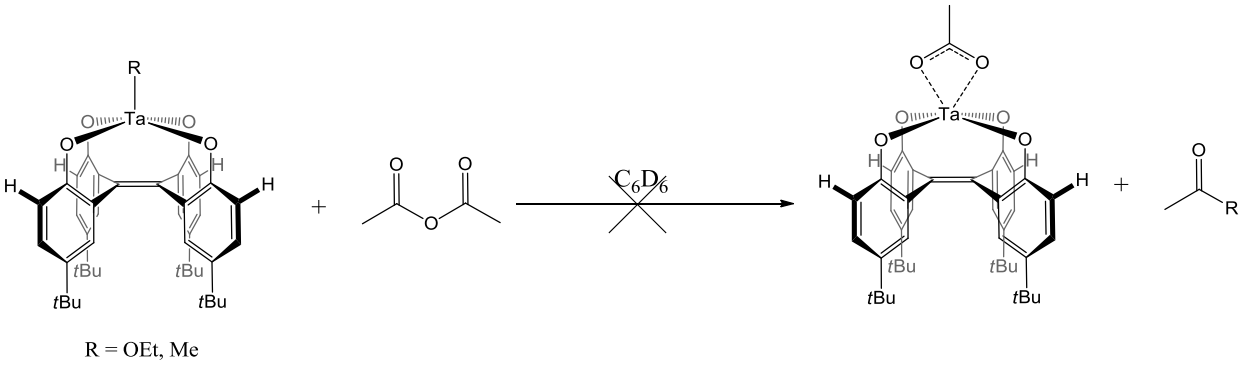

Scheme 20. Attempted Synthesis of Acetate TPO Complex.

2.6 Density Functional Theory Calculations

Complex **7** was analyzed by using the B3LYP/LANL2DZ level of theory for all the atoms in the complex. LANL2DZ was chosen as the basis set since it applies to the elements H, Li-La and Hf-Bi. All the elements in complex **7** are within that range. Energy calculations on the geometry optimized and unoptimized structure, using the atom coordinates of the solid state structure **7**, were completed. Energy minimized calculations, optimized, were completed so that the net inter-atomic force on each atom in space is close to zero. This would therefore give a better representation of the molecule without any other intermolecular forces acting upon it.

This DFT study was conducted to further provide evidence of π-interactions between Ta1 and the apical ligand N1, as well as π-interactions between Ta1 and O_{basal} in complex **7**. Once the structure was optimized it was split into three fragments: one fragment for the TPO moiety, one for the tantalum metal center and the third the dimethylamido moiety. Each fragment was resubmitted for DFT analysis using the B3LYP/LANL2DZ level of theory for all the atoms. Each fragment along with the parent optimized structure where then analyzed using the AOMix software. The AOMix software is used for molecular orbital (MO) analysis, calculating the MO compositions in terms of the constituent chemical fragments in the molecule. The software also enables the analysis of chemical structure such as the bonding or antibonding nature of molecular orbitals using overlap populations. [151,152] The optimized structure was analyzed for molecular orbital interactions between the tantalum metal center and the apical dimethyl amido ligand.

When analyzing the optimized structure, the HOMOs were investigated. HOMO-3 shows the interaction between the atomic orbitals on Ta1 and N1 (Figure 13). There is significant π orbital overlap between Ta1 and N1from the apical dimethylamido in the molecule. HOMO-3 is comprised of 59% p_y from the nitrogen and 3.9% from the tantalum d_{yz} orbital. This indicates

that the atomic orbital contribution significantly comes from the nitrogen atom in the formation of the molecular orbital. The percentage contributions do not add to 100% because there are MO interactions from other atoms on the complex; lobes can be seen around the hydrogens and oxygen atoms (Figure 13). The AOMix software only provides composition in terms of most important AOs therefore not all the percentage contribution will be listed in the software. Additionally, molecular orbitals, HOMO-13 and HOMO-23, show σ and π orbital interactions between N1 and Ta1 and O_{basal} (Figures 14 and 15). The major orbital contribution of HOMO-13 is 5.3% p_y O1, 4.4% p_y O2, 5.3% p_y O3, 5.3% p_y O4 and 3.3% d_{yz} Ta1 and 2.4% p_y Ta, with molecular orbitals also present on the phenoxide moieties contributing to the rest of HOMO-13. The majority of the orbital composition comes from the oxygens on the basal plane, ~78%, leaving ~22% contribution from tantalum. Molecular orbital lobes can be seen when looking at the basal oxygens to the tantalum metal center (Figure 14). Upon further analysis HOMO-71 (Figure 16) shows π orbital interaction between the apical nitrogen atom and the central tantalum metal. The AOMix software output showed that the most important atomic orbital composition comes from 15% p_x N1 and 2% d_{xy} Ta1. This further indicates that the nitrogen on the apical ligand contributes more in the formation of the bond to tantalum. This evidence further supports the strong π-interaction associated with N1 and Ta1 which was seen when analyzing the crystal structure of complex **7**. Furthermore, many more orbital interactions are present between Ta1 and O_{basal}: (1) HOMO-4 shows orbital overlap between Ta1 and O_{basal} (Figure 17): (2) HOMO-10 and HOMO-15 also show the orbital overlap between Ta1 and O_{basal} (Figure 18) though the orbital overlap between the atoms isn't as considerable. For example, HOMO-10 is composed mostly from orbitals on the oxygens. π-interactions 6.1% p_y O1, 6.0% p_y O2, 5.1% p_y O3, 5.1% p_y O4, and π-interactions 5.6% p_z O3, 4.7% p_z O1. This demonstrates that the bond formed from

the basal oxygens to tantalum contributes significantly more from oxygens atomic orbitals. The AOMix software shows that the most important AOs are on the oxygens. The contribution from the tantalum therefore must not be as large.

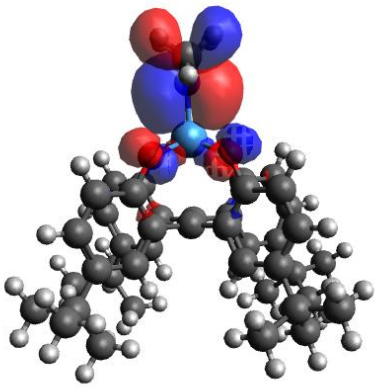

Figure 13. HOMO-3 Representation of Complex 7 Optimized Using B3LYP/LANL2DZ Level of Theory.

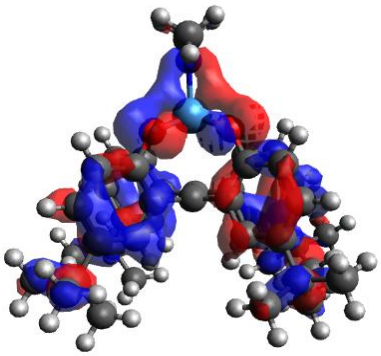

Figure 14. HOMO-13 Representation of Complex 7 Optimized Using B3LYP/LANL2DZ Level of Theory.

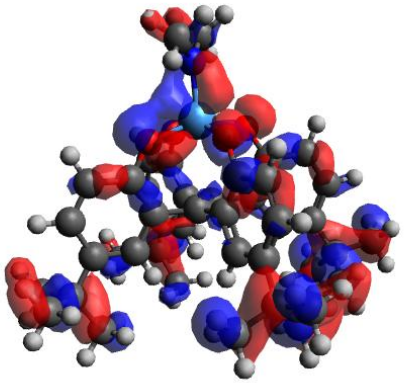

Figure 15. HOMO-23 Representation of Complex 7 Optimized Using B3LYP/LANL2DZ Level of Theory.

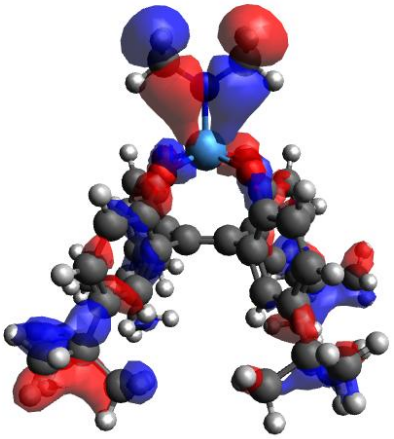

Figure 16. HOMO-71 Representation of Complex 7 Optimized Using B3LYP/LANL2DZ Level of Theory.

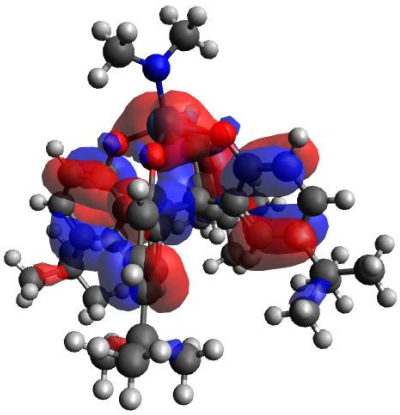

Figure 17. HOMO-4 Representation of Complex 7 Optimized Using B3LYP/LANL2DZ Level of Theory.

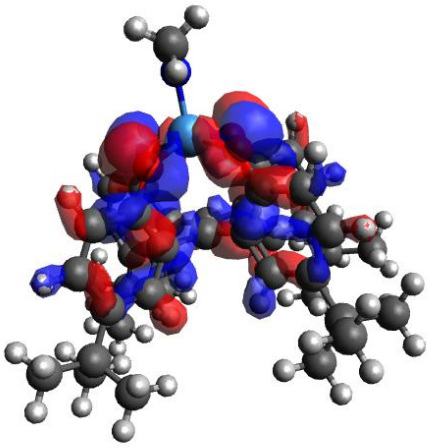

Figure 18. HOMO-10 Representation of Complex 7 Optimized Using B3LYP/LANL2DZ Level of Theory.

When comparing the optimized structure to the unoptimized structure of complex **7**, differences can be distinguished. Firstly, the energy of the optimized structure is lower than that of the unoptimized structure by 0.957 a.u. ($2.96*10^{-4}$ kJ/mol). The energy is lower because the complexes bond distances and angles have now been corrected for best symmetry orientations. Moreover, the optimized structure has bond angles that give a better representation of the molecule without any other intermolecular forces acting upon it. The geometry-optimized structure has the dimethyl amido group in the most geometrically favoured position. The methyl groups on dimethyl amido ligand are between the oxygens on the complex, unlike the unoptimized structure where the methyl groups are almost overtop of the oxygens (O1 and O4).

Table 2 compares some selected bond lengths and angles between the solid state structure and the DFT geometry optimized complex **7**. The Ta1–$O_{(basal)}$ bond lengths on the geometry optimized structure are less varied with the range being 1.947 – 1.952 Å. Also the bond angles between N1–Ta1–$O_{(basal)}$ are not as varied, ranging from 104.44–105.01°. The DFT geometry optimized structure has all 4 basal oxygens contributing to the tantalum metal center almost equally. Moreover, the Ta1–N1 bond length is slightly longer than in the solid state structure. The solid state structure shows more π-interaction between the apical ligand and tantalum metal center. Furthermore, the bond angles between Ta1–N1–C43/C44, C43–N1–C44 are very similar to the solid state structure.

Table 2. Selected Bond Lengths and Angles for Complex **7** - Solid State vs. DFT Geometry Optimized

	Solid State	DFT Geometry Optimized
Bond Lengths Selected Bond Lengths (Å)		
Ta1–O1	1.964(3)	1.952
Ta1–O2	1.923(3)	1.947
Ta1–O3	1.979(3)	1.952
Ta1–O4	1.918(3)	1.948
Ta1–N1	1.922(3)	1.949
C1–C2	1.332(6)	1.371
N1–C43	1.454(6)	1.479
N1–C44	1.464(6)	1.479
Selected Bond Angles (deg)		
N1–Ta1–O1	102.22(14)	104.44
N1–Ta1–O2	106.18(14)	104.92
N1–Ta1–O3	103.96(14)	104.64
N1–Ta1–O4	103.06(15)	105.01
Ta1–N1–C43	122.8(3)	123.00
Ta1–N1–C44	124.5(3)	123.03
C43–N1–C44	112.7(4)	113.97

For the unoptimized structure similar orbital interactions can be seen between N1 on the apical ligand and Ta1. HOMO-4 shows orbital interactions distinctly between N1 on the apical dimethyl amido ligand and Ta1. Large molecular orbitals are present between the two atoms (Figure 19). In addition, when analyzing the lower energy MO's HOMO-72 shows orbital overlaps between the apical N1 and Ta1 (Figure 20). The orbital overlaps are very similar to HOMO-71 from the optimized structure. Orbital overlap can be seen between N1 to Ta1 to O_{basal} in HOMO-16 and HOMO-21 (Figures 21 and 22). The lobes stretch from O_{basal} to the Ta1, indicating a bonding interaction. Moreover, O_{basal} to Ta1 bonding interactions is also evident

HOMO-11, HOMO-12 and HOMO-17 (Figures 23, 24, 25), albeit less significant than in HOMO-16 and HOMO-21.

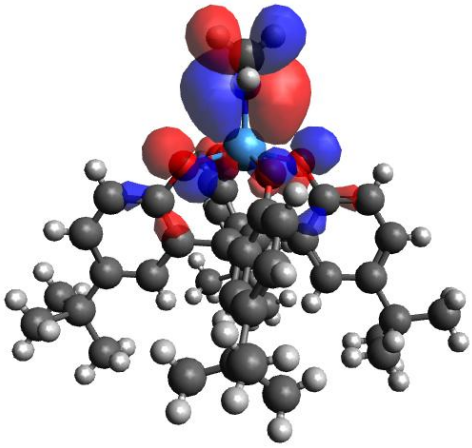

Figure 19. HOMO-4 Representation of Complex 7 Unoptimized Using B3LYP/LANL2DZ Level of Theory.

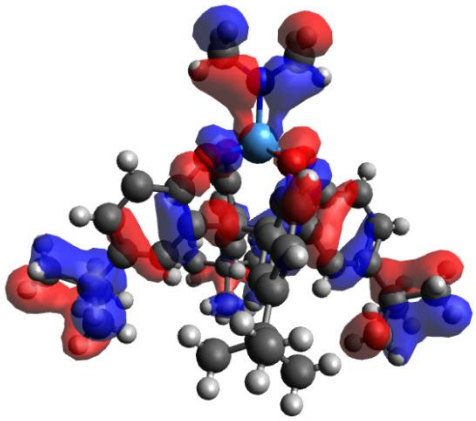

Figure 20. HOMO-72 Representation of Complex 7 Unoptimized Using B3LYP/LANL2DZ Level of Theory.

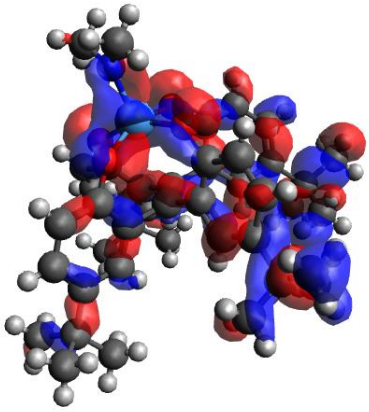

Figure 21. HOMO-16 Representation of Complex 7 Unoptimized Using B3LYP/LANL2DZ Level of Theory.

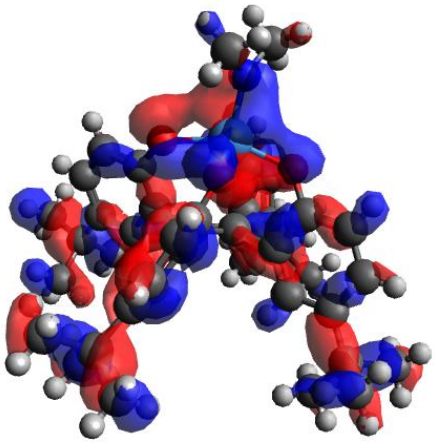

Figure 22. HOMO-21 Representation of Complex 7 Unoptimized Using B3LYP/LANL2DZ Level of Theory.

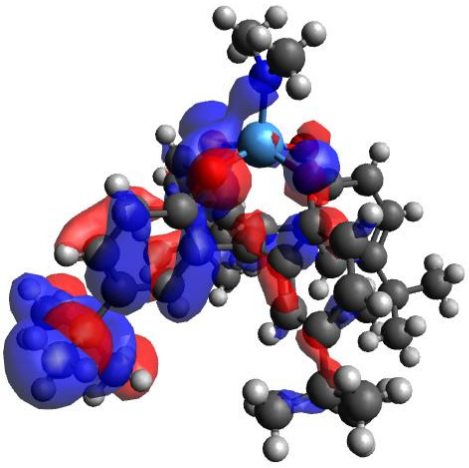

Figure 23. HOMO-11 Representation of Complex 7 Unoptimized Using B3LYP/LANL2DZ Level of Theory.

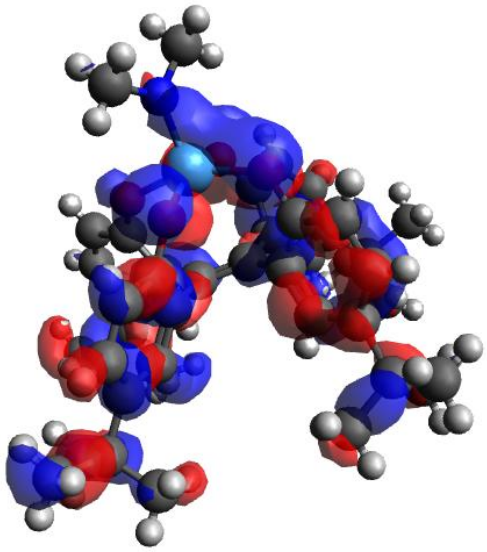

Figure 24. HOMO-12 Representation of Complex 7 Unoptimized Using B3LYP/LANL2DZ Level of Theory.

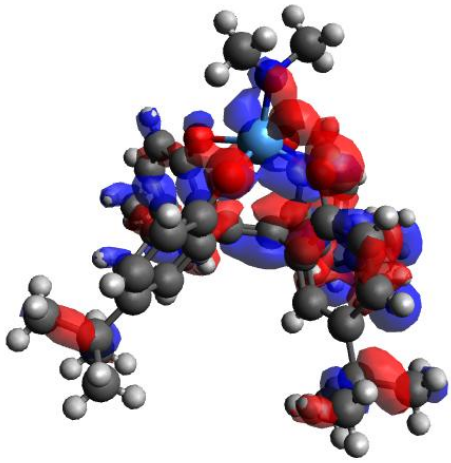

Figure 25. HOMO-17 Representation of Complex 7 Unoptimized Using B3LYP/LANL2DZ Level of Theory.

2.7 Coordination of 2,2',2",2"'-(1,2-Ethenediylidene)tetrakis[4-*tert*-butylphenol] **5b** to Group 6 Metals

The work described above on tantalum(V) has confirmed the hypothesis that the TPO ligand system imparts a square planar binding mode on the metal center. The crystal structures showed that complexes **6** and **7** both have square pyramidal geometries, as predicted, TPO forming the base of the square pyramid with the ethoxide or dimethylamide in the apical position. In addition, the work on tantalum showed that the complexes favour strong π-interactions. However, using tantalum for nitrogen activation would be difficult, and for this reason we became interested in group 6 metals. Group 6 metals are more suited when completing nitrogen fixation studies since they can support a wide range of oxidation states and have d-electrons required for nitrogen fixation. Furthermore, molybdenum has been shown to be a good metal for nitrogen fixation. For example much of the work by Schrock was based on molybdenum.[40,42,43]

Nitrogen fixation experiments are quite difficult when working with group 5 metals such as tantalum since reduction is challenging and tantalum complexes tend to remain in the +5 oxidation state, though there are reports in the literature for Ta(V) reducing to Ta(IV).[153] Keane et al. have shown that a Ta(V) hydrazido chloride can be chemically reduced, with potassium graphene compound, KC_8, at -30°C, to a mononuclear Ta(IV) hydrazido complex.[153]

Diamagnetic (d^0) group 6 metals were still first looked at before leading into any other less oxidized or paramagnetic species. Synthetic routes started by attempting synthesis with 2 precursors: molybdenum(VI) and tungsten (VI) oxychloride. This would access the coordination chemistry of TPO on group 6 metals. Syntheses were attempted by treating the metal tetrachloride oxide species with sodium methoxide to make $WO(OMe)_4$, which is analogous to $Ta(OEt)_5$ used to prepare complex **6**. The goal was now to replace all 4 methoxide ligands with

the TPO ligand. The methoxide species would then be added to one equivalent of $(TPO)H_4$ (Scheme 21). The synthesis for molybdenum and tungsten tetramethoxide oxide species has not been reported in the literature.

Unfortunately, these reactions did not produce any desired metal (VI) oxymethoxide precursors. After work-up, filtering out the solid and drying the filtrate in vacuo, the ^{1}H NMR spectrum was acquired. No proton resonances corresponding to the methoxide could be seen. The only resonances in the ^{1}H NMR spectrum corresponded to the solvent. One possibility is that the metal center could have reduced forming paramagnetic species which would have made the ^{1}H NMR spectrum very difficult to analyze.

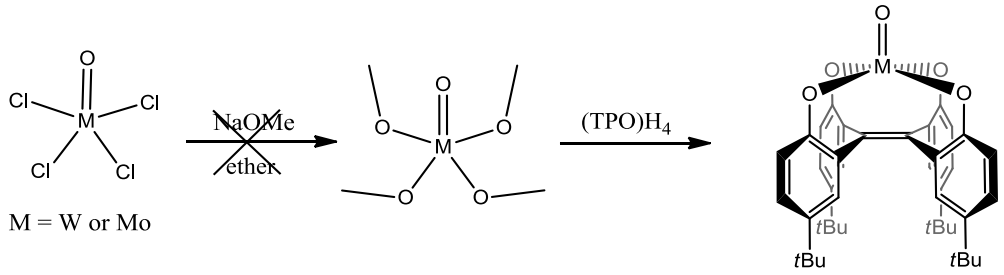

Scheme 21. Attempted Synthesis of Mo or W(VI) with $(TPO)H_4$.

Alternate synthetic routes were also attempted using the same metal precursors by exploring the literature for insight. The reactions of molybdenum(VI) oxychloride with calixarenes have been previously reported in the literature. The metal precursor was reacted with the calixarene ligand to obtain the transition metal complex, leaving HCl to bubble off as the by-product.[154,155] Since calixarenes have a tetraalkoxide binding mode similar to the TPO ligand, the reactions of molybdenum(VI) and tungsten(VI) oxychloride with $(TPO)H_4$ were attempted (Scheme 22). The metal oxychloride complex and $(TPO)H_4$ were added to an NMR tube with benzene-d_6 and the reaction was monitored by ^{1}H NMR spectroscopy. The reactions did not

produce any desirable results with no pure complex formed. The ^{1}H NMR spectrum showed far more resonances than anticipated, both in the aromatic and aliphatic regions of the spectrum in addition to broad resonances. The reactions did not produce complexes that were hoped for. The reactions were even heated to 70°C and monitored by ^{1}H NMR spectroscopy. This was an attempt to shift the equilibrium of the reaction to the products, but it also did not yield the targeted products. The HCl byproduct may have been reacting with the oxygens on TPO ligand as the product forms. The HCl may have been protonating the oxygens on TPO and creating a mixture of compounds. Additionally, if any water were present in the solution it would have decomposed the molybdenum complex to form molybdates.[155]

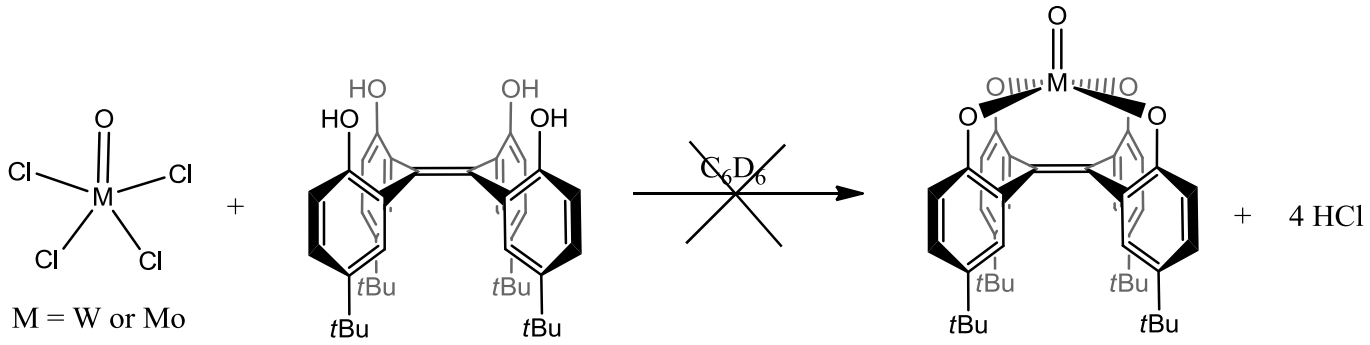

Scheme 22. Attempted synthesis of Mo or W (VI) species containing TPO.

Deprotonation of $(TPO)H_4$ using strong bases, sodium bis(trimethylsilyl)amide and sodium hydride, followed by the addition of the metal precursor in situ seemed to produce more desirable results (Scheme 23). The reaction was completed using tungsten(VI) oxychloride as the metal precursor, which was added to the reaction mixture and left to react for several hours. The product was obtained by filtering out the NaCl, drying in vacuo and washing with *n*-pentane. The product was characterized using ^{1}H NMR spectroscopy. The synthetic route that used sodium hydride was favoured since the spectrum looked more promising. The spectrum contained 3

resonances in the aromatic region and one resonance in the aliphatic region, consistent with what is expected, refer to ^{1}H NMR spectrum of complex **10** (**6.0** NMR Spectra). There also seems to be coordinated THF to the complex, as indicated by broad resonances assigned to THF. Though this tungsten complex is not fully characterized, preliminary results show that using this synthetic route seems to work more favourably. This synthesis can be the starting point of more group 6 transition metal complexes containing TPO.

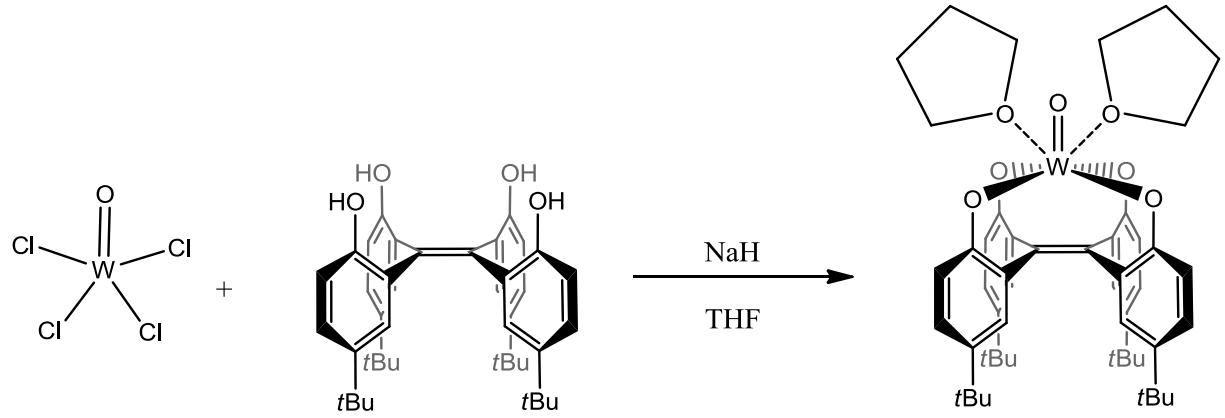

Scheme 23. Coordination of $(TPO)H_4$ to $WO(Cl)_4$ Forming Complex **10**.

3.0 Conclusions

Substituted (ethenediylidene)tetraphenoxides TPO provide a unique opportunity to study square pyramidal complexes. In our coordination study of TPO to tantalum(V), the ethoxide (**6**) and dimethylamide (**7**) complexes were isolated and structurally characterized, both showing significant double-bond character between the metal and the apical ligand. This confirmed our initial hypothesis that the square pyramidal geometry enforced by the TPO spectator ligand could facilitate π-interactions between the metal and the apical ligand. DFT studies on complex **7** also provided more evidence of the double bond character between the apical ligand and the metal center. Additional calculations completed using the AOMix program showed the AO compositions between tantalum and nitrogen, with nitrogen contributing significantly more to the MO.

Reactions of these complexes with trimethylaluminum cleanly led to the corresponding tantalum methyl complex (**8**). Reactivity studies showed that weak Brønsted acids such as ethanol and dimethylamine effectively engage in proton transfer to the apical ligand. In contrast, strong Brønsted acids gave mixtures of compounds that could not be effectively isolated and characterized, possibly due to competing protonation to the oxygens on the spectator ligand. Moreover, bulky Brønsted acids, such as phenol or benzoic acid, did not engage in any proton transfer with the apical ligand. In addition, no reaction between complexes **6**, **7** and **8** with acid chlorides/bromides were observed. Reactions with amines did not lead to the formation of any more isolated complexes with metal nitrogen bonds as were hoped for. The absence of isocyanide or hydride coordination to tantalum suggests a relatively electron-rich metal center, due to donation of π-electron density from TPO to the metal. Interestingly, reactions of acacH with complex **6** showed evidence of acac coordinating to the tantalum metal center with the

protonation of the spectator ligand, though a species could not be isolated. hfacH and MacacH were also employed in reactions but unfortunately also did not lead to any isolated species. Furthermore, the use of acetic anhydride to replace an apical ligand did not yield a product. Early coordination studies with group 6 metals suggests that tungsten(VI) species can be formed. This work shows that more complexes of mid-transition metals may be synthesized and further work can be investigated.

Work with the TPO ligand will continue in the future since it has shown to enforce square pyramidal geometries on transition metal centers. The coordination of TPO to transition metals that can accommodate a +7 oxidation state could also be targeted in future work, possibly using group 7 rhenium as it could support the M≡N (nitrido) species associated with dinitrogen reduction. This is an important intermediate in the nitrogen fixation cycle therefore further work in that direction would be an objective.

4.0 Experimental

4.1 General Experimental

All the reactions were conducted under an inert atmosphere at room temperature unless otherwise stated, using either an mBraun glovebox or standard Schlenk techniques. Toluene, ether, THF, MeCN, dichloromethane and *n*-pentane were purchased from Caledon Labs, dried using an MBraun solvent purification system fitted with activated alumina columns and stored over molecular sieves under a positive pressure of argon gas. Anhydrous benzene-d_6 was obtained by vacuum distilling over sodium and stored under argon. Anhydrous CD_2Cl_2 and $CDCl_3$ were obtained by vacuum distilling over calcium hydride and stored under argon. Anhydrous methanol and ethanol were purchased from Sigma-Aldrich and used as received. Tantalum(V) chloride, pentamethylcyclopendadienyltantalum tetrachloride, tantalum(V) ethoxide, and titanium (III) chloride were purchased from Strem Chemicals and used as received. Pentakis(dimethylamido)tantalum(V), trimethylaluminum (2.0 M in toluene), triisobutylaluminum (25 wt. % in hexanes), triethylaluminum (1.0 M in hexanes), sodium bis(trimethylsilyl)amide, methyllithium (1.6 M in diethylether), triethylammine, *n*-butyllithium (2.5 M in hexanes), dimethylcarbamoyl chloride, boron tribromide (1.0 M in CH_2Cl_2), diethylaluminum chloride (1.0 M in hexanes), 4-*tert*butylphenol, anisole, MeI, HCl (2.0 M in diethyl ether and 4.0 M in dioxane), triflic acid, chlorotrimethylsilane, dimethylamine (2.0 M in THF), *tert*-butylamine, *n*-butylamine, hydrazine (1.0 M in THF), acetyl chloride, acetyl bromide, benzoyl chloride, phenol, benzoic acid, dicyclopentadiene, triethylammonium chloride, silyltriflate, ammonium hexafluorphosphate, *tert*-butylisocyanide, 2,6-xylylisocyanide, acetylacetone, hexamethylacetylacetone, hexafluoroacetylacetone, sodium methoxide, molybdenum(VI) oxychloride and tungsten(VI) oxychloride were all purchased from Sigma-

Aldrich and used as received. Diethylzinc (15% w/w in hexanes) and N,N,N',N'-tetramethylethylenediamine were purchased from Alfa Aesar. Zn(Cu) couple was made from zinc dust and copper sulfate both purchased from Sigma-Aldrich. Methylaluminoxane and anilinium tetrakis(pentafluorophenyl)borate were donated by Albermarle Corp. $(TPO)H_4$ was prepared following published literature procedures.[101-103] Reactions where H_2 gas was used were carried out in J. Young NMR tubes.

NMR spectra were recorded on a Bruker AV 400 (^1H at 400 MHz, ^{13}C at 100 MHz) or Bruker AV 300 (^1H at 300 MHz, ^{13}C at 75.5 MHz) spectrometer and are at room temperature. VT NMR spectroscopy was completed on a Bruker AV 400 (^1H at 400 MHz, ^{13}C at 100 MHz) spectrometer by cooling to -80°C in intervals and slowly increasing the temperature back to room temperature. The spectra were referenced internally relative to the residual protio solvent (^1H) and solvent (^{13}C) resonances. Chemical shifts are reported with respect to $\delta = 0$ for TMS. Chemical shifts (δ) are reported in ppm and multiplicities are shown by s (singlet), d (doublet), t (triplet), q (quartet), and m (multiplet). Elemental analyses were determined by Chemistar Guelph Chemical Laboratories Incorporated.

4.2 Preparations

2,2',2",2"'-(1,2-Ethenediylidene)tetrakis(4-*tert*-butylphenoxide) Tantalum(V) Ethoxide (**6**). A solution of $Ta(OC_2H_5)_5$ (35 µL, 0.14 mmol) in toluene (3 mL) was added to a suspension of $(TPO)H_4$ (84.0 mg, 0.135 mmol in 6 mL toluene) and stirred for approximately 18 h. The pale yellow reaction mixture was filtered. The filtrate was collected and the volatiles removed in vacuo. The resulting solid was washed with cold pentane to give the product as a pale yellow solid (111 mg, 0.131 mmol, 97%). Addition of anhydrous ethanol (1.1 µL, 0.018 mmol) to complex **8** (15 mg, 0.018 mmol) in benzene-d_6 (1.5 mL) also gave a reaction product with spectroscopic data consistent with complex **6**, along with the formation of methane. ^{1}H NMR (400 MHz, C_6D_6): δ 7.44 (d $^4J_{HH}$ = 2.3 Hz, 4H, Ar), 6.83 (dd $^4J_{HH}$ = 2.3 Hz, $^3J_{HH}$ = 8.6 Hz 4H, Ar), 6.66 (d $^3J_{HH}$ = 8.6 Hz, 4H, Ar), 4.27 (q $^3J_{HH}$ = 7.0 Hz, 2H, OCH_2CH_3), 1.16 (s, 36H, $CH_{3(t\text{-butyl})}$), 1.08 (t $^3J_{HH}$ = 7.0 Hz, 3H, OCH_2CH_3) ppm. $^{13}C\{^1H\}$ NMR (100 MHz, C_6D_6): δ 159.1, 155.4, 143.9, 131.0, 125.8, 124.1, 117.2, 74.8 (OCH_2CH_3), 34.1 (CMe_3), 31.6 (CMe_3), 17.7 (OCH_2CH_3) ppm. Anal. Calcd. for $C_{44}H_{53}O_5Ta$ (%): C, 62.70; H, 6.34; N, 0.00; Found (%): C, 62.46; H, 6.17; N, <0.10 (below detection limit).

2,2',2",2"'-(1,2-Ethenediylidene)tetrakis(4-*tert*-butylphenoxide) Tantalum(V) Dimethylamide (**7**). A suspension of $(TPO)H_4$ (200 mg, 0.322 mmol) in toluene (5 mL) was transferred to an orange solution of $Ta(N(CH_3)_2)_5$ (129 mg, 0.322 mmol) in toluene (5 mL). The mixture was stirred overnight at room temperature. The resulting yellow solution was filtered. The filtrate was collected and the volatiles were removed in vacuo. The yellow brown solid was washed with cold pentane, yielding a light yellow solid (140 mg, 0.166 mmol, 52%). Addition of dimethylamine (2.0M in THF; 9.2 µL, 0.018 mmol) to complex **8** (15 mg, 0.018 mmol) in

benzene-d_6 (1.5 mL) also gave a reaction product with spectroscopic data consistent with complex **6**, along with the formation of methane. ^{1}H NMR (400 MHz, C_6D_6): δ 7.44 (d $^4J_{HH}$ = 2.3 Hz, 4H, Ar), 6.86 (dd $^4J_{HH}$ = 2.3 Hz, $^3J_{HH}$ = 8.5 Hz 4H, Ar), 6.69 (d $^3J_{HH}$ = 8.5 Hz, 4H, Ar), 3.40 (s, 6H, C$H_{3(amido)}$), 1.17 (s, 36H, C$H_{3(t\text{-butyl})}$) ppm. ^{13}C{^{1}H} NMR (100 MHz, C_6D_6): δ 159.1, 154.0, 143.7, 131.0, 125.6, 124.3, 117.1, 43.8 (NMe_2), 34.1 (CMe$_3$), 31.6 (CMe_3) ppm. Anal. Calcd. for $C_{44}H_{53}O_5Ta$ (%): C, 62.77; H, 6.47; N, 1.66; Found (%): C, 62.53; H, 6.68; N, 1.47.

2,2',2",2"'-(1,2-Ethenediylidene)tetrakis(4-*tert*-butylphenoxide) Tantalum(V) Methyl (**8**). Trimethylaluminum (2 M in toluene, 125 μL, 0.249 mmol) was added to a solution of complex **1** (105 mg, 0.125 mmol) in 5 mL of toluene. The solution was stirred at room temperature for approximately 18 h. The solution was filtered and the volatiles were removed from the filtrate under vacuum. The resulting solid was washed with cold *n*-pentane, giving complex **8** as a pale brown solid (66 mg, 0.081 mmol, 65%). ^{1}H NMR (300 MHz, C_6D_6): δ 7.44 (d $^4J_{HH}$ = 2.40 Hz, 4H, Ar), 6.80 (dd $^4J_{HH}$ = 2.40 Hz, $^3J_{HH}$ = 8.60 Hz, 4H, Ar), 6.65 (d $^3J_{HH}$ = 8.60 Hz, 4H, Ar), 1.63 (s, 3H Ta–CH_3), 1.15 (s, 36H, $CH_{3(t\text{-Bu})}$) ppm. ^{13}C{^{1}H} NMR (100 MHz, C_6D_6): δ 159.2, 153.2, 144.4, 131.3, 125.7, 124.2, 116.7, 53.4 (Ta–*Me*), 34.1 (CMe$_3$), 31.5 (CMe_3) ppm. Anal. Calcd. for $C_{43}H_{51}O_4Ta$ (%): C, 63.54; H, 6.32; N, 0.00; Found (%): C, 63.57; H, 6.11; N,<0.1 (below detection limit).

General Procedures for Ethylene Polymerization

Ethylene polymerization was performed at atmospheric pressure and room temperature; the reaction took place in a 500 mL Polymerization Flask containing a magnetic stir bar. The flask was first dried in an oven at 160°C for a minimum of 12 hours prior to use. Next the flask was placed under vacuum until it reached room temperature, after which it was back-filled with

ethylene gas. This cycle was repeated 3 times to ensure only ethylene gas was present in the flask. Now under an atmosphere of ethylene, the flask was charged with 25 mL of dry toluene. Other trials used 1000 equivalents of methylaluminoxane (2 M in toluene) and some in the absence of methylaluminoxane (2 M in toluene); **2.0** Results and Discussion for details. The solution was stirred for several minutes before the catalyst (10.3 mmol) in 1 mL of toluene was added to the polymerization flask using a syringe. The solution was vigorously stirred for 10 min after adding the catalyst. Additionally some trials were stirred for 24 hours. The reaction subsequently quenched with a 50:50 mixture of concentrated hydrochloric acid and methanol. Afterwards the mixture was filtered but in all case no solid were observed and nothing was collected.

General Procedure for Cyclopentadiene Synthesis

Cyclopentadiene was synthesized from its corresponding dimer using literature procedures, dicyclopentadiene via a Diels–Alder reaction, since as a monomer it dimerizes quite easily at room temperature.[156] Cyclopentadiene was prepared on a laboratory scale by thermolysis of dicyclopentadiene, by addition of dicyclopentadiene to a flask in high-boiling oil, at 250-260°C. The vapors were fractionated to remove from reflux and the cyclopentadiene was collected by distilling into a flask cooled to -78°C. The monomer, cyclopentadiene, was stored in the freezer (-40°C) until needed for the use as a reactant.

4.3 Supporting Information

Detailed crystallographic data for all structures including structure refinement parameters, tables of atomic coordinates with isotropic and anisotropic displacement parameters, bond lengths and angles that have been published can be found on the Cambridge Crystallographic Data Center (CCDC) website. CCDC reference numbers for each compound are given in parentheses **6** (CCDC reference number 1032147) and **7** (CCDC reference number 1032148).

X-ray Crystallography

Crystallographic data were collected at the University of Toronto on a Bruker Kappa APEX-DUO diffractometer using a monochromated Mo-Kα radiation (Bruker Triumph; λ = 0.71073 Å) at 150K. Data were measured using a combination of ϕ scans and ω scans, and were processed using APEX2 and SAINT.[157] Absorption corrections were carried out using SADABS.[157] Both structures were solved and refined using WinGX[158] with SHELXS-97 for full-matrix least-squares refinement that was based on F^2.[159] All H atoms were included in calculated positions and allowed to refine in riding-motion approximation with U_{iso} tied to the carrier atom.

Table 3. Crystal Data and Structure Refinement for Compound **6**.

Identification code	d1411
Empirical formula	C44 H53 O5 Ta
Formula weight	842.81
Temperature	147(2) K
Wavelength	0.71073 Å
Crystal system, space group	Triclinic, P-1
Unit cell dimensions	a = 11.3470(14) Å alpha = 103.694(3) °.
	b = 13.0316(16) Å beta = 101.905(3) °.
	c = 15.3105(19) Å gamma = 108.362(2) °.
Volume	1988.4(4) $Å^3$
Z, Calculated density	2, 1.408 Mg/m^3
Absorption coefficient	2.806 mm^{-1}
F(000)	860
Crystal size	0.28 x 0.12 x 0.05 mm^3
Theta range for data collection	1.44 to 27.55°.
Limiting indices	-14<=h<=14, -16<=k<=15, -19<=l<=19
Reflections collected / unique	65839 / 9030 [R(int) = 0.0181]
Completeness to theta = 27.55	98.5 %
Absorption correction	Semi-empirical from equivalents
Max. and min. transmission	0.7456 and 0.6135
Refinement method	Full-matrix least-squares on F^2
Data / restraints / parameters	9030 / 0 / 526
Goodness-of-fit on F^2	1.078
Final R indices [I>2sigma(I)]	R1 = 0.0149, wR2 = 0.0377
R indices (all data)	R1 = 0.0159, wR2 = 0.0384
Largest diff. peak and hole	0.767 and -0.406 $e.A^{-3}$

Table 4. Crystal Data and Structure Refinement for Compound **7**.

Identification code	d13219
Empirical formula	C44 H54 N O4 Ta
Formula weight	841.83
Temperature	147(2) K
Wavelength	0.71073 Å
Crystal system, space group	Triclinic , P-1
Unit cell dimensions	a = 11.6837(10) Å alpha = 104.204(2)°.
	b = 13.1820(10) Å beta = 99.842(2)°.
	c = 15.0808(11) Å gamma = 110.239(2)°.
Volume	2027.4(3) $Å^3$
Z, Calculated density	2, 1.376 Mg/m^3
Absorption coefficient	2.751 mm^{-1}
F(000)	856
Crystal size	0.23 x 0.100 x 0.025 mm^3
Theta range for data collection	1.74 to 27.62°.
Limiting indices	-15<=h<=6, -15<=k<=17, -18<=l<=19
Reflections collected / unique	29966 / 9147 [R(int) = 0.0405]
Completeness to theta = 27.62	97.0 %
Absorption correction	Semi-empirical from equivalents
Max. and min. transmission	0.7456 and 0.6135
Refinement method	Full-matrix least-squares on F^2
Data / restraints / parameters	9147 / 0 / 527
Goodness-of-fit on F^2	1.051
Final R indices [I>2sigma(I)]	R1 = 0.0363, wR2 = 0.0749
R indices (all data)	R1 = 0.0578, wR2 = 0.0846
Largest diff. peak and hole	2.704 and -1.021 $e.A^{-3}$

5.0 References

1. Housecrofft, E. C.; Sharpe, G. A. In *Catalysis and some Industrial Processes;* Inorganic Chemistry; Pearson: Englans, 2008; pp 905.

2. McCoy, M.; Reisch, M.; Tullo, A. H. Facts & Figures of the Chemical Industry. *Chem. Eng. News* **2006**, *84*, 35.

3. Parshall, G. W.; Putscher, R. E. Organometallic Chemistry and Catalysis in Industry. *J. Chem. Educ.* **1986**, *63*, 189.

4. Storck, W. J. The ChemicalIindustry Enters 2006 with Many of the Concerns it had in 2005. *Chem. Eng. News* **2006**, *84*, 12-15.

5. Weare, W. W.; Dai, X.; Byrnes, M. J.; Chin, J. M.; Schrock, R. R.; Müller, P. Catalytic Reduction of dinitrogen to Smmonia at a Single Molybdenum Center. *Proceedings of the National Academy of Sciences* **2006**, *103*, 17099-17106.

6. Leigh, G. *The World's Greatest Fix - A History of Nitrogen and Agriculture;* Oxford University Press, 2004 .

7. Fryzuk, M. D. N_2 Coordination. *Chem.Commun.* **2013**, *49*, 4866-4868.

8. AnonymousAll Nobel Prizes in Chemistry. *http://www.nobelprize.org/nobel_prizes/chemistry/laureates/* (accessed February/04, 2015).

9. Sellmann, D.; Sutter, J. In Quest of Competitive Catalysts for Nitrogenases and Other Metal Sulfur Enzymes. *Acc. Chem. Res.* **1997**, *30*, 460-469.

10. Weast, R. C., Ed. *; CRC Handbook of Chemistry and Physics*; CRC Press: Boca Raton, FL: 1985; , pp E-81.

11. MacKay, B. A.; Fryzuk, M. D. Dinitrogen Coordination Chemistry: On the Biomimetic Borderlands. *Chem. Rev.* **2004**, *104*, 385-402.

12. Nishibayashi, Y.; Takemoto, S.; Iwai, S.; Hidai *, M. Formation of Ammonia in the Reactions of a Tungsten Dinitrogen with Ruthenium Dihydrogen Complexes under Mild Reaction Conditions. *Inorg. Chem.* **2000**, *39*, 5946-5957.

13. Kandemir, T.; Schuster, M. E.; Senyshyn, A.; Behrens, M.; Schlögl, R. The Haber–Bosch Process Revisited: On the Real Structure and Stability of "Ammonia Iron" under Working Conditionsnss. *Angew. Chem. Int. Ed.* **2013**, *52*, 12723-12726.

14. Apodaca, L. U. S. Geological Survey. **2011**.

15. Alwin Mittasch, W. F. Early Studies of Multicomponent Catalysts. *Adv. Catal.* **1950**, *2*, 81-104.

16. Barański, A.; Kotarba, A.; Łagan, J. M.; Pattek-Janczyk, A.; Pyrczak, E.; Reizer, A. Kinetics of Activation of the Industrial and Model Fused Iron Catalysts for Ammonia Synthesis. *Applied Catalysis A: General* **1994**, *112*, 13-36.

17. Hinrichsen, S.; Broda, H.; Gradert, C.; Soncksen, L.; Tuczek, F. Recent Developments in Synthetic Nitrogen Fixation. *Annu. Rep. Prog. Chem. , Sect. A: Inorg. Chem.* **2012**, *108*, 17-47.

18. Bazhenova, T. A.; Shilov, A. E. Nitrogen Fixation in Solution. *Coord. Chem. Rev.* **1995**, *144*, 69-145.

19. Seefeldt, L. C.; Hoffman, B. M.; Dean, D. R. Mechanism of Mo-Dependent Nitrogenase. *Annu. Rev. Biochem.* **2009**, *78*, 701-722.

20. Seefeldt, L. C.; Dean, D. R. Role of Nucleotides in Nitrogenase Catalysis. *Acc. Chem. Res.* **1997**, *30*, 260-266.

21. Eady, R. R. Structure-Function Relationships of Alternative Nitrogenases. *Chem. Rev.* **1996**, *96*, 3013-3030.

22. Georgiadis, M. M.; Komiya, H.; Chakrabarti, P.; Woo, D.; Kornuc, J. J.; Rees, D. C. Crystallographic Structure of the Nitrogenase Iron Protein from Azotobacter Vinelandii. *Science* **1992**, *257*, 1653-1659.

23. Hoffman, B. M.; Dean, D. R.; Seefeldt, L. C. Climbing Nitrogenase: Toward a Mechanism of Enzymatic Nitrogen Fixation. *Acc. Chem. Res.* **2009**, *42*, 609-619.

24. Kim, J.; Rees, D. Structural Models for the Metal Centers in the Nitrogenase Molybdenum-Iron Protein. *Science* **1992**, *257*, 1677-1682.

25. Dance, I. Mimicking Nitrogenase. *Dalton Trans.* **2010**, *39*, 2972-2983.

26. Ritleng, V.; Yandulov, D. V.; Weare, W. W.; Schrock, R. R.; Hock, A. S.; Davis, W. M. Molybdenum Triamidoamine Complexes that Contain Hexa-tert-butylterphenyl, Hexamethylterphenyl, or p-Bromohexaisopropylterphenyl Substituents. An Examination of Some Catalyst Variations for the Catalytic Reduction of Dinitrogen. *J. Am. Chem. Soc.* **2004**, *126*, 6150-6163.

27. Allen, A.; Harris, R.; Loescher, B.; Stevens, J.; Whiteley, R. Dinitrogen Complexes of the Transition Metals. *Chem. Rev.* **1973**, *73*, 11-20.

28. Chatt, J.; Leigh, G. Nitrogen Fixation. *Chem. Soc. Rev.* **1972**, *1*, 121-144.

29. Fryzuk, M. D.; Shaver, M. Activation of Molecular Nitrogen: Coordination, Cleavage and Functionalization of N2 Mediated By Metal Complexes. *Adv. Synth. Catal.* **2003**, *345*, 1061-1076.

30. Crossland, J. L.; Tyler, D. R. Iron–Dinitrogen Coordination Chemistry: Dinitrogen Activation and Reactivity. *Coord. Chem. Rev.* **2010**, *254*, 1883-1894.

31. Rocklage, S. M.; Turner, H. W.; Fellmann, J. D.; Schrock, R. R. Preparation of Tantalum μ-Dinitrogen Complexes from Molecular Nitrogen and Reduced Tantalum Complexes. *Organometallics* **1982**, *1*, 703-707.

32. O'Regan, M. B.; Liu, A. H.; Finch, W. C.; Schrock, R. R.; Davis, W. M. A study of high-oxidation-state complexes of the type [W (η 5-C_5Me_5) $Me_2X]_2$(μ-N_2), including X-ray structures of [W(η 5-C_5Me_5) $Me_2(OC_6F_5)]_2$(μ-N_2) and [W(η 5-C_5Me_5)Me_2(S-2, 4,6-$C_6H_2Me_3$)] $_2$(μ-N_2). *J. Am. Chem. Soc.* **1990**, *112*, 4331-4338.

33. Hidai, M.; Tominari, K.; Uchida, Y.; Misono, A. A Trans-Dinitrogen Complex of Molybdenum. *Journal of the Chemical Society D: Chemical Communications* **1969**, 1392-1392.

34. Senoff, C. V. The Discovery of $Ru(NH_3)_5N_2]^{2+}$: A Case of Serendipity and the Scientific Method. *J. Chem. Educ.* **1990**, *67*, 368.

35. Rocklage, S. M.; Turner, H. W.; Fellmann, J. D.; Schrock, R. R. Preparation of Tantalum μ-Dinitrogen Complexes from Molecular Nitrogen and Reduced Tantalum Complexes. *Organometallics* **1982**, *1*, 703-707.

36. Fellmann, J.; Turner, H.; Schrock, R. Tantalum-Neopentylidene Hydride and Tantalum-Neopentylidyne Hydride Complexes. *J. Am. Chem. Soc.* **1980**, *102*, 6608-6609.

37. Fryzuk, M. D.; Haddad, T.; Rettig, S. J. Reduction of Dinitrogen by a Zirconium Phosphine Complex to Form a Side-on-Bridging N2 Ligand. Crystal Structure of {[$Pr^{i}_{2}PCH_{2}SiMe_{2})_{2}N$] ZrCl} 2 (μ-η 2: η 2-$N_2$). *J. Am. Chem. Soc.* **1990**, *112*, 8185-8186.

38. Fryzuk, M. D.; Johnson, S. A.; Rettig, S. J. New Mode of Coordination for the Dinitrogen Ligand: A Dinuclear Tantalum Complex with a Bridging N2 Unit That Is Both Side-On and End-On. *J. Am. Chem. Soc.* **1998**, *120*, 11024-11025.

39. Barrière, F. Modeling of the Molybdenum Center in the Nitrogenase FeMo-Cofactor. *Coord. Chem. Rev.* **2003**, *236*, 71-89.

40. Yandulov, D. V.; Schrock, R. R. *. Reduction of Dinitrogen to Ammonia at a Well-Protected Reaction Site in a Molybdenum Triamidoamine Complex. *J. Am. Chem. Soc.* **2002**, *124*, 6252-6253.

41. Yandulov, D. V.; Schrock, R. R. Catalytic Reduction of Dinitrogen to Ammonia at a Single Molybdenum Center. *Science* **2003**, *301*, 76-78.

42. Yandulov, D. V.; Schrock, R. R. Catalytic Reduction of Dinitrogen to Ammonia at a Single Molybdenum Center. *Science* **2003**, *301*, 76-78.

43. Schrock, R. R. Catalytic Reduction of Dinitrogen to Ammonia at a Single Molybdenum Center. *Acc. Chem. Res.* **2005**, *38*, 955-962.

44. Hetterscheid, D. G. H.; Hanna, B. S.; Schrock, R. R. Molybdenum Triamidoamine Systems. Reactions Involving Dihydrogen Relevant to Catalytic Reduction of Dinitrogen. *Inorg. Chem.* **2009**, *48*, 8569-8577.

45. Kinney, R. A.; McNaughton, R. L.; Chin, J. M.; Schrock, R. R.; Hoffman, B. M. Protonation of the Dinitrogen-Reduction Catalyst [HIPTN3N]MoIII Investigated by ENDOR Spectroscopy. *Inorg. Chem.* **2011**, *50*, 418-420.

46. Schrock, R. R. Catalytic Reduction of Dinitrogen to Ammonia by Molybdenum: Theory versus Experiment. *Angew. Chem. Int. Ed.* **2008**, *47*, 5512-5522.

47. Yandulov, D. V.; Schrock, R. R.; Rheingold, A. L.; Ceccarelli, C.; Davis, W. M. Synthesis and Reactions of Molybdenum Triamidoamine Complexes Containing Hexaisopropylterphenyl Substituents. *Inorg. Chem.* **2003**, *42*, 796-813.

48. Weare, W. W.; Schrock, R. R.; Hock, A. S.; Muller, P. Synthesis of Molybdenum Complexes that Contain Hybride Triamidoamine Ligands, (Hexaisopropylterphenyl-$NCH_2CH_2)_2NCH_2CH_2N$-aryl]$^{3-}$, and Studies Relevant to Catalytic Reduction of Dinitrogen. *Inorg. Chem.* **2006**, *45*, 9185-9196.

49. Vincent Ritleng , Dmitry V. Yandulov , Walter W. Weare , Richard R. Schrock ,* Adam S. Hock , and William M. Davis Molybdenum Triamidoamine Complexes that Contain Hexa-*tert*-butylterphenyl, Hexamethylterphenyl, or*p*-Bromohexaisopropylterphenyl Substituents. An Examination of Some Catalyst Variations for the Catalytic Reduction of Dinitrogen. *J. Amer. Chem. Soc.* **2004**, *126*, 6150.

50. Reithofer, M. R.; Schrock, R. R.; Muller, P. Synthesis of $(DPPNCH_2CH_2)_3N]_3$ Molybdenum Complexes (DPP = 3,5-(2,5-Diisopropylpyrrolyl)$_2C_6H_3$) and Studies Relevant to Catalytic Reduction of Dinitrogen. *J. Am. Chem. Soc.* **2010**, *132*, 8349-8358.

51. Chin, J. M.; Schrock, R. R.; Müller, P. Synthesis of DiamidoPyrrolyl Molybdenum Complexes Relevant to Reduction of Dinitrogen to Ammonia. *Inorg. Chem.* **2010**, *49*, 7904-7916.

52. Anderson, J. S.; Rittle, J.; Peters, J. C. Catalytic Conversion of Nitrogen to Ammonia by an Iron Model Complex. *Nature* **2013**, *501*, 84-87.

53. Creutz, S. E.; Peters, J. C. Catalytic Reduction of N_2 to NH_3 by an Fe-N_2 Complex Featuring a C-Atom Anchor. *J. Am. Chem. Soc.* **2014**, *136*, 1105-1115.

54. Nishibayashi, Y. Molybdenum-Catalyzed Reduction of Molecular Dinitrogen Under Mild Reaction Conditions. *Dalton Trans.* **2012**, *41*, 7447-7453.

55. Arashiba, K.; Miyake, Y.; Nishibayashi, Y. A molybdenum Complex Bearing PNP-Type Pincer Ligands Leads to the Catalytic Reduction of Dinitrogen into Ammonia. *Nat. Chem.* **2011**, *3*, 120-125.

56. Arashiba, K.; Miyake, Y.; Nishibayashi, Y. A molybdenum Complex Bearing PNP-Type Pincer Ligands Leads to the Catalytic Reduction of Dinitrogen into Ammonia. *Nat. Chem.* **2011**, *3*, 120-125.

57. Kuriyama, S.; Arashiba, K.; Nakajima, K.; Tanaka, H.; Kamaru, N.; Yoshizawa, K.; Nishibayashi, Y. Catalytic Formation of Ammonia from Molecular Dinitrogen by Use of Dinitrogen-Bridged Dimolybdenum–Dinitrogen Complexes Bearing PNP-Pincer Ligands: Remarkable Effect of Substituent at PNP-Pincer Ligand. *J. Am. Chem. Soc.* **2014**, *136*, 9719-9731.

58. Skoog, S. J.; Mateo, C.; Lavoie, G. G.; Hollander, F. J.; Bergman, R. G. Synthesis of Novel Group 4 Complexes Bearing the Tropidinyl Ligand: Investigations of Dynamic Behavior, Reactivity, and Catalytic Olefin Polymerization. *Organometallics* **2000**, *19*, 1406-1421.

59. Zhang, W.; Loebach, J. L.; Wilson, S. R.; Jacobsen, E. N. Enantioselective Epoxidation of Unfunctionalized Olefins Catalyzed by Salen Manganese Complexes. *J. Am. Chem. Soc.* **1990**, *112*, 2801-2803.

60. Xia, Q.; Ge, H.; Ye, C.; Liu, Z.; Su, K. Advances in Homogeneous and Heterogeneous Catalytic Asymmetric Epoxidation. *Chem. Rev.* **2005**, *105*, 1603-1662.

61. Du, G.; Abu-Omar, M. M. Oxo and Imido Complexes of Rhenium and Molybdenum in Catalytic Reductions. *Curr. Org. Chem.* **2008**, *12*, 1185-1198.

62. Andrikopoulos, P. C.; Michel, C.; Chouzier, S.; Sautet, P. In Silico Screening of Iron-Oxo Catalysts for CH Bond Cleavage. *ACS Catalysis* **2015**.

63. Gunay, A.; Theopold, K. H. C−H Bond Activations by Metal Oxo Compounds. *Chem. Rev.* **2010**, *110*, 1060-1081.

64. G de Noronha, R.; C Fernandes, A. High Valent Oxo-molybdenum Complexes as Efficient Catalysts for CX Bond Forming Reactions. *Curr. Org. Chem.* **2012**, *16*, 33-64.

65. Saouma, C. T.; Peters, J. C. ME and ME Complexes of Iron and Cobalt that Emphasize Three-Fold Symmetry (E = O, N, NR). *Coord. Chem. Rev.* **2011**, *255*, 920-937.

66. Rocklage, S. M.; Schrock, R. R. Tantalum Imido Complexes. *J. Am. Chem. Soc.* **1980**, *102*, 7808-7809.

67. Mindiola, D. J.; Hillhouse, G. L. Terminal Amido and Imido Complexes of Three-Coordinate Nickel. *J. Am. Chem. Soc.* **2001**, *123*, 4623-4624.

68. Waterman, R.; Hillhouse, G. L. Group Transfer From Nickel Imido, Phosphinidene, and Carbene Complexes to Ethylene with Formation of Aziridine, Phosphirane, and Cyclopropane Products. *J. Am. Chem. Soc.* **2003**, *125*, 13350-13351.

69. Gianetti, T. L.; La Pierre, H. S.; Arnold, J. Group 5 Imides and Bis (imide) s as Selective Hydrogenation Catalysts. *Eur. J. Inorg. Chem.* **2013**, *2013*, 3771-3783.

70. Berry, J. F. Terminal Nitrido And Imido Complexes of The Late Transition Metals. *Comments Inorg. Chem.* **2009**, *30*, 28-66.

71. Mehn, M. P.; Peters, J. C. Mid- to High-Valent Imido and Nitrido Complexes of Iron. *J. Inorg. Biochem.* **2006**, *100*, 634-643.

72. Crossland, J. L.; Tyler, D. R. Iron–Dinitrogen Coordination Chemistry: Dinitrogen Activation and Reactivity. *Coord. Chem. Rev.* **2010**, *254*, 1883-1894.

73. Schrock, R. R. Catalytic Reduction of Dinitrogen to Ammonia at a Single Molybdenum Center. *Acc. Chem. Res.* **2005**, *38*, 955-962.

74. Yandulov, D. V.; Schrock, R. R. Studies Relevant to Catalytic Reduction of Dinitrogen to Ammonia by Molybdenum Triamidoamine Complexes. *Inorg. Chem.* **2005**, *44*, 1103-1117.

75. Ray, K.; Heims, F.; Pfaff, F. F. Terminal Oxo and Imido Transition-Metal Complexes of Groups 9–11. *European Journal of Inorganic Chemistry* **2013**, *2013*, 3784-3807.

76. Christian, G.; Stranger, R.; Yates, B. F.; Cummins, C. C. Rationalizing the Different Products in the Reaction of N_2 with Three-Coordinate MoL_3 Complexes. *Dalton Trans.* **2007**, 1939-1947.

77. Creutz, S. E.; Peters, J. C. Catalytic Reduction of N_2 to NH_3 by an Fe–N_2 Complex Featuring a C-Atom Anchor. *J. Am. Chem. Soc.* **2014**, *136*, 1105-1115.

78. Laplaza, C. E.; Johnson, M. J.; Peters, J. C.; Odom, A. L.; Kim, E.; Cummins, C. C.; George, G. N.; Pickering, I. J. Dinitrogen Cleavage by Three-Coordinate Molybdenum (III) Complexes: Mechanistic and Structural Data1. *J. Am. Chem. Soc.* **1996**, *118*, 8623-8638.

79. Neese, F. The Yandulov/Schrock Cycle and the Nitrogenase Reaction: Pathways of Nitrogen Fixation Studied by Density Functional Theory. *Angewandte Chemie International Edition* **2006**, *45*, 196-199.

80. Schenk, S.; Le Guennic, B.; Kirchner, B.; Reiher, M. First-principles Investigation of the Schrock Mechanism of Dinitrogen Reduction Employing the Full HIPTN3N Ligand. *Inorg. Chem.* **2008**, *47*, 3634-3650.

81. Schenk, S.; Kirchner, B.; Reiher, M. A Stable Six-Coordinate Intermediate in Ammonia–Dinitrogen Exchange at Schrock's Molybdenum Catalyst. *Chemistry-A European Journal* **2009**, *15*, 5073-5082.

82. Cummins, C. C. Reductive Cleavage and Related Reactions Leading to Molybdenum–Element Multiple Bonds: New Pathways Offered by Three-Coordinate Molybdenum (III). *Chemical Communications* **1998**, 1777-1786.

83. Laplaza, C. E.; Cummins, C. C. Dinitrogen Cleavage by a Three-Coordinate Molybdenum(III) Complex. *Science* **1995**, *268*, 861-863.

84. Fryzuk, M. D.; Kozak, C. M.; Bowdridge, M. R.; Jin, W.; Tung, D.; Patrick, B. O.; Rettig, S. J. Macrocyclic Complexes of Niobium (III): Synthesis, Structure, and Magnetic Behavior of Mononuclear and Dinuclear Species that Incorporate the [P2N2] System. *Organometallics* **2001**, *20*, 3752-3761.

85. Fryzuk, M. D.; Kozak, C. M.; Bowdridge, M. R.; Patrick, B. O.; Rettig, S. J. Nitride Formation by Thermolysis of a Kinetically Stable Niobium Dinitrogen Complex. *J. Am. Chem. Soc.* **2002**, *124*, 8389-8397.

86. Guha, A. K.; Phukan, K. A. Why Vanadium Complexes Perform Poorly in Comparison to Related Molybdenum Complexes in the Catalytic Reduction of Dinitrogen to Ammonia (Schrock Cycle): A Theoretical Study. *Inorg. Chem.* **2011**, *50*, 8826-8833.

87. Ciampolini, M. In *Spectra of 3d Five-Coordinate Complexes;* Structure and Bonding; Springer: 1969; pp 52-93.

88. Orioli, P. L. The Stereochemistry of Five-Coordinate Nickel(II) and Cobalt(II) Complexes. *Coord. Chem. Rev.* **1971**, *6*, 285-308.

89. Fryzuk, M. D.; Love, J. B.; Rettig, S. J.; Young, V. G. Transformation of Coordinated Dinitrogen by Reaction with Dihydrogen and Primary Silanes. *Science* **1997**, *275*, 1445-1447.

90. Morello, L.; João Ferreira, M.; Patrick, B. O.; Fryzuk, M. D. Side-on Bound Dinitrogen Complex of Zirconium Supported by a P2N2 Macrocyclic Ligand. *Inorg. Chem.* **2008**, *47*, 1319-1323.

91. Beer, P. D. Transition-Metal Receptor Systems for the Selective Recognition and Sensing of Anionic Guest Species. *Acc. Chem. Res.* **1998**, *31*, 71-80.

92. Caselli, A.; Solari, E.; Scopelliti, R.; Floriani, C.; Re, N.; Rizzoli, C.; Chiesi-Villa, A. Dinitrogen Rearranging over a Metal-Oxo Surface and Cleaving to Nitride: From the End-On to the Side-On Bonding Mode, to the Stepwise Cleavage of the N∶N Bonds Assisted by Nb^{III}-calix[4]arene. *J. Am. Chem. Soc.* **2000**, *122*, 3652-3670.

93. Kojima, M.; Taguchi, H.; Tsuchimoto, M.; Nakajima, K. Tetradentate Schiff Base–Oxovanadium(IV) Complexes: Structures and Reactivities in the Solid State. *Coord. Chem. Rev.* **2003**, *237*, 183-196.

94. Śliwa, W. Calixarene Complexes with Transition Metal Ions. *J. Inclusion Phenom. Mol. Recognit. Chem.* **2005**, *52*, 13-37.

95. Blagg, R. J.; Connelly, N. G.; Haddow, M. F.; Hamilton, A.; Lusi, M.; Orpen, A. G.; Ridgway, B. M. Isomerism in Rhodium (I) N, S-Donor Heteroscorpionates: Ring Substituent and Ancillary Ligand Effects. *Dalton Trans.* **2010**, *39*, 11616-11627.

96. Couzijn, E. P.; Slootweg, J. C.; Ehlers, A. W.; Lammertsma, K. Stereomutation of Pentavalent Compounds: Validating the Berry Pseudorotation, Redressing Ugi's Turnstile Rotation, and Revealing the Two-and Three-Arm Turnstiles. *J. Am. Chem. Soc.* **2010**, *132*, 18127-18140.

97. Moberg, C. Stereomutation in Trigonal-Bipyramidal Systems: A Unified Picture. *Angewandte Chemie International Edition* **2011**, *50*, 10290-10292.

98. Stalick, J. K.; Corfields, P.; Meek, D. W. Trigonal-Bipyramidal and Square-Pyramidal Five-Coordinate Cobalt (II). Crystal and Molecular Structures of the Red and Green Isomers of Chlorobis [1, 2-bis(Diphenylphosphino)ethane] Cobalt(II) Trichlorostannate(II). *Inorg. Chem.* **1973**, *12*, 1668-1675.

99. BisiáCastellani, C. Five-Coordinated Copper (II) Complexes: a New Look at the Isomerization from Trigonal-Bipyramidal to Square-Pyramidal Geometry in Bis(bipyridyl)-(Monodentate Ligand) Copper(II) and Related Complexes. *Dalton Trans.* **1990**, 2895-2902.

100. Chung, M.; Qi, G.; Stryker, J. M. Synthesis of Sterically Hindered Ortho-Substituted Tetraphenylethenes. Electronic Effects in the McMurry Olefination Reaction. *Org. Lett.* **2006**, *8*, 1491-1494.

101. Chung, M.; Lightbody, O. C.; Stryker, J. M. Ortho-Silylated Derivatives of Tetrakis(2-hydroxyphenyl)ethene: A Sterically Isolated Structural Model for Oxo-Surface Binding Domains. *Org. Lett.* **2008**, *10*, 3825-3828.

102. Fujita, M.; Lightbody, O. C.; Ferguson, M. J.; McDonald, R.; Stryker, J. M. Quasi-Planar Homopolymetallic and Heteropolymetallic Coordination Arrays. Surface-Like Molecular Clusters of Magnesium and Aluminum. *J. Am. Chem. Soc.* **2009**, *131*, 4568-4569.

103. Verkerk, U.; Fujita, M.; Dzwiniel, T. L.; McDonald, R.; Stryker, J. M. Tetrakis(2-hydroxyphenyl)ethene and Derivatives. A Structurally Preorganized Tetradentate Ligand System for Polymetallic Coordination Chemistry and Catalysis. *J. Am. Chem. Soc.* **2002**, *124*, 9988-9989.

104. Floriani, C. Metal Reactivity on Oxo Surfaces Modeled by Calix [4] arenes: Metal-Driven Reactions in an Oxo-Quasiplanar Environment. *Chemistry-A European Journal* **1999**, *5*, 19-23.

105. Wieser, C.; Dieleman, C. B.; Matt, D. Calixarene and Resorcinarene Ligands in Transition Metal Chemistry. *Coord. Chem. Rev.* **1997**, *165*, 93-161.

106. Middel, O.; Greff, Z.; Taylor, N. J.; Verboom, W.; Reinhoudt, D. N.; Snieckus, V. The First Lateral Functionalization of Calix [4] arenes by a Homologous Anionic ortho-Fries Rearrangement. *J. Org. Chem.* **2000**, *65*, 667-675.

107. Zanotti-Gerosa, A.; Solari, E.; Giannini, L.; Floriani, C.; Chiesi-Villa, A.; Rizzoli, C. Self-Assembling of p-*tert*-Butylcalix[4]arene into Supramolecular Structures Using Transition-Metal Derivatization. *Chem. Commun.* **1996**, 119-120.

108. Shinkai, S.; Araki, K.; Manabe, O. Does the Calixarene Cavity Recognise the Size of Guest Molecules? On the 'Hole-Size Selectivity' in Water-Soluble Calixarenes. *Chem. Commun.* **1988**, 187-189.

109. Liu, L.; Zakharov, L. N.; Golen, J. A.; Rheingold, A. L.; Watson, W. H.; Hanna, T. A. Molybdocalixarene Structure Control via Rim Deprotonation. Synthesis, Characterization, and Crystal Structures of Calix[4]arene Mo (VI) Monooxo Complexes and Calix[4]arene Alkali Metal/Mo (VI) dioxo Complexes. *Inorg. Chem.* **2006**, *45*, 4247-4260.

110. Cozzi, P. G. Metal–Salen Schiff Base Complexes in Catalysis: Practical Aspects. *Chem. Soc. Rev.* **2004**, *33*, 410-421.

111. Katsuki, T. Some Recent Advances in Metallosalen Chemistry. *Synlett* **2003**, 281-297.

112. O'Mahony, C. P.; McGarrigle, E. M.; Renehan, M. F.; Ryan, K. M.; Kerrigan, N. J.; Bousquet, C.; Gilheany, D. G. Asymmetric Alkene Epoxidation with Chromium Oxo-Salen Complexes. A Systematic Study of Salen Ligand Substituents. *Org. Lett.* **2001**, *3*, 3435-3438.

113. Chen, H.; White, P. S.; Gagné, M. R. Synthesis and Reactivity of Titanium (IV)-Salen Complexes Containing Oxygen and Chloride Ligands. *Organometallics* **1998**, *17*, 5358-5366.

114. Haikarainen, A.; Sipilä, J.; Pietikäinen, P.; Pajunen, A.; Mutikainen, I. Synthesis and Characterization of Bulky Salen-Type Complexes of Co, Cu, Fe, Mn and Ni with Amphiphilic Solubility Properties. *Dalton Trans.* **2001**, 991-995.

115. McGarrigle, E. M.; Gilheany, D. G. Chromium-and Manganese-Salen Promoted Epoxidation of Alkenes. *Chem. Rev.* **2005**, *105*, 1563-1602.

116. Kojima, M.; Taguchi, H.; Tsuchimoto, M.; Nakajima, K. Tetradentate Schiff base–Oxovanadium (IV) Complexes: Structures and Reactivities in the Solid State. *Coord. Chem. Rev.* **2003**, *237*, 183-196.

117. Mathew, M.; Carty, A.; Palenik, G. J. Unusual Complex Containing Bridging Vanadyl Groups. Crystal Structure of N, N'-Propylenebis (Salicylaldiminato) Oxovanadium (IV). *J. Am. Chem. Soc.* **1970**, *92*, 3197-3198.

118. Fujii, H.; Funahashi, Y. A Trigonal-Bipyramidal Ferric Aqua Complex with a Sterically Hindered Salen Ligand as a Model for the Active Site of Protocatechuate 3, 4-Dioxygenase. *Angewandte Chemie* **2002**, *114*, 3790-3793.

119. Thomas A. Albright, Jeremy K. Burdett, Myung-Hwan Whangbo In *Five Coordiantion;* Orbital Interactions in Chemistry; John Wiley & Sons, Inc.: Canada, 1985; Vol. 1, pp 310-338.

120. Elian, M.; Hoffmann, R. Bonding Capabilities of Transition Metal Carbonyl Fragments. *Inorg. Chem.* **1975**, *14*, 1058-1076.

121. Spees, S. T.; Perumareddi, J. R.; Adamson, A. W. Crystal Field Energy Levels for Various Symmetries. *J. Phys. Chem.* **1968**, *72*, 1822-1825.

122. Caride, A.; Panepucci, H.; Zanette, S. Analysis of the Ligand Field Spectra of Some Low Spin Pentacoordinate Co2 Complexes. *J. Chem. Phys.* **1971**, *55*, 3651-3654.

123. Gray, H. B.; Preer, J. R. Electronic Structures of Low-Spin, Square-Pyramidal complexes of Nickel (II). *J. Am. Chem. Soc.* **1970**, *92*, 7306-7312.

124. Spees Jr, S. T.; Perumareddi, J. R.; Adamson, A. W. Substitution Reactions of Inorganic Complexes. Concerning the Prediction of Activation Energies and Reaction Mechanisms by Crystal field Theory. *J. Am. Chem. Soc.* **1968**, *90*, 6626-6635.

125. Rossi, A. R.; Hoffmann, R. Transition Metal Pentacoordination. *Inorg. Chem.* **1975**, *14*, 365-374.

126. Housecrofft, E. C.; Sharpe, G. A. In *d-Block Metal Chemistry: Coordination Complexes;* Inorganic Chemistry; Pearson: England, 2008; pp 637-685.

127. McNaughton, R. L.; Roemelt, M.; Chin, J. M.; Schrock, R. R.; Neese, F.; Hoffman, B. M. Experimental and Theoretical EPR Study of Jahn-Teller-Active [HIPTN3N]MoL Complexes (L = N2, CO, NH3). *J. Am. Chem. Soc.* **2010**, *132*, 8645-8656.

128. McNaughton, R. L.; Chin, J. M.; Weare, W. W.; Schrock, R. R.; Hoffman, B. M. EPR Study of the Low-Spin d3; S =1/2], Jahn-Teller Active, Dinitrogen Complex of a Molybdenum Trisamidoamine. *J. Am. Chem. Soc.* **2007**, *129*, 3480-3481.

129. O'Donoghue, M. B.; Davis, W. M.; Schrock, R. R. Derivatization of Dinitrogen by Molybdenum in Triamidoamine Complexes. *Inorg. Chem.* **1998**, *37*, 5149-5158.

130. Kol, M.; Schrock, R. R.; Kempe, R.; Davis, W. M. Synthesis of Molybdenum and Tungsten Complexes That Contain Triamidoamine Ligands of the Type $(C_6F_5NCH_2CH_2)_3N$ and Activation of Dinitrogen by Molybdenum. *J. Am. Chem. Soc.* **1994**, *116*, 4382-4390.

131. Schrock, R. R. Transition Metal Complexes That Contain a Triamidoamine Ligand. *Acc. Chem. Res.* **1997**, *30*, 9-16.

132. Fryzuk, M. D. Side-on End-on Bound Dinitrogen: An Activated Bonding Mode That Facilitates Functionalizing Molecular Nitrogen. *Acc. Chem. Res.* **2009**, *42*, 127-133.

133. Shilov, A. E. Catalytic Reduction of Molecular Nitrogen in Solutions. *Russ. Chem. Bull.* **2003**, *52*, 2555-2562.

134. Chang, Y.; Chan, P.; Tsai, Y.; Lee, G.; Hsu, H. Catalytic Reduction of Hydrazine to Ammonia by a Mononuclear Iron(II) Complex on a Tris(thiolato)phosphine Platform. *Inorg. Chem.* **2014**, *53*, 664-666.

135. Verkerk, U. H.; McDonald, R.; Stryker, J. M. Coordination Chemistry of the Tetrakis(2-hydroxyphenyl)ethene Support Mimic - Polymetallic Magnesium, Aluminum, and Titanium Derivatives. *Can. J. Chem.* **2005**, *83*, 922-928.

136. Kim, Y.; Kapoor, P. N.; Verkade, J. G. (RO)2Tatris(2-oxy-3,5-dimethylbenzyl)amine]: Structure and Lactide Polymerization Activities. *Inorg. Chem.* **2002**, *41*, 4834-4838.

137. Pyykkö, P.; Atsumi, M. Molecular Double-Bond Covalent Radii for Elements Li–E112. *Chem. Eur. J.* **2009**, *15*, 12770-12779.

138. Pyykkö, P.; Atsumi, M. Molecular Single-Bond Covalent Radii for Elements 1–118. *Chem. Eur. J.* **2009**, *15*, 186-197.

139. Werndrup, P.; Verdenelli, M.; Chassagneux, F.; Parola, S.; Kessler, V. G. Powders and Dense Thin Films of Late Transition Metal Oxide Nanocomposites From Structurally Characterized Single-Source Precursors. *J. Mater. Chem.* **2004**, *14*, 344-350.

140. Hayatifar, M.; Marchetti, F.; Pampaloni, G.; Zacchini, S. Synthesis, X-ray Characterization, and Reactivity of α-Aminoacidato Ethoxide Complexes of Niobium(V) and Tantalum(V). *Inorg. Chem.* **2013**, *52*, 4017-4025.

141. Castellano, B.; Zanotti-Gerosa, A.; Solari, E.; Floriani, C.; Chiesi-Villa, A.; Rizzoli, C. Metal-Carbon and Carbon-Oxygen Related Reactivity in Tantalum p-*tert*-Butylcalix[4]arene Complexes Undergoing Organic Functionalization. *Organometallics* **1996**, *15*, 4894-4896.

142. Tonks, I. A.; Henling, L. M.; Day, M. W.; Bercaw, J. E. Amine, Amido, and Imido Complexes of Tantalum Supported by a Pyridine-Linked Bis(phenolate) Pincer Ligand: Ta-N π-Bonding Influences Pincer Ligand Geometry. *Inorg. Chem.* **2009**, *48*, 5096-5105.

143. Elorriaga, D.; Galajov, M.; Garcia, C.; Gomez, M.; Gomez-Sal, P. Hydridotris(3,5-dimethylpyrazolyl)borate Dimethylamido Imido Niobium and Tantalum Complexes: Synthesis, Reactivity, Fluxional Behavior, and C-H Activation of the NMe2 Function. *Organometallics* **2012**, *31*, 5089-5100.

144. Tanski, J. M.; Parkin, G. Tantalum Amido and Imido Complexes Supported by Tris(2-indolyl)methyl]amine, a Tetradentate Trianionic Ligand with Reduced π-Donor Character. *Inorg. Chem.* **2003**, *42*, 264-266.

145. Mashima, K.; Tanaka, Y.; Nakamura, A. Synthesis, Characterization, and Reactions of a Mononuclear Tantalum-Benzyne Complex, Ta(η5-C_5Me_5)(η4-C_4H_6)(η.2-C_6H_4). *Organometallics* **1995**, *14*, 5642-5651.

146. Pyykkö, P.; Atsumi, M. Molecular Single-Bond Covalent Radii for Elements 1–118. *Chem. Eur. J.* **2009**, *15*, 186-197.

147. Fryzuk, M. D.; Johnson, S. A.; Rettig, S. J. New Mode of Coordination for the Dinitrogen Ligand: A Dinuclear Tantalum Complex with a Bridging N_2 Unit That Is Both Side-On and End-On. *J. Am. Chem. Soc.* **1998**, *120*, 11024-11025.

148. Brookhart, M.; Grant, B.; Volpe, A. F. $(3,5\text{-}(CF_3)_2C_6H_3)_4B]\text{-}H(OEt_2)_2]^+$: a Convenient Reagent for Generation and Stabilization of Cationic, Highly Electrophilic Organometallic Complexes. *Organometallics* **1992**, *11*, 3920-3922.

149. Belford, R. L.; Martell, A.; Calvin, M. Influence of Fluorine Substitution on the Properties of Metal Chelate Compounds—I Copper (II) Chelates of Bidentate Ligands. *Journal of Inorganic and Nuclear Chemistry* **1956**, *2*, 11-31.

150. Olmstead, W. N.; Bordwell, F. G. Ion-Pair Association constants in Dimethyl Sulfoxide. *J. Org. Chem.* **1980**, *45*, 3299-3305.

151. Gorelsky, S. AOMix: program for molecular orbital analysis. *York University, Toronto* **1997**.

152. Gorelsky, S.; Lever, A. Electronic structure and spectra of ruthenium diimine complexes by density functional theory and INDO/S. Comparison of the two methods. *Journal of Organometallic Chemistry* **2001**, *635*, 187-196.

153. Keane, A. J.; Zavalij, P. Y.; Sita, L. R. N-N Bond Cleavage of Mid-Valent Ta(IV) Hydrazido and Hydrazidium Complexes Relevant to the Schrock Cycle for Dinitrogen Fixation. *J. Am. Chem. Soc.* **2013**, *135*, 9580-9583.

154. Corazza, F.; Floriani, C.; Chiesi-Villa, A.; Guastini, C. The Oxo-Molybdenum (VI) Group over a calixarene-Oxo Surface: Calix[4]arene Complexing Inorganic and Organic Functionalities. *J.Chem.Soc., Chem.Commun.* **1990**, 640-641.

155. Millar, A. J.; White, J. M.; Doonan, C. J.; Young, C. G. Synthesis and Characterization of Monomeric Oxo Dichloro 1, 3-Dialkyl p-*tert*-butylcalix[4]arene Complexes of Molybdenum(VI, V) and tungsten(VI, V). *Inorg. Chem.* **2000**, *39*, 5151-5155.

156. Magnusson, G. A Convenient Preparation of Cyclopentadiene from its Dimer. *J. Org. Chem.* **1985**, *50*, 1998-1998.

157. APEX, S., SADABS. Bruker AXS, Inc. **Madison, Wisconsin, USA, 2007**.

158. Farrugia, L. J. WinGX Suite for Small-Molecule single-Crystal Crystallography. *J. App. Cryst.* **1999**, *32*, 837-838.

159. Sheldrick, G. M. Phase Annealing in SHELX-90: Direct Methods for Larger Structures. *Acta Crystallogr.* **1990**, *46*, 467-473.

6.0 NMR Spectroscopy

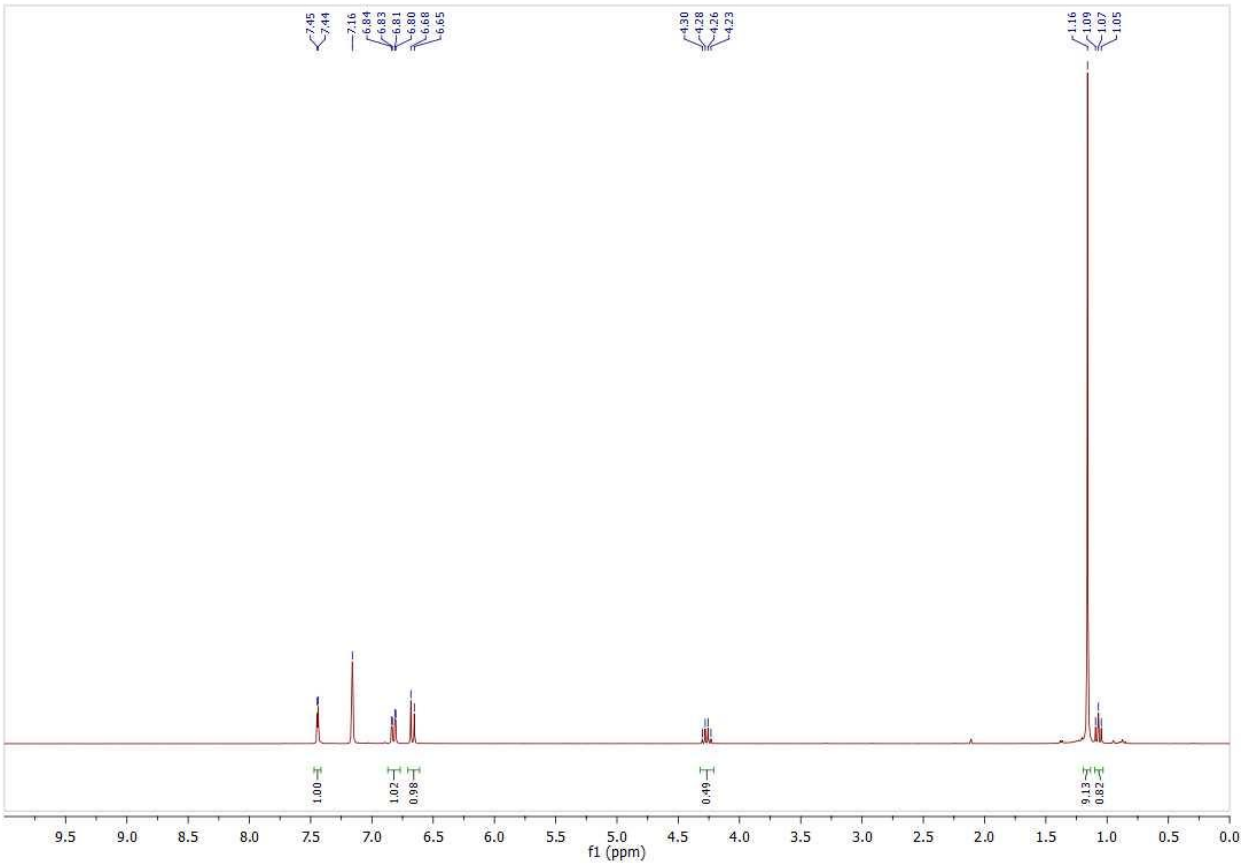

^{1}H NMR (400 MHz, C_6D_6) of Complex 6

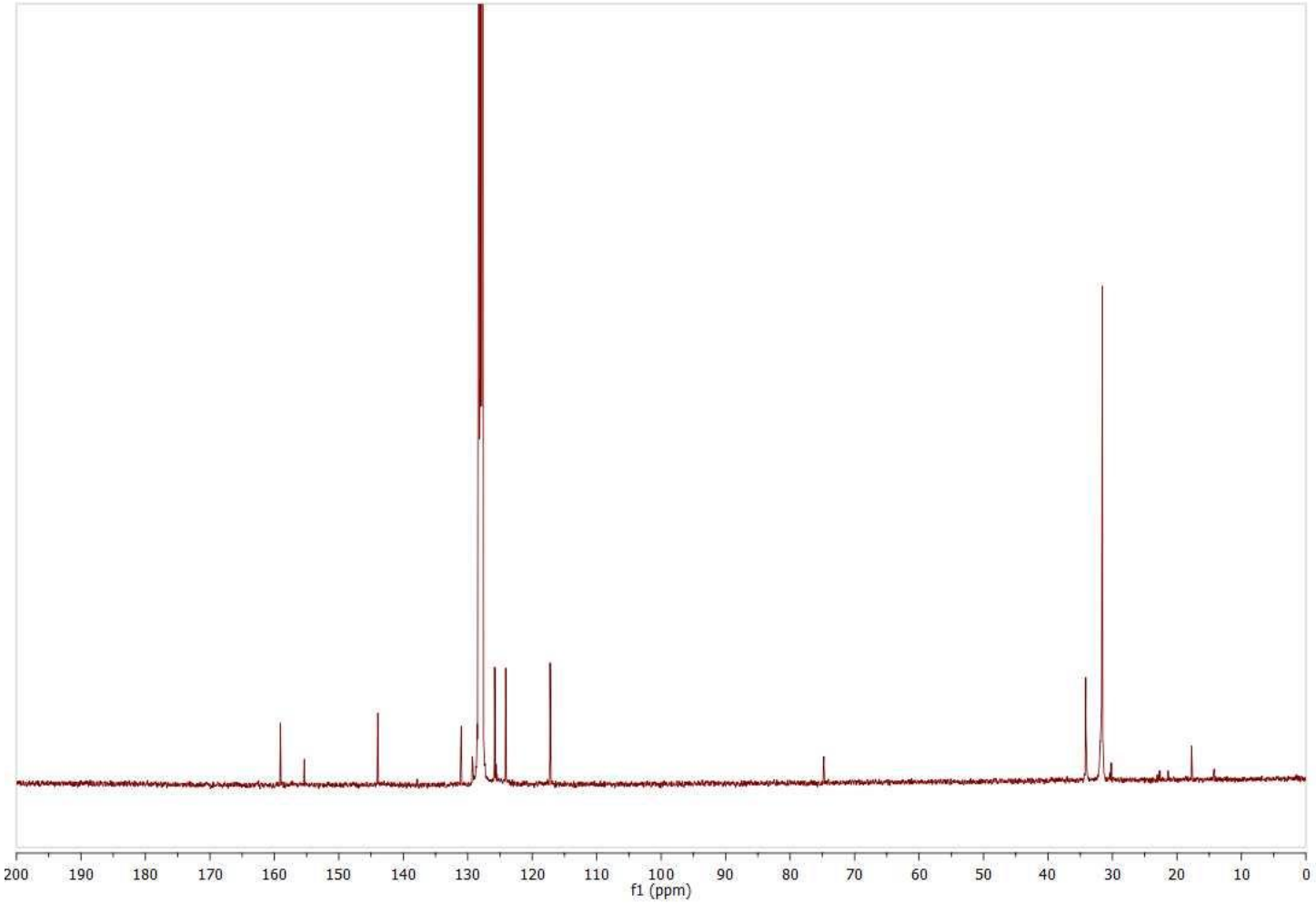

$^{13}C\{^{1}H\}$ NMR (100 MHz, C_6D_6 of Complex 6

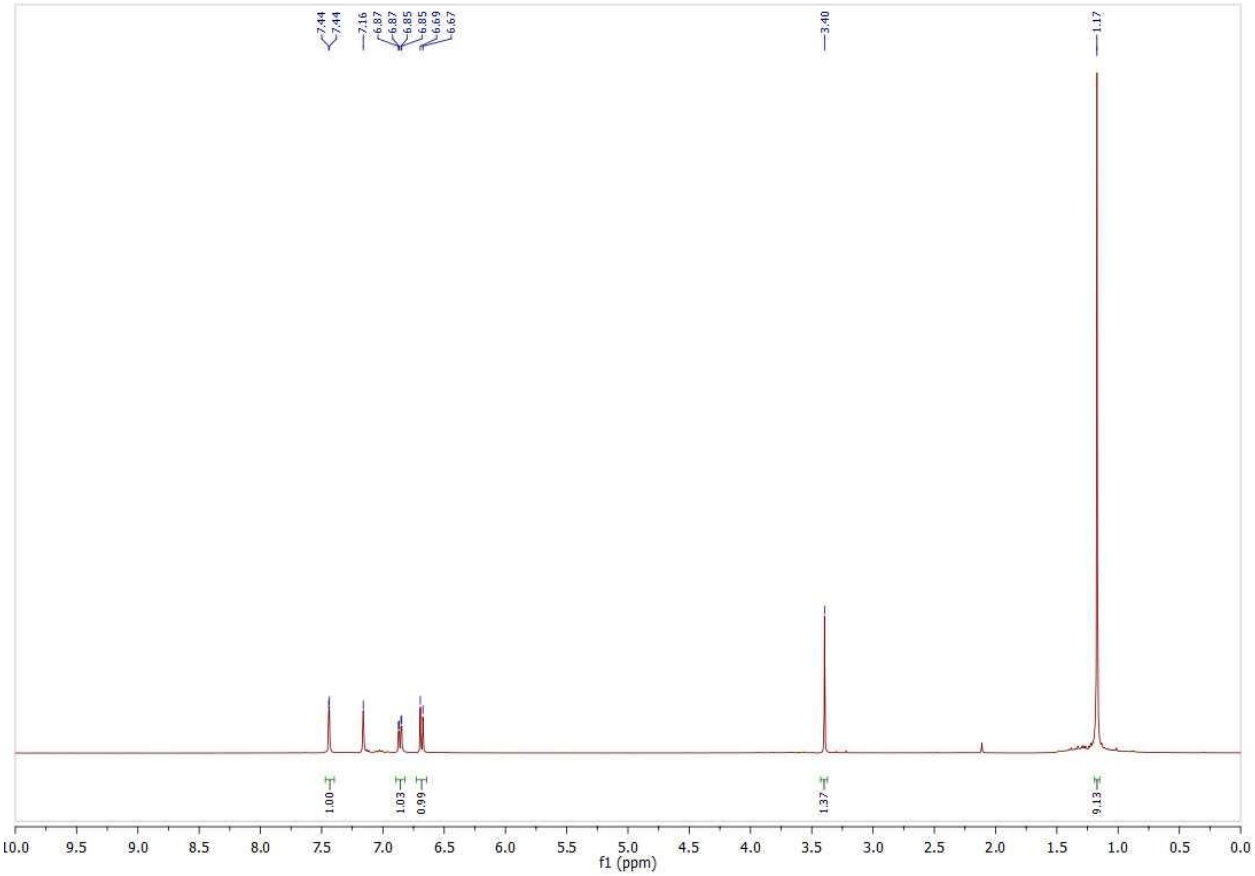

^{1}H NMR (400 MHz, C_6D_6) of Complex 7

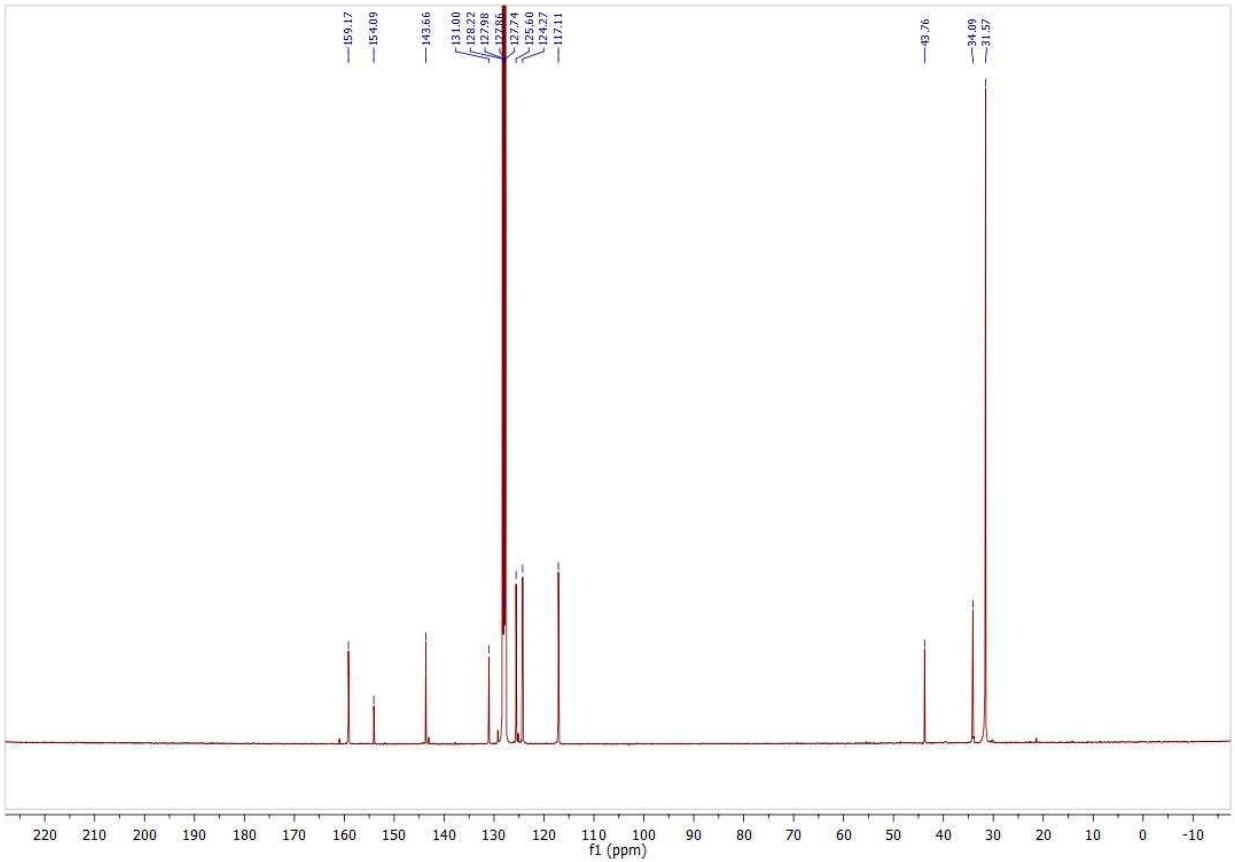

$^{13}C\{^{1}H\}$ NMR (100 MHz, C_6D_6 of Complex 7

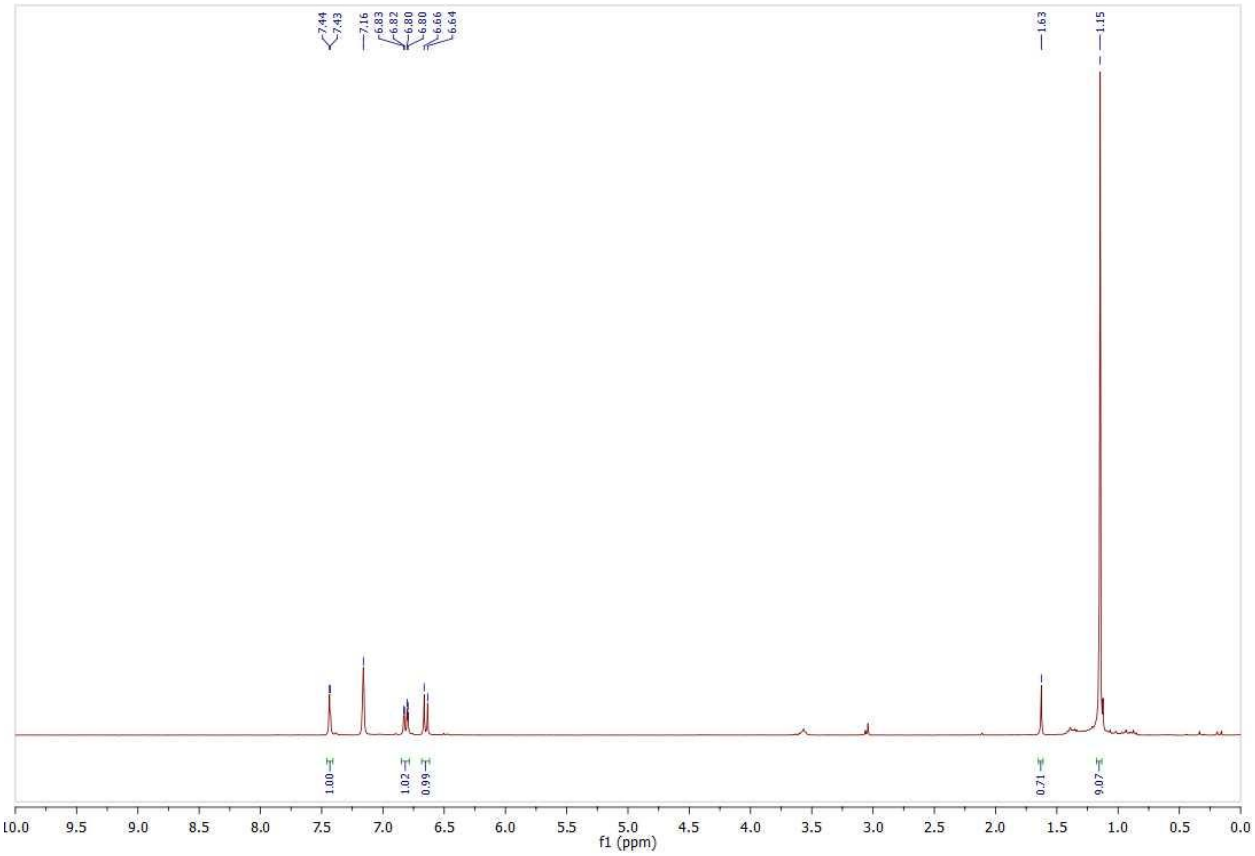

^{1}H NMR (400 MHz, C_6D_6) of Complex 8

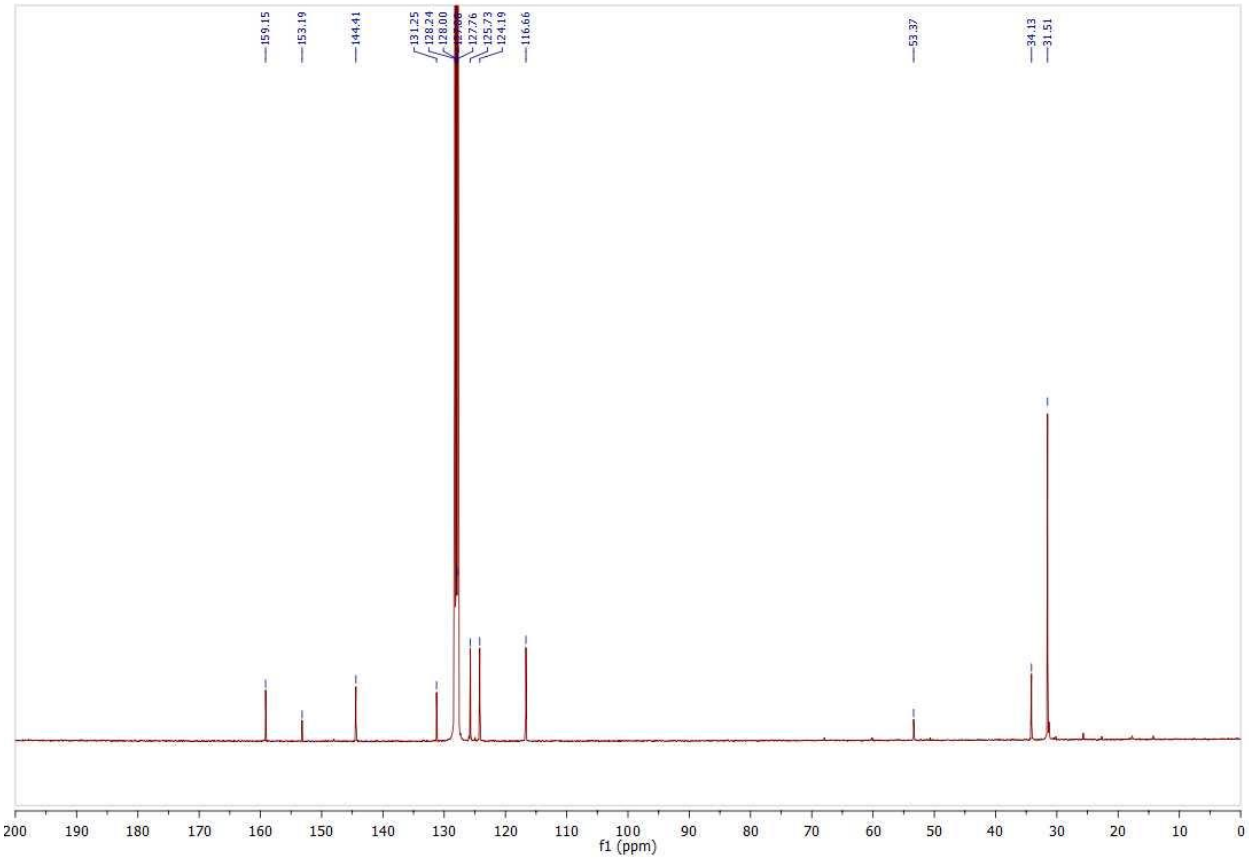

$^{13}C\{^{1}H\}$ NMR (100 MHz, C_6D_6 of Complex 8

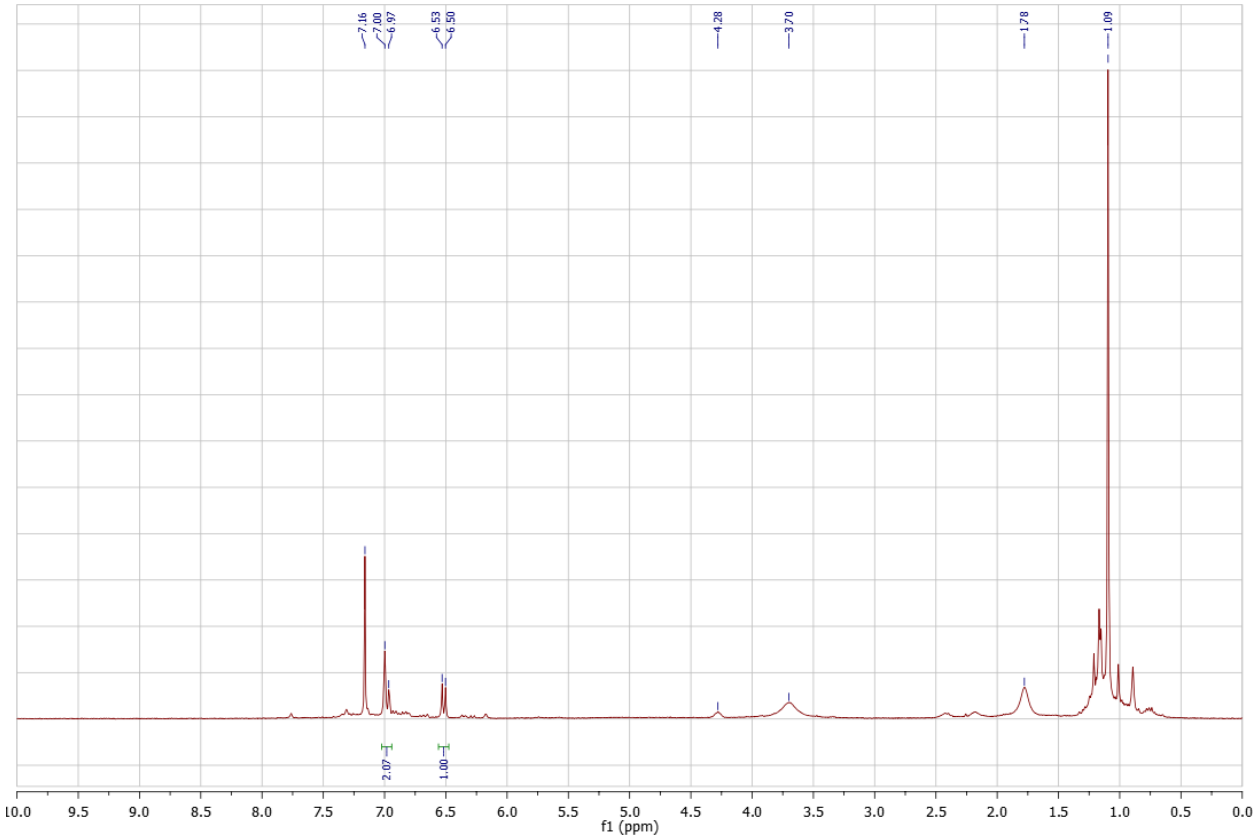

^{1}H NMR (400 MHz, C_6D_6) of Complex 10